RIGA TECHNICAL UNIVERSITY

Jaymin Vrajlal Sanchaniya

STUDY ON FABRICATION TECHNIQUE, PROPERTIES, AND APPLICATIONS OF PAN NANOFIBERS

Doctoral Thesis

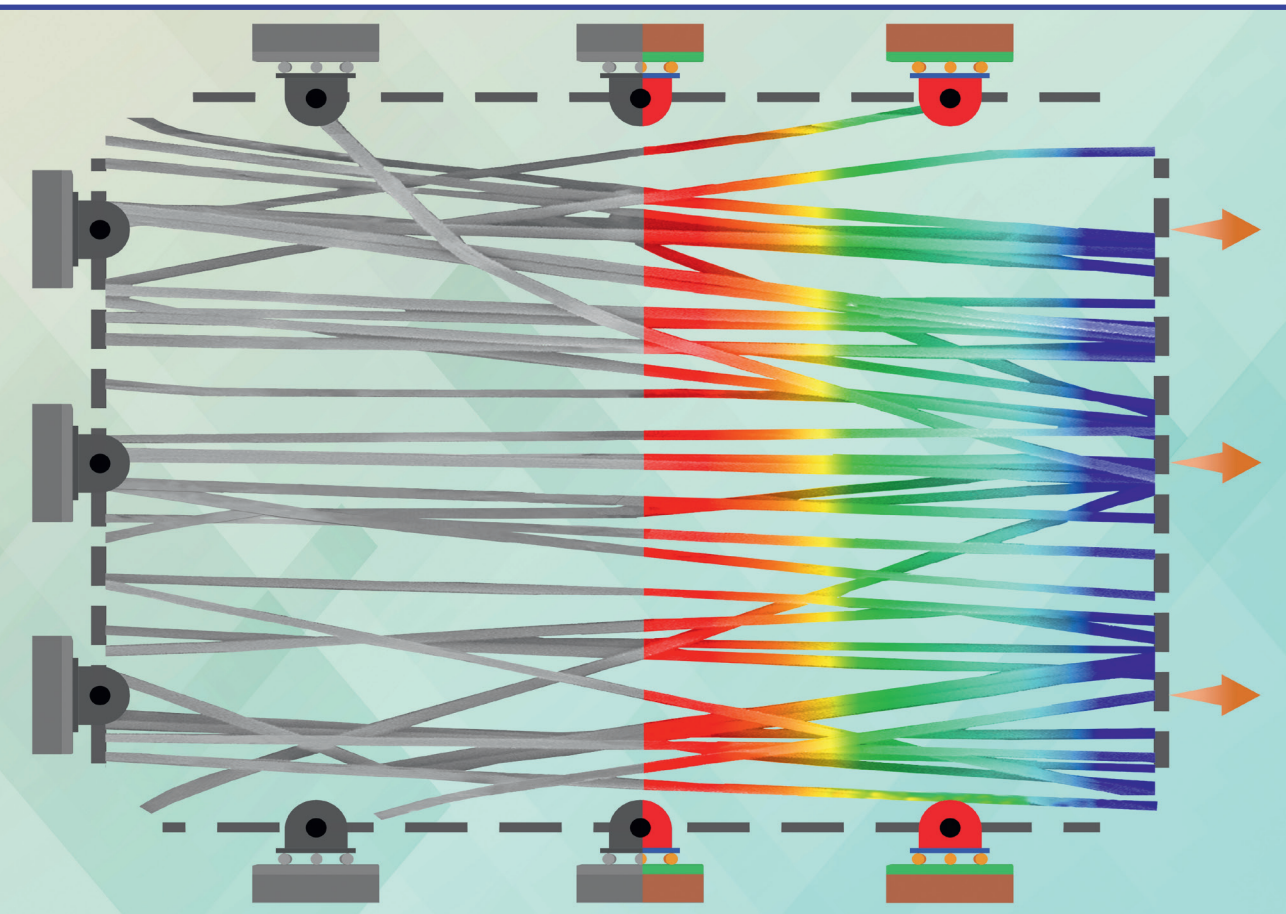

RTU Press
Riga 2024

RIGA TECHNICAL UNIVERSITY
Faculty of Civil and Mechanical Engineering

Jaymin Vrajlal Sanchaniya
Doctoral Student of the Study Programme
"Mechanical Engineering and Mechanics (Applied Mechanics)"

A STUDY ON FABRICATION TECHNIQUE, PROPERTIES, AND APPLICATIONS OF PAN NANOFIBERS

Doctoral Thesis

Scientific supervisors:
Associate Professor Dr. sc. ing.
INGA ĻAŠENKO
Professor Dr. sc. ing.
ANDREJS KRASŅIKOVS

Riga 2024

ANOTĀCIJA

Nanotehnoloģiju joma, jo īpaši nanopavedienu izpēte un izmantošana, ir materiālzinātnes priekšplānā, piedāvājot nepārspējamas inovāciju iespējas daudzās jomās. Šī doktora disertācija ar nosaukumu "A Study on Fabrication Technique, Properties, And Applications of PAN Nanofibers" (Pan Nanošķiedru Izgatavošanas Tehnoloģijas, Īpašību Un Lietojuma Izpēte), iedziļinās sarežģītajā poliakrilnitrila (PAN) šķiedru no nanomateriāla pasaulē, pievēršot uzmanību to izgatavošanai, mehāniskajām un termiskajām īpašībām, kā arī to potenciālajam pielietojumam. Izmantojot izsmeļošu literatūras pārskatu un virkni rūpīgu eksperimentālu pētījumu, šī darba mērķis ir novērst būtiskas nepilnības esošajās zināšanās par nanošķiedru tehnoloģiju, īpaši koncentrējoties uz PAN nanošķiedrām.

Sākot ar plašu nanošķiedru tehnoloģiju apskatu, šajā darbā uzsvērts ražošanas paņēmienu progress, īpašu uzmanību pievēršot elektrovērpšanai. Elektrovērpšanas unikālā spēja ražot nanošķiedras ar atšķirīgām īpašībām padara to nenovērtējamu filtrēšanas, biomedicīnisko ierīču un strukturālo materiālu pielietošanai. Pētījumā rūpīgi izpētīta eksperimentāla PAN nanošķiedru paklāju izgatavošana, izmantojot dažādas elektrovērpšanas metodes, lai izpētītu to ietekmi uz šķiedru orientāciju un paklāja struktūru. Ievērojams šī pētījuma sasniegums ir galīgo elementu (FE) modeļa formulēšana un apstiprināšana, kas precīzi prognozē elektrovītinātu nanošķiedru paklāju mehānisko uzvedību.

Pētījuma 3. nodaļā pētīta strukturālās orientācijas ietekme uz nanošķiedru paklājiem, atklājot, ka orientētiem paklājiem ir ievērojami lielāka izturība - aptuveni par 300 % lielāka nekā nejauši strukturētiem paklājiem, kā to apstiprina 4. nodaļā izstrādātais FE modelis. Ceturtajā nodaļā tiek veikta FE modeļa pilnveidošana, rūpīgi pārbaudot, kā strukturālie parametri ietekmē PAN nanošķiedru paklāju mehāniskās īpašības.

Piektajā nodaļā eksperimentāli tiek pētīta atkarsēšanas ietekme uz PAN nanošķiedru paklājiem. Tika novērots, ka atlaidināšana 70 grādu temperatūrā pēc Celsija var palielināt nanošķiedru paklāja stingrību par aptuveni 7 %, savukārt temperatūras virs 100 grādiem pēc Celsija paklāju padara trauslu šķīdinātāja iztvaikošanas dēļ. Turklāt pēc atkarsēšanas stiklošanās temperatūra pazeminājās par 5,21 %, un TGA analīzēs tika novērots sākotnējs 3 % masas zudums, kas saistīts ar šķīdinātāja iztvaikošanu.

Šā pētījuma 6. nodaļā ir izklāstīts šā pētījuma jaunais aspekts, izmantojot iegremdēšanas metodi un PVA šķīdumu ar zemu koncentrāciju kā leģējošo vielu, kā rezultātā PVA tiek iestrādāts PAN nanopavedienu paklājos kā lokalizētas aglomerācijas un plāns pārklājums uz nanopavedieniem, vienlaikus saglabājot to porainību. Stiepes testi parādīja, ka

PVA piedevas rezultātā ievērojami palielinājās gan nanošķiedru paklāju elastības modulis, gan stiepes izturība, un uzlabojuma lielums bija tieši atkarīgs no izmantotās PVA koncentrācijas. Konkrēti, pie 2 % PVA koncentrācijas elastības modulis garenvirzienā palielinājās par aptuveni 78,33 %, bet UTS - par aptuveni 84,34 %. Šķērsvirzienā elastības modulis un UTS palielinājās attiecīgi par aptuveni 159,57 % un 200,88 %, kas norāda, ka PVA piedevas efektīvi pastiprināja šķiedru savstarpējās saites un nodrošināja papildu strukturālo atbalstu.

Termiskās analīzes, tostarp termogravimetriskā analīze (TGA) un diferenciālā skenējošā kalorimetrija (DSC), parādīja, ka ar PVA dopētajiem nanošķiedru paklājiem ir izmainītas termiskās degradācijas īpašības un stiklošanās temperatūras, kas atspoguļo PVA ietekmi uz to termisko stabilitāti. Novērotais siltuma absorbcijas pieaugums, pieaugot PVA koncentrācijai DSC karsēšanas ciklu laikā, liecina, ka PAN nanošķiedru un PVA mijiedarbība būtiski ietekmē kompozīta termiskās īpašības. Otrā sildīšanas cikla laikā tika novērots ievērojams PVA plēves stiklošanās temperatūras (Tg) pieaugums par 63,02 %. Turpretī kompozīta Tg būtiski nemainījās, kas norāda uz kompozīta spēju saglabāt stiklošanās temperatūru tuvu nepiesātināto PAN nanošķiedru paklāju stiklošanās temperatūrai, neskatoties uz PVA tilpuma palielināšanos.

7. nodaļā atklāts, ka nanošķiedru tieša elektrovērpšana uz tekstilmateriāliem, kuras mērķis ir ražot laminētus tekstilmateriālus, kas integrēti ar elektrovērptām nanošķiedrām, atklāj iespēju radīt nešķīstošus tekstilkompozītus, izmantojot PAN nanošķiedras dažādiem lietojumiem. Šī inovatīvā pieeja demonstrē elektrovītņu PAN nanošķiedru potenciālu uzlabot tekstilmateriālu strukturālo integritāti un funkcionālās īpašības, paverot jaunas iespējas progresīvu kompozītmateriālu izstrādei. PAN nanošķiedru iekļaušana tekstilmateriālos ne tikai uzlabo šo kompozītu mehāniskās īpašības, bet arī ievieš papildu funkcijas, piemēram, uzlabotu termisko stabilitāti un filtrēšanas spējas, uzsverot nanošķiedru integrācijas pārveidojošo ietekmi uz tekstilrūpniecību un materiālzinātni.

Kopumā šis darbs veicina dziļāku izpratni par PAN nanošķiedrām, sākot no to ražošanas un mehāniskajām īpašībām līdz to pielietojumam, paverot ceļu turpmākai pētniecībai un attīstībai nanošķiedru tehnoloģiju jomā.

ABSTRACT

The domain of nanotechnology, particularly the exploration and utilization of nanofibers, stands at the forefront of materials science, offering unrivalled opportunities for innovation across a multitude of fields. This doctoral thesis, titled "PAN Nanofibers: A Comprehensive Study on Fabrication Technique, Properties, and Applications," ventures into the sophisticated world of polyacrylonitrile (PAN) nanofibers, focusing on their fabrication, mechanical and thermal characteristics, and their potential applications. Through an exhaustive review of the literature coupled with a series of rigorous experimental investigations, this work aims to bridge significant gaps in the existing knowledge of nanofiber technology, specifically concentrating on PAN nanofibers.

Initiating with an extensive survey of nanofiber technologies, this thesis emphasizes the progression of fabrication techniques, with a particular focus on electrospinning. The unique capability of electrospinning to produce nanofibers with distinct properties makes it invaluable for applications in filtration, biomedical devices, and structural materials. The research meticulously explores the experimental fabrication of PAN nanofiber mats using various electrospinning methods to examine their impact on fibre orientation and mat structure. A notable achievement of this research is the formulation and validation of a finite element (FE) model that accurately predicts the mechanical behaviour of electrospun nanofiber mats.

In Chapter 3, the investigation extends into the impact of structural orientation on nanofiber mats, unveiling that oriented mats exhibit a remarkable enhancement in strength—approximately 300% greater than randomly structured mats, as validated by the developed FE model in the chapter 4. Chapter 4 delves into the refinement of the FE model, scrutinizing how structural parameters influence the mechanical properties of PAN nanofiber mats.

Chapter 5 embarks on an experimental inquiry into the effects of annealing on PAN nanofiber mats. It was observed that annealing at 70 degrees Celsius could enhance the stiffness of the nanofiber mat by approximately 7%, whereas temperatures above 100 degrees Celsius rendered the mat brittle due to solvent evaporation. Additionally, annealing led to a decrease in the glass transition temperature by 5.21%, and an initial 3% mass loss was noted in TGA analyses, attributed to solvent evaporation.

Chapter 6 introduces the novel aspect of this study through the use of a dip-coating method and low-concentration PVA solution as a dopant, resulting in PVA being incorporated into the PAN nanofiber mats as localized agglomerations and a thin coating on the nanofibers while still preserving their porosity. Tensile testing indicated that PVA doping led to a

significant increase in both the elastic modulus and ultimate tensile strength of the nanofiber mats, with the magnitude of improvement directly related to the concentration of PVA used. Specifically, at a concentration of 2% PVA, the elastic modulus in the longitudinal direction increased by approximately 78.33%, and the UTS increased by approximately 84.34%. In the transverse direction, the elastic modulus and UTS exhibited increases of approximately 159.57% and 200.88%, respectively, indicating that PVA doping effectively reinforced their inter-fibre bonds and provided additional structural support.

Thermal analyses, including thermogravimetric analysis (TGA) and differential scanning calorimetry (DSC), demonstrated that PVA-doped nanofiber mats exhibited altered thermal degradation behaviour and glass transition temperatures, reflecting the influence of PVA on their thermal stability. The observed increase in heat absorption with rising PVA concentration during the DSC heating cycles suggests that the interaction between PAN nanofibers and PVA significantly affects the composite's thermal behaviour. During the second heating cycle, a notable increase to 67.0 ℃ from 41.1 ℃ in the glass transition temperature (Tg) of the PVA film was observed. Conversely, the Tg of the composite did not show a significant change, indicating the ability of the composite to maintain the glass transition temperatures close to those of the undoped PAN nanofiber mats despite the increase in PVA volume.

Chapter 7 unveils that the direct electrospinning of nanofibers onto textiles, aimed at producing laminated textiles integrated with electrospun nanofibers, reveals the feasibility of creating non-crimping textile composites using PAN nanofibers for diverse applications. This innovative approach demonstrates the potential of electrospun PAN nanofibers to enhance the structural integrity and functional properties of textiles, opening new avenues for the development of advanced composite materials. The incorporation of PAN nanofibers into textile materials not only augments the mechanical performance of these composites but also introduces additional functionalities, such as improved thermal stability and filtration capabilities, underscoring the transformative impact of nanofiber integration on textile engineering and material science.

In summary, this thesis contributes to a deeper understanding of PAN nanofibers, from their production and mechanical properties to their applications, paving the way for further research and advancements in nanofiber technology.

PREFACE

This Dissertation Thesis encapsulates the culmination of my research endeavours undertaken at the Riga Technical University, specifically within the Mechanics and Biotextile Research Laboratory, during the period from October 2020 to March 2024. While embarking on this doctoral journey, my initial intrigue in the scientific exploration and the challenges that research presents propelled me toward the study of nanofibers—a field initially daunting due to my background primarily rooted in manufacturing, CAD, FEM, and Solid Mechanics.

The journey, characterised by its rigorous demands and steep learning curve, ultimately turned into a rewarding exploration, culminating in more than twenty scientific publications, including five Q1 journal articles. This achievement is not solely mine, but a testament to the collective support and guidance provided by my esteemed supervisors, Associate Professor Inga Lasenko and Professor Andrejs Krasikovs. Their insightful consultations and unwavering support were instrumental in navigating the complexities of my research.

I extend my heartfelt gratitude to Riga Technical University for providing me with the platform and resources to pursue my PhD studies. Special thanks to the Doctoral Department and the ERASMUS Department, whose funding and support were crucial to my work. My research journey was further enriched by visits to other prestigious institutions, including The University of Rouen Normandy, RWTH Aachen University, Latvian University, and Tallinn University of Technology. The collaboration and insights gained from these visits were invaluable for my doctoral thesis.

My journey was made all the more enriching and bearable by the companionship of my fellow Ph.D. candidates and friends. Their camaraderie played a significant role in smoothing the arduous path of doctoral studies. I am particularly grateful to Umesh Vavaliya and Sanjay Vejanand for their help and support during this period.

In closing, my deepest appreciation goes to my family: my parents, my brother, and especially my wife Rashmi. Their understanding, patience, and unwavering support have been my anchor throughout this challenging but fulfilling journey. This thesis, while a significant academic milestone, represents something far greater: the collective effort, support, and belief of everyone who has been a part of this journey.

Jaymin Sanchaniya

Riga, 03 March 2024

TABLE OF CONTENTS

LIST OF FIGURES

LIST OF TABLES

LIST OF PUBLICATIONS

The research conducted for this doctoral thesis has contributed significantly to the field of nanofiber technology, resulting in notable publications in both high-impact journals and prestigious conference proceedings. The dissemination of the findings has been structured as follows:

Q1 Journal Articles:

1. **Sanchaniya, J. V.**, Lasenko, I., Gobins, V., & Kobeissi, A. (2024). A Finite Element Method for Determining the Mechanical Properties of Electrospun Nanofibrous Mats. Polymers (Basel), 16(6), 852. https://doi.org/10.3390/polym16060852.

2. **Sanchaniya, J. V.**, Lasenko, I., Vijayan, V., Smogor, H., Gobins, V., Kobeissi, A., & Goljandin, D. (2024). A Novel Method to Enhance the Mechanical Properties of Polyacrylonitrile Nanofiber Mats: An Experimental and Numerical Investigation. Polymers (Basel), 16(7), 992. https://doi.org/10.3390/polym16070992.

3. **Sanchaniya, J. V.**, Lasenko, I., Kanukuntala, S.-P., Smogor, H., Viluma-Gudmona, A., Krasnikovs, A., Gobins, V., & Tipans, I. (2023). Mechanical and thermal characteristics of annealed-oriented PAN nanofibers. Polymers (Basel). https://doi.org/10.3390/polym15153287.

4. **Sanchaniya, J. V.**, Lasenko, I., Kanukuntla, S. P., Mannodi, A., Viluma-gudmona, A., & Gobins, V. (2023). Preparation and Characterization of Non-Crimping Laminated Textile Composites Reinforced with Electrospun Nanofibers. Nanomaterials, 13(13), 1949. https://doi.org/10.3390/nano13131949.

Q3 Journal Article:

5. **Sanchaniya, J. V.** (2024). Comparative Analysis of Thermal Characteristics: Virgin Polyacrylonitrile (PAN) Versus Electrospun PAN Nanofiber Mats. Latvian Journal of Physics and Technical Sciences. Accepted Article.

Other Journal Articles and Conference Proceedings:

The peripheral research findings have been presented in 14 additional scientific publications, encompassing a wide range of topics relevant to the development and application of nanofiber technologies. These contributions have been documented in journals and peer-reviewed conference proceedings, further showcasing the breadth and depth of the research undertaken.

6. **Sanchaniya, J. V.**, Dobariya, S. P., & Lasenko, I. (2024). Mechanical and Thermal Properties of Nanocomposites Reinforced with Pan Nanofiber Mats. Latvian Journal of physics and technical sciences. Accepted Article.

7. **Sanchaniya, J. V.**, Rana, V., & Vejanand, S. R. (2024). Optimization of Electrospinning Parameters for High-Strength Oriented Pan Nanofiber Mats. Latvian Journal of physics and technical sciences. Accepted Article.

8. **Sanchaniya, J. V.**, Muraleedharan, H. K., & Lasenko, I. (2024). Influence of Iron (III) Oxide Nanorods on The Mechanical and Thermal Properties of Pan Nanofiber Mats. Latvian Journal of physics and technical sciences. Accepted Article.

9. **Sanchaniya, J. V.**, & Moothedath, G. (2024). Deformation Behaviour of Oriented Electrospun Pan Nanofiber Mats. Latvian Journal of physics and technical sciences. Accepted Article.

10. **Sanchaniya, J. V.,** Soni, T., & Lasenko, I. (2024). Development and Characterization of Biaxial Pan Nanofiber Mats. Latvian Journal of physics and technical sciences. Accepted Article.

11. Lasenko, I., **Sanchaniya, J.V.**, Kanukuntla, S.P., Ladani, Y., Viluma-gudmona, A., Kononova, O., Lusis, V., Tipans, I., & Selga, T. (2023). The mechanical properties of nanocomposites reinforced with PA6 electrospun nanofibers. Polymers (Basel), 15, doi:10.3390/polym15030673.

12. Lasenko, I., Grauda, D., Butkauskas, D., **Sanchaniya, J.V.,** Viluma-Gudmona, A., & Lusis, V. (2022). Testing the physical and mechanical properties of polyacrylonitrile nanofibers reinforced with succinite and silicon dioxide nanoparticles. Textiles, 2, 162–173, doi:10.3390/textiles2010009.

13. **Sanchaniya, J.V.**, Kanukuntla, S.P., & Senyurt, K.B. (2023). Fabrication and mechanical properties of polymer composte nanofiber mats. 22nd Int. Sci. Conf. Eng. Rural Dev. Proc. 2023, 22, 85-90, doi:10.22616/ERDev.2023.22.TF014.

14. Kanukuntla, S.P., **Sanchaniya, J.V.**, & Kardani, U. (2023). Numerical simulation of polymeric composite nanofiber mat. 22nd Int. Sci. Conf. Eng. Rural Dev. Proc. 2023, 22, pp. 790–795, doi:10.22616/ERDev.2023.22.TF156.

15. Kanukuntla, S., **Sanchaniya, J. V.**, & Beresnevics, V. (2023). Comparative dsc analysis of virgin and nanofiber mats of pa6. 22nd Int. Sci. Conf. Eng. Rural Dev. Proc. 2023, 22, 539–543, doi:10.22616/ERDev.2023.22.TF113.

16. **Sanchaniya, J. V.**, & Kanukuntla, S. (2023). Morphology and mechanical properties of PAN nanofiber mat. J. Phys. Conf. Ser. 2023, 2423, 012018, doi:10.1088/1742-6596/2423/1/012018.

17. **Sanchaniya, J. V.**, Kanukuntla, S. P., Modappathi, P., & Macanovskis, A. (2022). Mechanical behaviour numerical investigation of composite structure, consisting of polymeric nanocomposite mat and textile. 21st Int. Sci. Conf. Eng. Rural Dev. Proc. 2022, 21, 720–726, doi:10.22616/erdev.2022.21.tf225.

18. **Sanchaniya, J. V.**, Kanukuntla, S.P., Shereef, A., & Kaneps, J. (2022). Modelling and analysis of composite polyacrylonitrile nanofiber mats utilized to strengthen motorbike side panel. 21st Int. Sci. Conf. Eng. Rural Dev. Proc. 2022, 21, 727–736, doi:10.22616/erdev.2022.21.tf226.

19. **Sanchaniya, J.V.**, Kanukuntla, S.P., Simon, S., & Gerina-Ancane, A. (2022). Analysis of mechanical properties of composite nanofibers constructed on rotating drum and collector plate. 21st Int. Sci. Conf. Eng. Rural Dev. Proc. 2022, 21, 737–744, doi:10.22616/erdev.2022.21.tf227.

20. Viluma-Gudmona, A., Lasenko, I., **Sanchaniya, J.V.**, & Podgornovs, A. (2021). Electro-resistant biotextile development based on fiber reinforcement with nano particles. In 20th Int. Sci. Conf. Eng. Rural Dev. Proc. 2021, pp. 804–812, doi: 10.22616/ERDev.2021.20.TF182.

21. Viluma-Gudmona, A., Lasenko, I., **Sanchaniya, J.V.**, & Abdelhadi, B. (2021). The amber nano fibers development prospects to expand the capabilities of textile 3D printing in the general process of fabrication methods. 20th Int. Sci. Conf. Eng. Rural Dev. Proc. 2021, pp. 248–257, doi: 10.22616/ERDev.2021.20.TF051.

Note: All listed publications have been indexed in reputable databases such as SCOPUS or Web of Science, ensuring their accessibility and visibility within the scientific community.

1. INTRODUCTION

Nanoscale science and technology, a pioneering field of research, focuses on phenomena measured in nanometres, to a length in a billionth of a meter. Over the past few decades, scientists have developed tools and methods that enhance our understanding of the fundamental aspects of the world at this minuscule scale.

Nanotechnology, defined as the manipulation of matter with at least one dimension ranging from 1 to 100 nanometres (nm) by the Nanotechnology Initiative, has unlocked the tremendous potential inherent in nanoscale objects. At this scale, materials exhibit unique properties due to quantum effects, size effects, and a significant surface-to-volume ratio or interface-to-volume ratio. Manipulating the nanoscale structure allows for precise control over material properties, including mechanical, thermal, electrical, magnetic, and optical characteristics. Figure 1.1 depicts the nanofiber mat produced through the process of electrospinning.

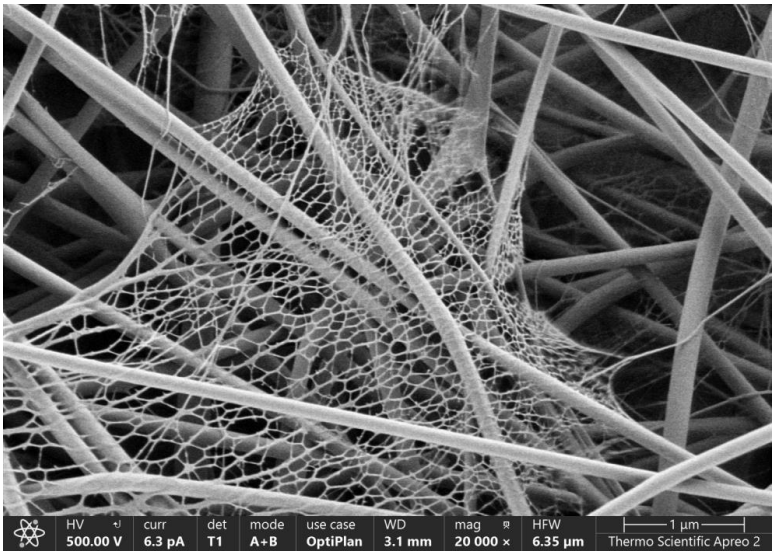

Figure 1.1 Electrospun nanofiber mat obtained using the electrospinning technique.

Materials developed at the nanoscale often surpass the properties of conventional materials, opening doors to a myriad of applications. The high surface-to-volume ratio of nanomaterials, for instance, finds utility in composites, chemical reactions, drug delivery, and energy storage. Nanosized catalysts hold promise for enhancing the efficiency of chemical reactions, illustrating the transformative potential of nanotechnology.

Anticipated to reshape existing technologies and spawn new industries, nanotechnology spans diverse fields such as surface science, organic chemistry, molecular biology, semiconductor physics, and microfabrication. Key research areas include the synthesis, characterization, and integration of nanomaterials, driven by the expansive range of potential applications in both industry and the military.

Within the realm of nanotechnology, nanomaterials emerge as a crucial subset. Defined as materials with at least one dimension less than 100 nm, nanomaterials possess unique physical and chemical properties, characterized by small size and high specific surface area, as well as quantum confinement. Scientists harness these distinctive features to create materials, devices, and systems at the nanometer scale, exploring novel phenomena and properties that arise at this dimension.

Nanomaterials are classified into zero-dimensional (e.g., nanoparticles), one-dimensional (e.g., nanofibers, nanotubes, and nanowires), and two-dimensional (e.g., nanoplatelets and nanofilms) categories. Notably, nanofiber mats, with a thickness of up to 200 micrometres, hold particular relevance for diverse applications such as filtration and medical applications due to their unique characteristics at this thickness. This research focuses on the fabrication and characterization of polyacrylonitrile (PAN) nanofiber mats, delving into their properties, novel applications, and the transformative impact of nanotechnology on materials science and technology.

Electrospinning, a cost-effective technique, stands out as a versatile method for producing polymer fibers within the nanoscale range, spanning from tens to a few hundred nanometres. The applications of electrospun nanofibers are diverse, encompassing optical materials (Tanioka et al., 2010), sensors (Mao et al., 2013), nanocomposites (Lasenko et al., 2022), tissue scaffolds (W. He et al., 2007), wound treatment (Vargas et al., 2010), drug delivery systems (Kenawy et al., 2002; W. Song et al., 2021; Y. Zhang et al., 2023), filtration, protective gear (Faccini et al., 2012), and smart textiles (J.-V. Sanchaniya et al., 2022). Figure 1.2 illustrates the straightforward electrospinning setup equipped with a syringe pump and a rotating drum collector.

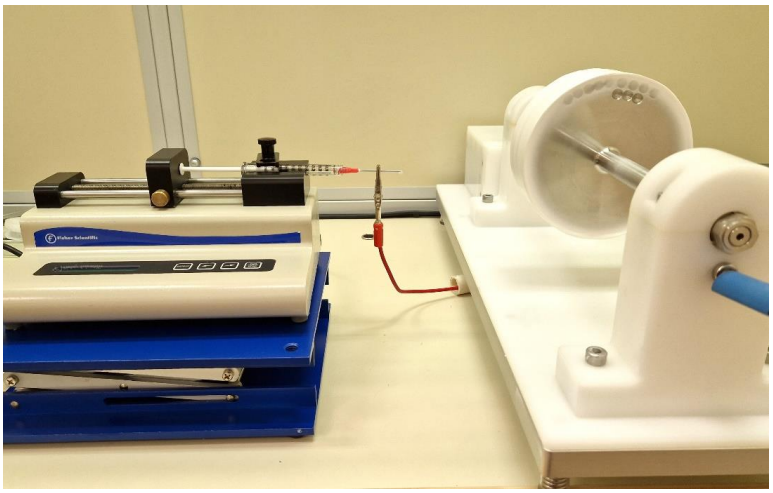

Figure 1.2 Simple electrospinning setup featuring a syringe pump and rotating drum collector.

Nanofibrous mat structures are composed of fibers characterized by an apparent endlessness, as their length far surpasses their diameter by orders of magnitude. This unique attribute arises from the electrospinning process, wherein a thin jet emanates from the tip of the Taylor cone, traverses a spatial distance, undergoes elongation, and eventually adheres to the collector, all while experiencing various instabilities. The longevity of these fibers becomes evident through microscopic analysis, such as scanning electron microscopy (SEM), where micrographs consistently reveal the absence of discernible fibre endings. This substantiates the remarkable length-to-diameter ratio of nanofibers, a defining feature imparted during their intricate formation process.

Polyacrylonitrile (PAN), a semicrystalline synthetic polymer, serves as a crucial material for electrospinning. Intrinsically hydrophobic and insoluble in many solvents, except for specific polar aprotic solvents and mineral salts (Musale & Kumar, 2000; Scharnagl & Buschatz, 2001), PAN's unique thermoplastic nature is characterized by a propensity to degrade before melting at heating rates below 80 °C/min. This degradation initiates at 250 °C, with a degradation temperature of 317 °C. Electrospun PAN nanofibers play a pivotal role in various applications, acting as the precursor for continuous carbon nanofibers, finding utility in filtration, and contributing to catalysis applications.

The versatility of PAN nanofibers extends to filtering applications, such as air and water filtration, biofluid purification, and the extraction of hazardous contaminants from polluted water sources (Duan et al., 2019; Zhou et al., 2022). Their expansive surface area and

electrostatic capabilities render them effective in capturing airborne particles and pollutants during air and water filtration, respectively. The biocompatibility and ecological safety of PAN nanofibers further enhance their suitability for medical and biological applications, serving as essential components in dialysis machines, wound dressings, and tissue engineering scaffolds (Radu et al., 2023).

Despite these advantages, the random orientation of electrospun fibre mats and the varied fibre diameters pose challenges in achieving optimal mechanical characteristics, limiting their practical applications. Rotating drum collectors emerge as a solution, facilitating the production of oriented nanofibers that enhance overall strength. The mechanical properties of these oriented nanofibers, crucial for industrial use, need comprehensive evaluation, especially in the longitudinal and transverse directions.

Understanding the strength of electrospun nanofibers involves considering factors such as polymer type, crystallization rate, and crystallinity level. The strength and deformation mechanisms of nonwoven materials, integral to electrospun nanofiber mats, are contingent upon the fibers and their bonds. However, the inherent challenges of random fibre alignment, lack of adhesion between fibers, and excessive porosity often necessitate improvements in the mechanical characteristics of electrospun nanofiber mats, unlocking their full potential for a wider range of applications.

1.1. Main Goal and Tasks of the Thesis

The primary goal of this thesis is to advance the understanding and application of PAN nanofiber mats by fabricating them and comprehensively evaluating their thermal, mechanical properties, and morphology. This research aims to not only enhance these properties through a conventional method, such as annealing, but also to explore unconventional methods, ensuring competitiveness in diverse applications.

To accomplish the defined objective, the following tasks are outlined:

1. Conducted a literature review on electrospinning methods, mechanical testing, and microstructure modeling of PAN nanofiber mats.
2. Fabricated PAN nanofibers using various collectors, achieving both random and aligned structures in the nanofiber mats.
3. Performed tensile, thermal, and morphological tests on the randomly and oriented structured PAN nanofiber mats.

4. Developed a finite element (FE) model to predict the mechanical properties of the electrospun PAN nanofiber mats.
5. Investigated the impact of various structural parameters on the overall strength of the nanofiber mats.
6. Applied conventional annealing methods to the PAN nanofiber mats to examine changes in mechanical, thermal, and morphological properties.
7. Prepared PAN nanofiber composite mats using a non-conventional dip-coating method with low-concentration PVA solutions (0.5%, 1%, and 2%).
8. Assessed the morphological, tensile, and thermal properties of the PAN nanofiber composite mats.
9. Developed an FE model to predict the mechanical behaviour of the composite PAN nanofiber mats.
10. Created non-crimping laminated textile composites by electrospinning PAN nanofibers onto textiles, then analysed and compared their mechanical and morphological properties with an analytical model.

By performing the above listed tasks the doctoral thesis entailed a systematic and detailed exploration of PAN nanofiber mats, incorporating a mix of traditional and innovative methodologies to push the boundaries of material science. The extensive experiments and modeling conducted provided deep insights into the behaviour and properties of these materials. The outcomes of this research have not only contributed to a robust academic understanding but are also expected to pave the way for future innovations in nanofiber applications across various industries. This comprehensive work underscores the potential of PAN nanofibers in enhancing material performance and introduces new possibilities for their practical deployment.

1.2. Research Gap and Unexplored Aspects of PAN Nanofiber Mats

The existing body of research in the field of fabricating and evaluating nanofibers has largely overlooked the specific area of aligned PAN nanofibers, especially for their potential use in filtration and biomedical applications. A significant gap exists in understanding how conventional processes like annealing impact these aligned PAN nanofibers. Furthermore, there is a notable lack of research in developing high-strength nanofiber mats while maintaining

their inherent porosity. These gaps indicate that the current understanding and utilization of PAN nanofibers in these applications are limited and require further exploration.

Unexplored aspects of the PAN nanofiber mats is that the majority of nanofiber applications utilize randomly collected fibers, which often results in low strength and high variability in their mechanical properties due to the random structure. The fabrication of highly aligned nanofibers and a thorough investigation of their mechanical and thermal properties have not been sufficiently explored. This lack of exploration extends to both conventional methods, such as annealing, and non-conventional methods, like creating spun bonds using PVA (Polyvinyl Alcohol) solution.

Moreover, the numerical modelling of nanofibers and their interactions remains an unexplored area. This gap in research highlights the need for a deeper understanding of the properties and potential applications of nanofibers. Addressing these unexplored aspects could lead to significant advancements in the use and effectiveness of PAN nanofiber mats in various fields.

1.3. Main Objective of the Each Chapter

In Chapter 1.3, the thesis delineates several pivotal tasks aligned with the overarching objectives. Most of the existing research on nanofibers has centred around those with random orientation, which often results in compromised mechanical properties such as lower strength and higher variability in tensile strength and elastic modulus. This research takes a different approach by focusing on the fabrication and potential of highly aligned PAN nanofibers. Aligned nanofibers offer a more uniform structure, which could lead to enhanced mechanical properties and make them more suitable for specific applications where strength and directionality of forces are crucial. After conducting the extensive literature review objective of each chapter are mentioned below.

The first objective involves (chapter 3) the fabrication of PAN nanofiber mats using varied collectors, including both rotating and stationary types. This step is critical for assessing the influence of collection methods on the nanofibers' characteristics. Following the fabrication, a rigorous analysis of the mechanical, thermal, and morphological properties of these mats is conducted, adhering to established industry standards.

The second objective addresses (chapter 5) the annealing of these fabricated nanofiber mats. Annealing, a conventional method for enhancing the strength of polymeric nanofibers, is applied at various temperatures. This process is carefully examined to understand its impact on

the nanofibers' mechanical, thermal, and morphological properties. Insights gathered from the literature guide this experimental phase, enabling a thorough comparison of the nanofiber mats before and after annealing.

The third objective (chapter 6) introduces a non-conventional enhancement method. This involves the use of low-viscosity PVA solution to penetrate and bind the PAN nanofiber mat. As the solution evaporates, it leaves behind PVA polymer, which solidifies and binds the nanofiber mat together. This technique aims to enhance the strength of the nanofiber mats while preserving their inherent porosity. A systematic evaluation of this method's impact on the mats' mechanical, thermal, and morphological properties is undertaken, benchmarked against industry standards.

The last objective (chapter 4 and 6) encompasses the development of a robust numerical model based on the experimental results obtained from the previous tasks. This model aims to predict the strength, mechanical behaviour, and thermal characteristics of the prepared nanofiber mats. It is validated against experimental data of PAN nanofibers, both in their standalone form and when bonded with PVA solution. The reliability and accuracy of this model are crucial for its applicability in predicting the behaviour of nanofiber mats under various conditions.

Finally, the fifth task introduces the development of laminated textiles reinforced with PAN nanofibers. This task involves the direct collection of electrospun nanofibers onto fabric, leading to the fabrication of non-crimping laminated textiles. The properties of these textiles, particularly focusing on their structural characteristics and mechanical properties, are then thoroughly investigated. This task marks a significant step towards exploring additional applications of nanofiber mats in advanced textile production.

Together, these tasks form the backbone of the thesis, each contributing to a comprehensive understanding of PAN nanofiber mats and their potential applications. The sequential approach from fabrication to modelling ensures a thorough exploration of the materials' properties and behaviours, laying the groundwork for future innovations in nanofiber technology.

1.4. Scientific Novelty of the Study

Chapter 1.4 of the thesis delves into the scientific novelty of the study, highlighting how this research contributes new insights and methodologies to the field of nanofiber technology, particularly focusing on PAN (Polyacrylonitrile) nanofiber mats.

1. Exploration of Aligned PAN Nanofibers: One of the primary novel aspects of this study is the comprehensive exploration of aligned PAN nanofibers. Unlike most existing research that predominantly focuses on randomly oriented nanofibers, this study ventures into understanding and leveraging the unique properties of alignment in PAN nanofibers. This alignment potentially enhances mechanical strength and uniformity, making these nanofibers particularly suitable for specialized applications such as filtration and biomedical devices.
2. Advanced Treatment Methods and Their Impacts: Another innovative aspect of this research is the detailed investigation of how various treatment methods, especially annealing, affect the properties of aligned PAN nanofibers. This study explores the thermal and mechanical implications of annealing on nanofibers, providing new insights into optimizing their properties for specific applications. The nuanced understanding of these treatment effects opens up possibilities for customizing nanofiber characteristics according to application requirements.
3. Novel Non-Conventional Enhancement Techniques: The thesis also introduces and evaluates non-conventional methods for enhancing nanofiber mats. Specifically, it investigates the use of low-viscosity PVA solutions as a binding agent, examining how this method can enhance the strength of PAN nanofiber mats while preserving their inherent porosity. This approach represents a significant advancement in the production of high-strength, porous nanofiber mats, a key challenge in the field.
4. Numerical Modelling: An additional novel contribution is the development of a robust numerical model to predict the mechanical and thermal behaviour of PAN nanofiber mats. This model, validated against experimental data, offers a powerful tool for predicting nanofiber behaviour under various conditions. It bridges the gap between theoretical analysis and practical application, enhancing the understanding of nanofiber mat behaviour in real-world scenarios.
5. Development of Laminated Textiles with Electrospun Nanofibers: Lastly, the thesis explores the fabrication of non-crimping laminated textiles using directly collected electrospun nanofibers onto fabric. This innovative approach to textile development leverages the unique properties of nanofibers to enhance the structural and mechanical properties of textiles. It represents a significant step forward in textile engineering, potentially leading to the creation of new types of advanced materials with wide-ranging applications.

The scientific novelty of this study lies in its holistic approach towards exploring new dimensions of PAN nanofiber mats. From investigating the effects of alignment and treatment methods to pioneering novel enhancement techniques and modelling approaches, this research significantly advances the understanding and application of nanofiber technology. It paves the way for future innovations and practical applications in various fields, marking a substantial contribution to the study of nanomaterials.

2. LITERATURE REVIEW

2.1. State of the Art & Recent Development in Nanofiber Mats

This chapter serves as an introduction to the world of nanofiber mats, discussing the state of the art and recent advancements in this field. It delves into various aspects including fabrication techniques, testing standards, and numerical models developed to predict the mechanical behaviour of nanofiber mats, setting the stage for a comprehensive understanding of their significance and applications.

Polyacrylonitrile (PAN) and its copolymers have been subjects of extensive research for nearly a century, primarily due to their potential for commercial and technological applications. PAN's ability to undergo crosslinking, which endows it with crucial properties like insolubility and resistance to swelling in organic solvents, has been a focal point of recent studies. These investigations have enhanced understanding of PAN processing and fibre-forming technologies. Among various precursors for carbon nanofibers (CNFs), PAN stands out as the most popular choice, attributed to its high carbon yield, structural flexibility in final CNF products, and the ease of obtaining stabilized products through ladder structure formation via nitrile polymerization (Nataraj et al., 2012; D. Papkov, Goponenko, et al., 2013).

The journey of PAN, from its initial recognition in 1893 as acrylonitrile (AN), has been marked by significant milestones. The transformation of PAN into a usable fibre, however, faced challenges due to difficulties in dissolving it for spinning, with notable progress made only around 1925. The development of the homopolymer of PAN into fibre-forming material took a leap in the 1940s after DuPont discovered a suitable solvent. PAN's solubility in various polar solvents, including DMF (Dimethylformamide), DMSO (Dimethyl Sulfoxide), DMAc (Dimethylacetamide), and solutions of ethylene carbonate, highlights its versatility. PAN's high solubility in DMF at elevated temperatures demonstrates its superiority over other solvents (Nataraj et al., 2012).

Nanofibers, including those made of PAN, find applications across a diverse range of industries. They are integral in energy storage (such as batteries), catalysis, wound dressing, scaffolds for tissue engineering, filtration, protective clothing, and sensors. These applications, each leveraging the unique properties of nanofibers, are illustrated in Figure 1.1.

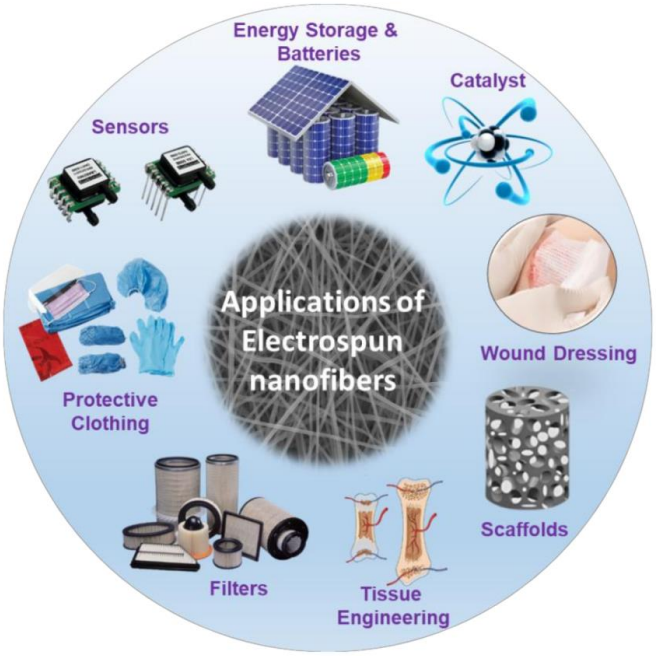

Figure 2.1 Applications of nanofibers (Nathanael & Oh, 2021)

The current state and recent advancements in nanofiber mats, specifically highlighting the diverse applications of these materials across various industries. The chapter aims to provide a comprehensive understanding of how nanofibers, particularly nanofibers and its derivatives, have evolved and found utility in numerous fields.

Energy Storage & Batteries:

In the realm of energy applications, significant progress has been made in utilizing electrospun nanofibers (NFs). These NFs have shown promising results in lithium-based batteries (LIBs, LSBs, and Li-O_2 batteries), fuel cells, dye-sensitized solar cells, and supercapacitors. The high surface area and porosity of electrospun NFs contribute to enhanced power capabilities and kinetic properties in lithium-based batteries by shortening Li+ diffusion pathways. In fuel cells, these NFs have been employed as electrode materials and electrolyte membranes, demonstrating high activities and durability as electrocatalysts and exhibiting high electrolyte uptakes and ionic conductivities as membranes. Furthermore, for dye-sensitized solar cells, electrospun NF photoelectrodes have shown high photoelectric conversion efficiencies. Similarly, supercapacitors utilizing NFs exhibit impressive specific capacities and

electrochemical performances, owing to the NFs' thermal stability and electrical conductivity (G. Sun et al., 2016).

Wound Dressing:

Electrospun nanofibers have shown great promise as wound dressings, owing to their similarity in morphology to skin's extracellular matrix (ECM). Their high surface area and porous structure enhance crucial functions like homeostasis, exudate absorption, and cellular processes, making them highly efficient wound dressing materials. However, the journey from research to commercialization faces challenges, including low production rates and lack of standardized procedures. The future of electrospun nanofiber wound dressings lies in multifunctional development, addressing various wound types and healing stages. The potential for commercialization is high, but the path involves overcoming production and reproducibility hurdles (K. Chen et al., 2022).

Scaffolds:

For drug delivery applications, electrospinning offers the flexibility to use either biodegradable or nondegradable materials. This control allows for precise management of drug release, either through diffusion or a combination of diffusion and scaffold degradation. The orientation and arrangement of electrospun fibers can be tailored to influence both mechanical properties and biological responses. Various drugs, including antibiotics, anticancer agents, proteins, DNA, and RNA, have been incorporated into electrospun scaffolds using different drug loading methods. Controlled drug delivery systems, especially fibrous carriers, offer site-specific drug delivery and the ability to encapsulate multiple drugs, enhancing therapeutic efficacy and reducing toxicity (Kanani & Bahrami, 2010).

Tissue Engineering:

In tissue engineering (TE), electrospun nanofibrous mats have emerged as a promising scaffold fabrication technique. These mats, characterized by increased porosity and large surface areas, provide an environment conducive to cell adhesion, proliferation, and differentiation. Electrospinning is celebrated for its cost-effectiveness, versatility, and ability to create ECM-like structures. Despite its advantages, limitations such as poor cell infiltration and low mechanical strength of conventional electrospun scaffolds are being addressed through innovative solutions. The future of TE lies in developing multifunctional scaffolds capable of physically promoting cell development and supporting tissue regeneration (Zulkifli et al., 2023).

Filters:

Nanofiber mats have made significant strides in filtration applications, particularly in air, water, and blood filtration. The introduction of electrostatic charging technologies has led to more open-structured filter media with lower pressure drops and high efficiency. The integration of antimicrobial agents like silver imparts additional antimicrobial properties to these filters (Sundarrajan et al., 2014).

Protective Clothing:

Electrospun fibres (super fibres and ultrafine) have potential applications in protective clothing (PC) for diverse environments, including industrial, laboratory, home, and military settings (D. Papkov et al., 2019; D. Papkov, Zou, et al., 2013). Despite extensive academic research and unique property claims, the transition of ENMs into commercial PC products faces challenges, primarily related to mass production and mechanical properties. Future development in the PC industry requires a coherent technical strategy, a multidisciplinary approach, and a focus on market applications (Gorji et al., 2017).

Sensors:

Electrospun sensors stand out for their exceptional properties such as fibre continuity, surface functionality, mechanical performance, and large surface-to-volume ratio. These characteristics endow electrospun sensors with high sensitivity, good recovery, and robust sensory response. Electrospun fibers have found applications in various types of sensors, including gas, biological, electrochemical, optical, and thermal sensors. Their high surface area and free energy facilitate the immobilization of biomolecules, leading to increased adsorption and activity (Aliheidari et al., 2019).

The production of high-strength PAN nanofiber mats and an in-depth understanding of their mechanical behaviour are crucial for several interconnected reasons. In industries like aerospace, military, and sports equipment manufacturing, the strength-to-weight ratio of PAN nanofibers is highly valued, making them ideal precursors for carbon fibers where both durability and lightness are crucial. Additionally, understanding their mechanical behaviour enables the design of materials that can withstand extreme conditions, which is critical in sectors like aviation and construction where material failure could have dire consequences.

Advancements in material science are driven by studies on PAN nanofiber mats, leading to the innovation of new composites and hybrid materials with tailored properties. This not only enhances our understanding of material science but also opens doors to novel applications in various sectors.

Furthermore, the safety and reliability of products made from high-strength PAN nanofiber mats depend on a comprehensive understanding of their mechanical behaviour. This

knowledge is particularly crucial in sectors like automotive and civil engineering, where material failure poses significant safety hazards.

Customization is a key aspect of material development, as different applications demand materials with specific properties. By understanding the mechanical properties of PAN nanofiber mats, they can be tailored to meet the unique requirements of various industries, leading to more efficient and effective products.

Finally, the economic and environmental benefits of stronger, more durable materials are significant. They can reduce the frequency of replacements, leading to long-term cost savings and sustainability by reducing waste and the need for new resources.

2.2. Nanofiber Fabrication Technique - Electrospinning

Nanofibers have emerged as a pivotal element in a wide range of industries, including packaging, purification, textiles, pharmaceuticals, and biomedicine, owing to their exceptional engineering properties. These fibers, often referred to as nanofibers, are fabricated from various polymers tailored to their specific applications. Their biodegradability, biocompatibility, and ability to form highly porous structures with outstanding properties make them invaluable in diverse areas such as drug delivery, medical implants, wound care, filtration, and water treatment. This chapter aims to present an in-depth overview of the techniques used in nanofiber synthesis.

Electrospinning stands out as a preferred method for nanofiber production, renowned for its effectiveness, versatility, affordability, and simplicity. Nanofibers created through electrospinning are distinguished by their large surface area, fine diameter (ranging from nano to microscale), and excellent porosity. A typical electrospinning setup consists of essential components like a high-voltage power supply, a syringe pump, a spinneret or blunt-tip needle, and a collector.

The process involves using a polymer and a suitable solvent to create a polymer solution, which may include additives like drugs, peptides, or nanoparticles. The application of high voltage aids in ejecting the polymer solution as jet strands from the spinneret towards a grounded collector. The electric field influences the interfacial tension of the polymer droplet, forming a “Taylor cone” from which the fibre jet emerges. As the jet travels through the air, solvent evaporation occurs, resulting in the deposition of solid polymer fibers on the collector and the formation of a nonwoven web. Key parameters in this process include polymer type,

concentration, conductivity, viscosity, flow rate, and the distance between the nozzle and collector.

Despite its widespread use, electrospinning has limitations, such as the requirement for high voltage (posing safety concerns), lower production yield, and the high cost of scaling up. The process involves three types of instabilities: axisymmetric Rayleigh instability, which fragments the polymer jet; an instability that arises under strong electric fields; and whipping instability caused by electrostatic repulsion, which leads to the bending and stretching of the jet, crucial for producing thinner nanofibers (Anusiya & Jaiganesh, 2022).

Over the past two decades, several electrospinning techniques have been developed, including solution electrospinning, melt electrospinning, multiple jet electrospinning, coaxial electrospinning, and magnetic field-assisted electrospinning. Coaxial electrospinning, for instance, is used to create core-shell nanofibers, where bioactive molecules are encapsulated within the core and released upon degradation of the outer polymer coating. This technique finds applications in skin regeneration, bone regeneration, and desalination.

Solution electrospinning has been instrumental in introducing conductive properties into scaffolds, enhancing biomineralization for bone regeneration. Melt electrospinning, meanwhile, is used to produce 3D scaffolds suitable for cell adhesion and proliferation, showing promise for dental and maxillofacial surgery.

Electrospinning is particularly effective and cost-efficient for lab-scale production of nanofiber mats. Given its versatility and effectiveness, electrospinning is the sole method employed in this thesis for fabricating nanofibers, providing a foundation for further research and development in the field of nanotechnology.

2.2.1. Principle of Electrospinning

Electrospinning is a sophisticated electrohydrodynamic technique used to create fibers from a liquid polymer solution or melt. This process, characterized by its simplicity and accessibility, is widely implemented in various laboratories. The fundamental components of an electrospinning setup include a high-voltage power supply, a syringe pump, a spinneret (often a blunted hypodermic needle), and a conductive collector as shown in Fig 1.2A. The power supply utilized in this process can be either direct current (DC) or alternating current (AC) (D. Li & Xia, 2004; Xue, Xie, et al., 2019).

The electrospinning process begins with the extrusion of the liquid polymer from the spinneret, forming a pendant droplet due to surface tension, altering the electrospinning process parameters, it is possible to control the morphology of nanofibers (Araujo et al., 2019; Di.

Papkov et al., 2019). When this droplet is subjected to an electrical charge, the electrostatic forces cause the droplet to deform into a Taylor cone. From this cone, a charged jet is emitted. Initially, this jet extends in a straight trajectory. However, as it moves away from the spinneret, it undergoes complex whipping motions, a result of bending instabilities. This dynamic motion stretches the jet, significantly reducing its diameter.

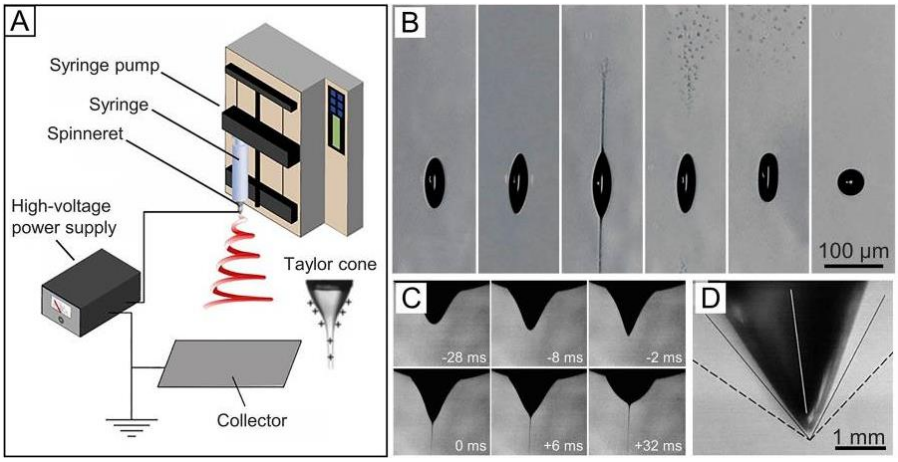

Figure 2.2 (A) Fundamental arrangement for electrospinning. (B) Rapid-capture images depicting the fragmentation of an ethylene glycol droplet at levitation, charged to the Rayleigh threshold, resulting in the release of dual jets. (C) Sequential images illustrating the transformation of a suspended PEO droplet in water from a spherical form to a conical structure, culminating in jet propulsion. (D) Image capturing the droplet at its pivotal moment (Xue, Wu, et al., 2019a).

As the jet travels towards the collector, it rapidly solidifies, resulting in the formation of ultrafine solid fibers that are deposited on the grounded collector (D. Li & Xia, 2004; Liao et al., 2018; B. Sun et al., 2014). This entire process can be categorized into four distinct stages:

Charging of the Liquid Droplet and Taylor Cone Formation: In this initial phase, the liquid droplet at the spinneret tip becomes charged due to the applied voltage. The electrostatic repulsion within the surface charges of the droplet leads to its elongation and eventual transformation into a characteristic cone shape known as the Taylor cone.

Jet Extension in a Straight Line: Following its formation, the charged jet extends linearly from the apex of the Taylor cone. During this stage, the jet remains relatively straight and stable as it begins its journey towards the collector.

Thinning of the Jet and Development of Instabilities: The electric field and the surrounding environment influence the thinning of the jet. This phase is critical as it involves the growth of electrical bending instabilities, often referred to as whipping instabilities. These

instabilities cause the jet to undergo complex motions, effectively stretching and thinning it to form finer fibers.

Solidification and Collection of the Fiber(s): The final phase involves the solidification of the jet as it reaches the collector. The rapid evaporation of the solvent (in the case of a solution) or cooling (in the case of a melt) leads to the formation of solid fibers, which are then collected on the grounded collector.

Each of these stages plays a crucial role in determining the final properties of the electrospun fibers, such as diameter, morphology, and internal structure. Understanding and controlling these stages are key to optimizing the electrospinning process for specific applications. The subsequent subchapters provide a more in-depth examination of these stages, offering insights into the complexities and nuances of the electrospinning process.

2.2.2. Taylor Cone upon Charging a Liquid Droplet

Electrospinning, an intricate electrohydrodynamic process, plays a pivotal role in transforming electrically charged liquid droplets into nanofibers. This fascinating mechanism can be exemplified by observing the behaviour of ethylene glycol droplets subjected to an electric field, as captured in Figure 1.2B (Duft et al., 2003). Initially, upon introduction into a levitator, these droplets assume a spherical form with a radius of about 58μm, bearing a charge of approximately 3.3 p_c. Due to the evaporation of neutral molecules, the droplets gradually diminish in size, reaching a critical Rayleigh stability radius of around 24μm in a mere 140 microseconds. At this juncture, they undergo a remarkable transformation from a spherical to an ellipsoidal shape, developing sharp tips at their poles. Almost instantaneously, two fine liquid jets emerge from these tips, propelled in opposite directions. The jets eventually disintegrate into smaller droplets, driven away from the parent droplet by the force of electrostatic repulsion. Following the jet ejection, the droplets retract to their original spherical shape within approximately 210 microseconds. This process vividly demonstrates the disintegration of a droplet charged to the brink of Rayleigh instability and the subsequent generation of Rayleigh jets. In scenarios where ethylene glycol is substituted with a sol–gel precursor solution, these Rayleigh jets can be stabilized for further characterization using advanced electron microscopy techniques (D. Li et al., 2007).

The electrospinning process begins with a controlled and consistent liquid feed through a spinneret, facilitated by a syringe pump. A crucial aspect of electrospinning is the creation of a potential difference between the spinneret and the collector. This results in the separation of positive and negative charges within the liquid, leading to the migration of charges similar to

the spinneret's polarity towards the droplet's surface, thereby accumulating excess charges. As the voltage increases, the surface charge density on the droplet also increases. This process involves a delicate balance between surface tension, which naturally favours a spherical shape to minimize the droplet's total surface free energy, and electrostatic repulsion, which endeavours to deform the droplet, thereby increasing its surface area to alleviate the repulsion (Reneker & Hao, 2006).

To comprehend the dynamics at play, it is helpful to consider the liquid in the droplet as an ideal conductor. In such a scenario, the electrostatic pressure (p_e) exerted on the droplet's surface by the external electric field can be quantified using the formula $p_e = \epsilon E^2/2$, where ϵ represents the dielectric constant of the medium surrounding the droplet, and E signifies the intensity of the electric field. Concurrently, the droplet experiences capillary pressure (p_c) due to surface tension, which can be articulated by the Young–Laplace equation: $p_c = 2\gamma/r$. In this equation, γ denotes the surface tension, and r refers to the mean radius of curvature of the droplet's surface. This radius can be approximated by the inner radius of the spinneret (Finn, 1999). When the electric field reaches a critical intensity at a certain critical voltage (V_c), p_e surpasses p_c. This indicates that the electrostatic repulsion has become strong enough to overcome the surface tension, compelling the droplet to morph into a conical shape.

The critical voltage required for this transformation can be calculated using the following equation (Taylor & Dyke, 1969):

$$V_c^2 = \frac{4H^2}{h^2}\left(ln\left(\frac{2h}{R}\right) - 1.5\right)(1.3\pi R\gamma)(0.09) \quad \ldots (1.1)$$

In this equation, H symbolizes the distance between the spinneret's tip and the collector, *h* is the length of the spinneret, and R is the outer radius of the spinneret. The units for H, *h*, and R are all in centimetres, while the surface tension (γ) is measured in dyn/cm, and the voltage is in kilovolts. The factor 1.3 is derived from. 2cos49.3°, considering that the cone typically has a semi-vertical angle close to 49.3°. The specific voltage needed to generate a conical shape in the droplet during electrospinning depends on the liquid's properties. For more viscous liquids, a higher critical voltage is required to generate an electrostatic repulsion force that can overpower both the surface tension and the viscoelastic force of the liquid (Reneker & Yarin, 2008; Yarin et al., 2001b). The transformation from a spherical to a conical shape before jet ejection, as exhibited in Figure 1.2C, is a clear demonstration of this phenomenon, where a droplet of poly (ethylene oxide) (PEO) in water is shown. Figure 1.2D captures this critical moment of droplet transformation, illustrating the precise point at which the droplet adopts a

conical shape. This conical shape is sustained throughout the electrospinning process, provided there is a steady supply of liquid to compensate for the volume ejected during the formation of fibers.

2.2.3. Stretching the Charged Jet

The intricate process of electrospinning involves stretching a charged jet from the apex of the Taylor cone, propelled and elongated by an electric field towards the collector. This jet extension is a critical aspect of electrospinning, shaping the final characteristics of the produced nanofibers. Various models, grounded in experimental evidence and electrohydrodynamic theories, offer insights into the jet's behaviour (R. T. Collins et al., 2008).

One approach conceptualizes the jet as a sequence of viscoelastic dumbbells connected in a string, with its 3D trajectory determined by linear Maxwell equations (Han et al., 2008). This model aligns well with experimental findings, providing a robust framework for understanding jet dynamics. Another perspective treats the jet as a long, slender entity, focusing on whipping movements rather than splaying to explain the electrospinning phenomenon. This model has been expanded to predict the whipping amplitude saturation and the resultant fibre diameter. A third approach incorporates nonlinear rheology to describe the jet's movement within an electric field, enhancing our comprehension of the electrospinning mechanics and aiding experimentalists in optimizing setup and parameters for desired fibre characteristics (J. J. Feng, 2002; Fridrikh et al., 2003; J. H. He et al., 2005; Hohman et al., 2001).

As depicted in Figure 3A (Reneker & Hao, 2006), the jet initially proceeds in a near-straight trajectory from the spinneret tip, known as the near-field region. In this phase, the fluid's viscoelastic properties suppress Rayleigh instability, which would otherwise cause the jet to disintegrate into droplets.

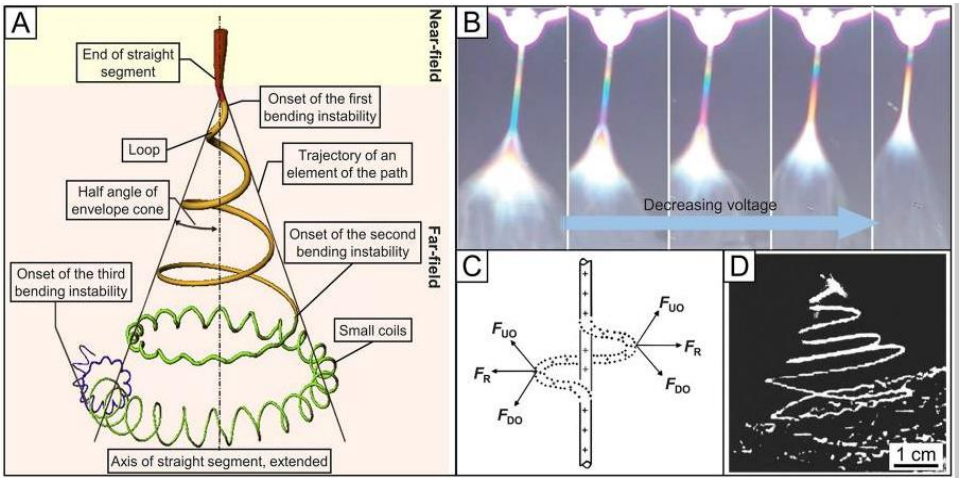

Figure 2.3 highlights various aspects of the electrospun jet's path:(A) Illustrates the jet's trajectory. (B) Shows the interference colours in a jet's straight segment, indicating the jet diameter and segment length variations with voltage changes. (C) Outlines the forces acting on a charged jet, where the net lateral electrostatic force (FR) bends the jet. FR grows exponentially as the radial displacement of the segment increases, leading to bending instabilities. (D) Provides a stereographic image of the bending jet at different stages of these instabilities (Xue, Wu, et al., 2019b).

The jet's surface charges move along, creating a current through it. The jet's velocity, length, and diameter in the straight segment are measurable (Helgeson et al., 2008; Reneker et al., 2002). The velocity at the end of this segment ranges from 1 to 15 m/s. The critical length (L) of the straight segment can be estimated using the following equation 1.2 (Gañán-Calvo, 1997; J. H. He et al., 2005):

$$L = \frac{4kQ^3}{\pi\rho^2 I^2}\left(\frac{1}{R_0^2} - \frac{1}{r_0^2}\right) \quad \ldots (1.2)$$

Where $R_0 = \left(\frac{2\sigma Q}{\pi k \rho E}\right)^{1/3}$, with σ as surface charge, Q as flow rate, κ as electrical conductivity, ρ as fluid density, E as electric field strength, I as the current through the jet, and r as the initial jet radius. Under certain conditions, such as a slow flow rate, the straight segment can be notably short. Figure 3B demonstrates the interference colors in a straight jet segment of aqueous PEO, with the observed color correlating to the jet's diameter (Y. Wang et al., 2018). The straight segment length and the voltage reduction have a direct relationship. In another study with a poly(ε-caprolactone) (PCL) solution, the straight segment was around 3 mm, with a 5-10μm diameter at the midpoint and a downward velocity near 1 m/s (Reneker et al., 2002).

2.2.4. Thinning the Jet

The electrospinning process involves the acceleration of a charged jet, which is integral to the thinning and eventual formation of nanofibers. As the jet extends as a straight line, surface tension and viscoelastic forces within it resist forward movement, gradually attenuating its acceleration. Concurrently, the jet's diameter reduces monotonically along its length due to continuous stretching. When acceleration stabilizes, any minor perturbation can disrupt the jet's straight trajectory, leading to instability predominantly caused by electrostatic repulsion among surface charges (J. H. He et al., 2005).

In the far-field region of the electrospinning process, the charged jet is susceptible to three distinct types of instabilities (Hohman et al., 2001; Yarin et al., 2001a):

Axisymmetric or Rayleigh Instability: Dominated by surface tension, it can lead to the jet's breakup into droplets. This instability is suppressed in strong electric fields.

Higher-Field Axisymmetric Instability: Occurs under stronger electric fields than Rayleigh instability.

Whipping or Bending Instability (Non-Axisymmetric): Caused by aerodynamic instability and a radial electrostatic force (FR), resulting from electrostatic repulsion among surface charges. This instability leads to long wave perturbations in the jet.

These instabilities, depicted in Figure 2.3C, are influenced by the jet's charge interactions and the external electric field. Their development and rate are further controlled by the liquid's physicochemical properties and the electrospinning parameters.

To create ultrafine nanofibers, the rapid growth of whipping instability is crucial. This instability, by producing lateral force (FR) perpendicular to the jet axis, causes the jet to bend sharply by about 90°, forming a series of loops and spirals (envelope cone) in the jet's trajectory, as shown in Figure 2.3A. These loops are where most elongation occurs, leading to a substantial reduction in the jet's diameter. The velocity components of these loops contribute to their downward movement, typically at a slower pace than the transverse velocity.

The whipping process effectively elongates the jet's length by up to 10,000 times in less than 0.05 seconds, with an incredibly high drawing rate (up to 1,000,000 s^{-1}). This dramatic stretching reduces the jet's diameter significantly, creating fibers with sub-micrometre and nanometer-scale diameters (F. Liu et al., 2009).

Figure 3D, captured using high-speed photography, illustrates the distinct stages of bending instabilities in a solution of poly(ethylene oxide) in water and alcohol. The image

clearly shows the envelope cone formed during the first bending instability and the onset of the second bending instability on the loop with the largest diameter.

The terminal diameter (dt) of the jet can be calculated using the equation:

$$d_t = (\gamma\varepsilon\frac{Q^2}{I^2}\frac{2}{\pi(2ln\aleph - 3)})^{1/3} \quad \ldots (1.3)$$

where γ is the surface tension, ε the dielectric constant, Q the flow rate, I the electric current, and χ the dimensionless wavelength of the bending instability.

Other instabilities, such as branching and capillary instability, are also observed in electrospinning. Branching occurs at high surface charge densities, leading to secondary jets from the primary one. Capillary instability, influenced by lower charge densities on the jet, disrupts the jet into droplets, resulting in beaded fibers. These phenomena contribute to the diversity of fibre structures achievable through electrospinning.

2.2.5. Solidification of the Jet

In the electrospinning process, the solidification of the jet into fibers is a critical phase. This transformation occurs either through solvent evaporation or the cooling of the melt, depending on the nature of the material being electrospun. The duration and efficiency of the solidification process significantly influence the characteristics of the resulting fibers.

If the solidification process unfolds slowly, it allows the charged jet to undergo prolonged elongation. This extended period of stretching contributes to the production of fibers with notably thinner diameters. A remarkable aspect of this elongation and solidification process is the significant reduction in the cross-sectional radius of the fibers compared to the initial jet. For instance, in one study, it was observed that the cross-sectional radius of a fully dried fibre was reduced to just 1.3×10^{-3} times that of the initial jet. This drastic reduction is primarily attributed to the combined effects of stretching and solvent evaporation during the electrospinning process (Yarin et al., 2005).

Post solidification, the fibers retain some of the charges on their surface, although the various instabilities that characterized the earlier stages of the jet's journey cease to occur. The persistence of these charges on the fibre surfaces can impact the behaviour of the fibers during their collection and subsequent handling.

The completion of solidification marks the end of the dynamic changes in the fibre structure. At this stage, the fibers have attained their final form, with their dimensions and properties now set. This phase is pivotal in defining the quality and applicability of the

electrospun fibers, as it determines their final diameter, strength, and overall structure, all of which are crucial for their intended use in various applications. Understanding and controlling the solidification process is, therefore, essential for tailoring the properties of electrospun fibers to meet specific requirements in diverse fields.

2.2.6. Deposition of the fibers

The deposition of fibers onto a grounded collector marks the culmination of the electrospinning process, significantly influencing the final fibre morphologies. The shape and structure of the deposited fibers are largely dependent on the stage of bending instability they undergo prior to deposition. Typically, fibers formed during the first bending instability's loop region are easily gathered as a nonwoven mat on either stationary or moving collectors.

Fibers generated during the second and third bending instabilities, often characterized by smaller, more intricate coils, can be deposited in a range of patterns. These include fibers with straight or wavy morphologies and even complex coils encompassing numerous turns. The diversity in the deposition patterns contributes to the versatility of electrospun fibers in various applications.

Once deposited, the fibers rapidly lose most of their charges to the grounded collector, owing to their direct contact. However, due to the generally low conductivity of the materials used in fibre production, a notable amount of residual charge often remains on the fibre surfaces. This retention of surface charges can influence the behaviour of subsequently arriving charged jets (Catalani et al., 2007; G. Collins et al., 2012).

The persistence of these residual charges on the collected fibers tends to repel incoming jets bearing similar charges, leading to a pendulum-like movement of the electrified jet (Han et al., 2008). Consequently, the thickness of a nonwoven mat composed of electrospun fibers is generally confined to an upper limit, typically ranging between 0.5 to 1 mm (Han et al., 2008). This limitation is rooted in the electrostatic interactions between the charged jet and the already deposited fibers, which inherently restrict the mat's build-up beyond a certain thickness.

This phenomenon underlines the intricacy of the electrospinning process, where not only the formation and stretching of the fibers are critical but also how these fibers interact with each other upon deposition. Understanding these interactions is vital for optimizing the electrospinning process for specific applications, particularly when precise control over mat thickness and fibre morphology is required.

2.2.7. Control of an Electrospinning Process

In electrospinning, the creation and diameter control of the fibers largely hinge on the precision with which processing parameters are managed. These parameters encompass the voltage applied, the flow rate of the solution, and the distance between the spinneret and the collector.

A static DC high voltage is commonly applied to the spinneret, creating an electric field that influences the behaviour of the liquid and consequently the formation of fibers. The voltage's polarity, either positive or negative, affects the distribution and type of charges that accumulate on the liquid's surface, thus impacting the nature of the jet. The chosen polarity is especially crucial for materials like electrolytes, where electrospinning efficiency is polarity dependent. The applied voltage is a critical factor in determining the amount of charge carried by the jet, the degree of electrostatic repulsion among these charges, and the jet's interaction with the external electric field (Terada et al., 2012; TONG & WANG, 2012). Higher voltages typically lead to the formation of thinner fibers, but they can also cause the ejection of more fluid, resulting in thicker fibers (Demir et al., 2002).

Using AC voltage in electrospinning produces different outcomes. With AC, the jet acquires alternating positive and negative charge segments, reducing electrostatic repulsion and thereby suppressing bending instability. The AC frequency is key: too high a frequency impedes effective charge transfer, while too low a frequency results in a predominantly single-charged jet (Balogh et al., 2016; Kessick et al., 2004; Stanishevsky et al., 2016). An optimal frequency facilitates the formation of a whipping cloud and the emergence of a visible thread downstream, as shown in Figure 1.4A,B (Maheshwari & Chang, 2009). This thread exhibits reduced attraction to the grounded collector, making deflection easier (Sarkar et al., 2007). AC electrospinning also leads to reduced net charges on the fibers, enabling extended collection on non-conductive substrates.

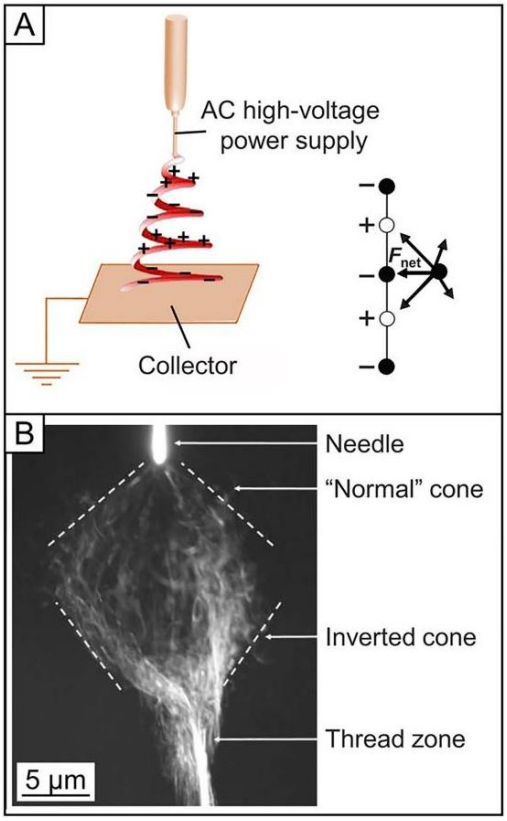

Figure 2.4 (A) Schematic representation of AC electrospinning, detailing the forces impacting a shifted segment of a charged jet. (B) Image capturing the jet in the process of AC electrospinning, taken with a 0.02-second exposure. Visible is the whipping envelope, appearing as a fusion of a standard cone and a reverse cone, with a clear thread zone observable beneath the peak of the reverse cone (Xue, Wu, et al., 2019b).

The flow rate of the spinning solution is another crucial parameter. Increasing the flow rate generally results in fibers with larger diameters. The distance between the spinneret and the collector is pivotal in determining the instability stage at which the jet solidifies and is deposited. Adequate distance ensures complete extension and solidification of the jet into solid fibers, with increased distance typically yielding thinner fibers. However, beyond a certain range, increasing the distance further does not reduce the fibre diameter due to early jet solidification.

In sum, the morphology and diameter of electrospun fibers are the outcomes of a complex interplay of processing parameters. For instance, an increase in flow rate necessitates adjustments in critical voltage and working distance to ensure proper jet extension and

solidification. Therefore, optimizing all processing parameters is essential for effective control over the electrospinning process, ensuring the desired fibre morphology and diameter.

2.3. Mechanical Testing Standards

Nonwoven fabrics are unique in their structure compared to traditional woven textiles. They lack a specific fibre arrangement, such as the warp and weft pattern found in woven fabrics, yet they retain many characteristics of conventional textiles. Nonwovens are composed of staple or continuous filaments, bonded through frictional entanglements or adhesive forces, sometimes enhanced by chemical, thermal, or mechanical treatments. The fibers used in nonwovens can be either natural or synthetic, typically within the micrometre range.

Defining nonwovens is complex due to their diverse nature. Different organizations have proposed various definitions to encapsulate their multifaceted characteristics. For instance, BS EN ISO 9092:2019 defines a nonwoven as an "engineered fibrous assembly" that gains structural integrity through physical and/or chemical means, explicitly excluding traditional methods like weaving or knitting. This standard emphasizes the significance of measurable tensile strength in nonwovens, underscoring their mechanical robustness.

Nonwovens are increasingly utilized in high-value applications, including medical devices, filters, technical clothing, and acoustic insulation. A critical factor in their functionality is fibre diameter, affecting properties like porosity, which influences filtration capacity. Interestingly, moving from microscale to nanoscale fibers significantly enhances mechanical properties. Nanofiber nonwovens have garnered attention for their high surface-to-volume ratio and exceptional characteristics, finding use in fields like tissue engineering and catalysis. Evaluating their mechanical properties is vital for assessing their applicability, with tensile testing being a common method. However, their highly porous and flexible nature poses challenges in obtaining reliable data for material design.

Handling nanofibrous mats for tensile testing is delicate, requiring specific attention to avoid damage, pre-tensioning, or slippage during testing. The use of a paper frame, which is cut before testing, aids in specimen handling and gauge length measurement. However, accurately measuring the cross-sectional area, particularly thickness, remains a challenge due to the high porosity of these materials. This measurement difficulty impacts the stress calculation (σ), making comparison of mechanical performances challenging, especially across different laboratories.

Existing standards, such as ISO 9073 and BS EN 29073, lack specificity for nanofibrous nonwovens, limiting their applicability. For example, BS EN 29073-3:1992, which focuses on tensile strength and elongation, suggests specimen dimensions that are impractical for nanofibrous mats. Furthermore, these standards often express breaking strength in newtons, reflecting breaking load rather than actual strength (σ at break).

The absence of a technical standard for tensile testing of nanofibrous nonwovens highlights a significant gap in the field. Despite their growing use, there is a lack of reliable and simple methods for tensile testing these materials, which impedes the ability to compare results reliably.

In addressing the challenges associated with the mechanical testing of nanofiber mats in this thesis, a specific approach was adopted, aligning with ASTM D882-18. These standard treats nanofiber mats akin to polymeric films and is aptly suited for nonwoven fabrics. Utilizing the standard strip method, the dimensions of the test specimens were set to 50 mm in length and 10 mm in width. This specification provided a feasible and practical framework for assessing the tensile properties of nanofibrous nonwovens.

To accurately measure the thickness of these nanofiber mats, a low force (5-7 N) micrometre was employed. This instrument is particularly effective for measuring thin, delicate materials like nanofibrous nonwovens. The use of a low force micrometre is crucial as it minimizes compression and deformation of the highly porous material, thereby providing more precise and reliable thickness measurements. This precision is vital, considering that nanofibrous mats have a high porosity level, often close to 90%, which can significantly influence the measured thickness. By using a low force micrometre, the impact of measurement pressure on the thickness readings was substantially reduced, leading to more accurate calculations of the cross-sectional area and, consequently, the stress (σ) values.

The adoption of this methodological approach, coupled with the use of a low force micrometre for thickness measurements, represents a significant step in overcoming the challenges associated with the mechanical testing of nanofibrous nonwoven materials. It ensures that the data obtained are reliable and can be effectively used for material design and comparison across various applications and research settings.

2.4. Microstructure Modelling of Nanofiber Mats

The field of nanofiber research has witnessed a surge in studies focusing on numerical and analytical methods to analyse the microstructure of randomly structured nanofibers. These

studies aim to predict the strength of nanofiber mats and to determine the strength of individual nanofibers within these mats. Each research work in this area brings its own set of assumptions and methodologies, reflecting the complexity of modelling nanofiber structures.

A prevalent method in this research (Yin et al., 2018; Yin & Xiong, 2018) involves assessing the area of single fibers to estimate the porosity of the nanofiber mat. This approach is crucial for understanding the spatial distribution of fibers and the void spaces within the mat, which significantly impact its mechanical properties. By analysing the fibre area relative to the total area of the mat, researchers can derive valuable insights into the density and structural configuration of the mat, which are essential for predicting its mechanical strength and behaviour.

Contrastingly, some researchers (Maccaferri et al., 2021; Rodriguez-Millan et al., 2018) have adopted an alternative strategy where the direct measurement of porosity is circumvented. Instead, they focus on determining the physical characteristics of the nanofiber samples by measuring their weight and dimensions. This approach allows for an estimation of the mat's thickness without directly measuring porosity. It's particularly useful in instances where the complex or irregular nature of the nanofiber mat makes direct porosity measurement challenging. By integrating the weight and dimensional data, researchers can approximate the thickness of the nanofiber mat, which, coupled with other material properties, provides a comprehensive understanding of the mat's overall structural and mechanical characteristics.

This diversity in methodologies underscores the need for versatile and multifaceted approaches in modelling nanofiber mats. As research progresses, there is an increasing emphasis on developing more nuanced and sophisticated models that can accurately simulate the intricate microstructure of nanofiber mats. These models not only aim to enhance our understanding of the material properties of nanofibers but also strive to pave the way for innovative applications across various scientific and engineering domains.

Focusing on the analytical analysis required to predict the strength and behaviour of these materials under tensile forces. The intricate relationships between various forces and strains acting on individual fibers and the entire nanofiber mat are explored in this section, employing mathematical formulations and equations.

When a nanofiber is subjected to tensile force, as illustrated in Figure 1.5, the force acting on a single fibre, oriented at an angle θ, can be represented by the variable f_{sn}.

$$f_{sn} = \frac{F}{cos\theta} \quad \ldots (1.1)$$

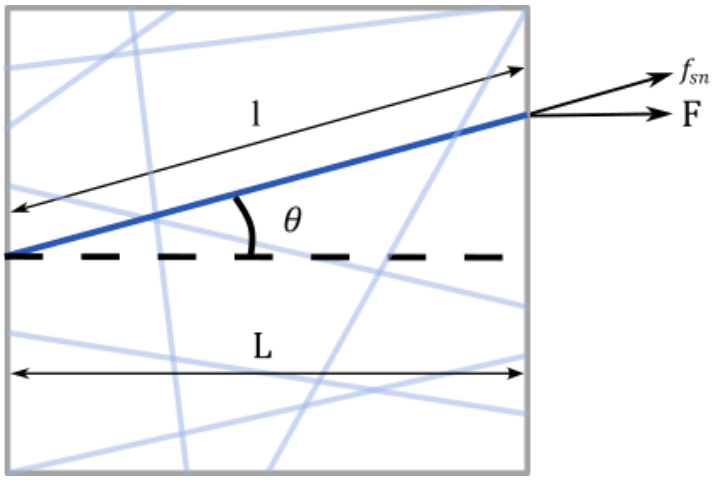

Figure 2.5 Force acting on the single nanofiber.

This relationship between the tensile force on a single nanofiber and the strain it undergoes follows a linear relationship, as depicted in Equation 1.2. In this equation, δ denotes the displacement in the fibre's direction, l is the length of the fibre, E_0 represents the elastic modulus of the single fibre, and A is the fibre's cross-sectional area.

$$f_{sn} = \frac{E_0 A}{l}\delta \quad \ldots (1.2)$$

There is also a specific relationship between fibre displacement and the displacement in the tensile direction, as shown in following equation:

$$\delta = \sqrt{(lsin\theta)^2 + (\delta_0 + lcos\theta)^2} - l \quad \ldots (1.3)$$

Where Δ_0 is the displacement in the tensile force direction. When the angle is close to the zero, it can be written as:

$$\frac{d\Delta}{d\Delta_0} = cos\theta \quad \ldots (1.4)$$

And the relation between the l and L can be written as,

$$l = \frac{L}{cos\theta} \quad \ldots (1.5)$$

Leading to Equations 1.4 and 1.5 and these are further substituted into Equation 2, which is then used to modify Equation 1.1, providing a comprehensive understanding of the forces acting in the tensile direction.

$$F = \frac{E_0 A}{L} cos^3\theta\delta_0 \quad \ldots (1.6)$$

The average force and displacement relationship for the entire nanofiber mat could determine by integrating fibre forces across various directions, considering the uniformity of the nanofiber mat in different angular orientations (for random structure). This leads to Equation 1.7, which addresses the equivalent cross-sectional area (A_0) of an oblique fibre in the tensile direction.

$$A = cos\theta A_0 \quad \ldots (1.7)$$

Following could be solved by substituting into the equation 1.6.

$$F = \frac{E_0 A_0}{L} cos^4\theta \delta_0 \quad \ldots (1.8)$$

$$\sigma_0' = \frac{F}{A_0} = E_0 cos^4\theta \varepsilon_0' \quad \ldots (1.9)$$

Where σ_0' is an equivalent stress of an oblique single fibre, and ε_0' is an equivalent strain of a single fibre. Therefore, we can obtain.

$$E_0' = E_0 cos^4\theta \quad \ldots (1.10)$$

Where E_0' is an equivalent elastic modulus of a single fibre.

Subsequent equations focus on deriving the equivalent stress and strain of a single fibre and its corresponding elastic modulus. The fibre distribution uniformity assumption allows for the calculation of the elastic modulus of the nanofiber mats using an integral formula that incorporates the volume fraction of the fibers (1 - P).

$$E_m^e = \frac{3}{8} E_0 (1 - P) \quad \ldots (1.11)$$

Where 1-P is the volume fraction of the fibre.

Till equation 1.11 it is considered for the all the nanofibers in the mat are straight. However, it could be in a curvature shape in the case where they are collected randomly. Those nanofibers go under unbending under force and changes stiffness. The elasticity modulus of the bending nanofibers is further explored as mentioned in (Pai et al., 2011), leading to Equation 1.12. The modulus of single fibers and fibrous mats is expressed in Equations 1.13 and 1.14, respectively.

$$E_m^e = \frac{3}{8} SR \times E_0 (1 - P) \quad \ldots (1.12)$$

Where SR represents the stiffness ratio of the straight nanofibers in the system and bended nanofibers in the system.

Elastic-Plastic model representing the elastic modulus for the single nanofiber can be expressed as mentioned in equation 1.13.

$$E_f = \begin{cases} E_0, & \sigma_0 \le \sigma_0^y \\ pE_0, & \sigma_0 > \sigma_0^y \end{cases} \quad \dots (1.13)$$

Similarly, Equation 1.14 represents the Elastic-Plastic modulus for the nanofiber mat.

$$E_m = \begin{cases} E_m^e, & \varepsilon_m \le \varepsilon_m^y \\ E_m', & \varepsilon_m > \varepsilon_m^y \end{cases} \quad \dots (1.14)$$

As tensile stress on the mats increases, fibers at different angular orientations enter the plastic phase at varying points. This behaviour is obtained in Equation 1.15, which divides the mat's stiffness into two parts: fibers still in the elastic phase and those in the plastic phase.

The focus is on understanding the force distribution across a nanofiber mat, particularly examining the role of individual nanofibers at various angular orientations, denoted by θ angle. The method for calculating the force acting on the entire nanofiber mat hinges on understanding the force acting on each nanofiber, with particular attention to their angular orientation relative to the applied force.

A critical aspect of this analysis is recognizing the sequence in which nanofibers at different angles reach their plastic deformation phase. Initially, fibers that are aligned straight (at a zero angle) transition into the plastic zone. This progression is followed by nanofibers positioned at an angle θ_1, and finally, those at an angle of $\frac{\pi}{2}$ or perpendicular to the applied force.

The model posits that when nanofibers at angle θ_1 begin to enter the plastic zone, the nanofiber mat exhibits a division into two distinct regions based on their angular orientation. Fibers that are oriented at angles greater than θ_1 remain in the elastic zone, retaining their original properties and response to stress. In contrast, fibers at angles smaller than θ_1 undergo plastic deformation, indicating a change in their mechanical behavior and response to the applied force.

$$\frac{E_m'}{E_m^e} = \frac{\int_{\theta_1}^{\frac{\pi}{2}} cos^4\theta d\theta + p\int_0^{\theta_1} cos^4\theta d\theta}{\int_0^{\frac{\pi}{2}} cos^4\theta d\theta} \quad \dots (1.15)$$

Equation 1.16 represents the tensile stress in the single nanofiber.

$$\sigma_0 = E_0 cos^2\theta \varepsilon_m \quad \dots (1.16)$$

Similarly, the strain of the fibers in the nanofiber mat can be written as,

$$cos^2\theta_1 = \frac{\varepsilon_m^y}{\varepsilon_m} \quad \dots (1.17)$$

Finally, by integrating the modulus of the plastic segment, a comprehensive stress-strain curve for the mats is obtained. This detailed modelling approach provides crucial insights

into the mechanical properties of nanofiber mats, crucial for applications where strength and durability are paramount.

In this thesis, a novel approach that combines experimental fabrication and Finite Element Method (FEM) modelling is introduced to analyse and predict the mechanical properties of nanofiber mats. This mixed-method strategy is particularly significant as it bridges the gap between the microstructural characteristics of individual nanofibers and the macroscopic behaviour of the entire mat.

The core of this approach lies in the fabrication of nanofiber mats with highly aligned fibers. By controlling the alignment of nanofibers, it becomes possible to study their individual mechanical properties more accurately. These properties are then utilized as foundational data for developing a comprehensive FEM model.

The core of this approach lies in the fabrication of nanofiber mats with highly aligned fibers. By controlling the alignment of nanofibers, it becomes possible to study their individual mechanical properties more accurately. These properties are then utilized as foundational data for developing a comprehensive FEM model. This model aims to simulate the behaviour of nanofiber mats under various mechanical loads, thereby predicting their overall strength and durability.

In Chapter 3, the methodology for fabricating both random and oriented nanofiber mats is discussed in depth. The process involves systematic testing of these mats to ascertain the mechanical characteristics of individual nanofibers. These characteristics are crucial in creating an accurate FEM model that reflects the real-world performance of the nanofiber mats. The FEM analysis presented in this thesis goes beyond traditional modelling techniques by incorporating both microstructural details of single fibers and macroscopic behaviour of the entire mat. This dual-scale analysis allows for a more precise prediction of the mechanical properties of nanofiber mats, a vital aspect in tailoring their use for specific applications.

Such an integrated approach to modelling is significant in advancing our understanding of nanofiber mats. It provides a comprehensive framework to predict how these materials will behave under different conditions, which is invaluable in designing nanofiber-based products for various industries, including biomedical, environmental, and structural applications. The detailed discussion of the FEM model in this thesis lays the groundwork for future research and development in the field of nanofiber technology, opening up new possibilities for innovative applications.

2.5. Conclusions of Literature Review

The extensive literature review presented in Chapter 1 of this thesis encompasses a detailed exploration of nanofiber technology, tracing its evolution, applications, fabrication techniques, and the nuances of numerical modelling. It begins with an in-depth look at the state of the art and recent developments in nanofiber mats, emphasizing the critical role of polyacrylonitrile (PAN) nanofibers. The unique properties of these nanofibers have led to their widespread use in diverse fields such as energy storage, catalysis, wound dressing, tissue engineering, and filtration. Their high surface area and porosity are particularly noted for their contribution to the effectiveness in these applications.

The review then delves into the methods of fabricating nanofibers, with a focus on electrospinning due to its efficiency, adaptability, and cost-effectiveness. The electrospinning process, involving a high-voltage power supply, a syringe pump, a spinneret, and a conductive collector, is elaborated in detail. The process steps, including the formation of the Taylor cone, stretching and thinning of the charged jet, solidification, and fibre deposition, are thoroughly explained.

Mechanical testing standards for nanofiber mats are also scrutinized, highlighting the challenges in testing such materials. This section underscores the importance of accounting for factors like porosity and thickness in mechanical testing, while pointing out the limitations in current standards and practices.

Moreover, the chapter delves into the numerical and analytical methods used to predict the strength and properties of nanofiber mats. Various modelling approaches and their underlying assumptions are discussed, illustrating the complexities involved in accurately representing the intricate structure of nanofibers. The application of finite element modelling (FEM) in predicting the mechanical behaviour of nanofibers, both as individual fibers and as mats, is highlighted, underscoring its significance in understanding and predicting their properties.

In summary, the literature review in Chapter 1 offers a comprehensive and multifaceted overview of nanofiber technology. It not only provides a historical perspective and insight into current advancements but also sheds light on the potential applications and the complexities involved in the fabrication and modelling of nanofibers. This overview sets the stage for the detailed investigations and novel contributions presented in the subsequent chapters of the thesis.

3. FABRICATION OF PAN NANOFIBER MATS

Chapter 3 delves into the fabrication process of PAN (Polyacrylonitrile) nanofiber mats, a cornerstone of this research. Nanofibers, due to their minute size and high surface area to volume ratio, present unique properties and challenges. This chapter focuses on producing these nanofibers using advanced electrospinning techniques, emphasizing the evaluation of their mechanical properties. The fabrication process, pivotal in determining the nanofibers' final properties and potential applications, is explored in detail. The content of this chapter is also available for reference in a published format (J. V. Sanchaniya, 2024; J. V. Sanchaniya, Lasenko, Gobins, et al., 2024).

3.1. Objectives of the Fabrication of PAN Nanofiber Mats

This chapter focuses on the production and examination of Polyacrylonitrile (PAN) nanofibers using two distinct methodologies for collection: employing a static plate and a dynamic rotating drum collector. This investigative segment is dedicated to evaluating how these varied collection techniques influence the mechanical attributes of the produced nanofibers. The PAN nanofiber mats thus fabricated serve as a benchmark for further developments presented in subsequent chapters, including the enhancements achieved through annealing processes detailed in Chapter 5, and the application of a bonded Polyvinyl Alcohol (PVA) solution discussed in Chapter 6. This methodical exploration is pivotal in comprehensively decoding the intrinsic properties of PAN nanofiber mats, their adaptability to enhancement strategies, and assessing alterations in thermal stability when juxtaposed with unprocessed PAN powder. This foundational research not only aims to elucidate the mechanical characteristics inherent to PAN nanofibers but also to establish a solid groundwork for advancing finite element modelling techniques in Chapter 4, thereby offering a multi-faceted view of the nanofibers' response to assorted refinement methodologies.

3.2. Materials and Methodology

In preparing for the electrospinning process, a solution of PAN is first created. PAN powder (an average molecular weight (MW) of 150,000 (typical) and a CAS number of 25014-41-9), obtained from Sigma-Aldrich (Merck KGaA, Darmstadt, Germany), is mixed with N, N-dimethylformamide (DMF), a solvent chosen for its compatibility with PAN. This mixture is heated and stirred at 80 °C for four hours using a Thermo Scientific™ Cimarec + TM Stirring

Hotplates Series magnetic stirrer. The purpose of this prolonged stirring at a controlled temperature is to ensure a homogenous solution, crucial for the consistency of the electrospun fibers. After preparation, the solution is left to stabilize at room temperature, a critical step to mitigate or eliminate air bubbles, which could adversely affect the spinning process.

The actual electrospinning takes place using a Fisherbrand TM Single Syringe Pump coupled with a needle-based electrospinning machine. The setup is calibrated to maintain a consistent room temperature of 22 ± 1 °C, vital for achieving reproducible results. The rotating drum collector, sourced from Shenzhen Tongli Tech Co. Ltd., is set to a constant speed of 2100 rpm. This speed is chosen to optimize the alignment and uniformity of the collected nanofibers. To obtain the random structure of the nanofiber mat flat plate collector was used. Aluminium foil is strategically placed on the drum to facilitate the efficient collection of nanofibers.

For morphological analysis, a Hitachi TM300 tabletop SEM is utilized. This high-precision instrument allows for a detailed examination of the nanofibers at a magnification of 1500x under a vacuum environment. The SEM images are further analysed using the OrientationJ plugin for the ImageJ program (Püspöki et al., 2016; Rezakhaniha et al., 2012; Schneider et al., 2012), enhancing the understanding of fibre orientation, a critical factor in determining the mechanical properties of the mats. The mean diameter and distribution of the nanofibers are accurately calculated by measuring over 100 fibers across various images, providing a comprehensive statistical analysis of their dimensions.

To assess the mechanical properties of the fabricated nanofibers, a Mecmesin Multi-Test 2.5-i tensile testing machine is employed. Equipped with sensors ranging from 10-N to 250-N, this machine measures the tensile strength of the nanofibers under controlled environmental conditions as specified in ISO 139:1973. The sample size and testing procedure adhere to the ASTM D882-18 standard, ensuring the reliability and comparability of the test results. The thickness of the nanofiber mats, a vital parameter for accurate mechanical testing, is meticulously measured using a digital micrometre (MDC-25PX, code No. 293-240-30, serial No. 71912410) from Mitutoyo, Japan. The specimen was cut parallel and perpendicular to the direction of the nanofibers for testing in the longitudinal and transverse directions, respectively. A 50 mm × 40 mm paper template was cut with an inside cut of 30 mm × 20 mm. Using double-sided thin scotch tape (3M Scotch Magic Tape (Matte Finish) 3/4" × 36-yard Desk Dispenser Refills), both ends of the specimen adhered to the paper template. After attaching the paper and sample to the tensile testing equipment, the sides of the paper template were cut with scissors.

Thermal properties of the nanofibers are investigated through Thermogravimetric Analysis (TGA) and Differential Scanning Calorimetry (DSC), both conducted under inert

nitrogen atmospheres. The TGA, performed using a NETZSCH TG 209 F1 Libra® thermomicrobalance, evaluates the thermal stability of the samples by measuring weight changes across a temperature range of 20 °C to 800 °C. The DSC, carried out using a NETZSCH DSC 214 Polyma differential scanning calorimeter, provides insights into thermal transitions such as glass transition temperatures of the samples. The DSC cycles include heating from –50 °C to 150 °C to eliminate impurities and moisture, followed by a repeat cycle to capture the glass transition temperature accurately as shown in g Figure 3.1.

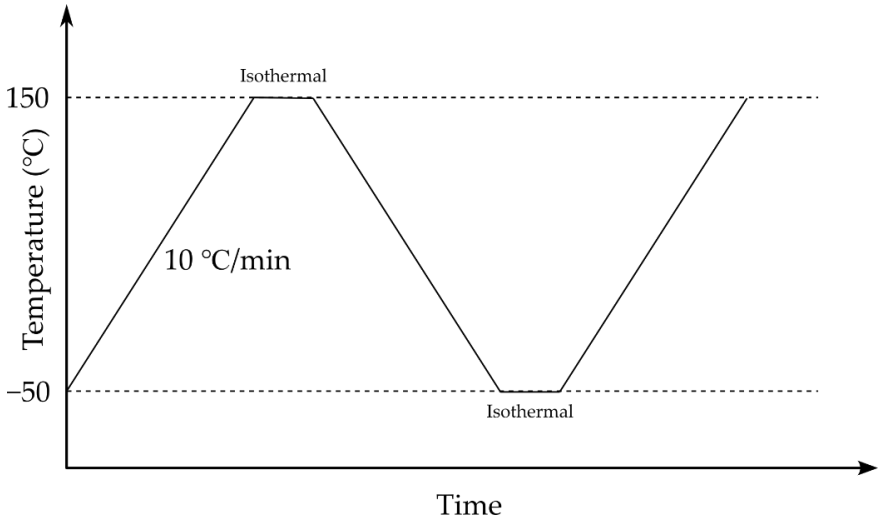

Figure 3.1 Heating cycle in DSC

To measure the weight of the sample, a laboratory scale (KERN ABT 5NM (KERN&Sohn GmbH, Balingen, Germany); maximum weight of 100 g; discreteness of 0.000001 g; serial number: WB22G0101; calibration certificate number: B61-389-2023-03/1, 24 March 2023) was used.

A density comparison method was employed for porosity testing of the nanofiber mats, involving the measurement of the nanofiber mat's mass to calculate its porosity. This method follows the equation:

$$P(\%) = \left(1 - \frac{M}{M_d}\right) \times 100 \qquad \ldots (3.1)$$

where P represents the porosity percentage, M is the measured mass of the nanofiber mat (µg), and M_d is the theoretical mass that the specimen would possess if it were fully dense.

The value of M_d is calculated using the formula V × ρ, where V represents the volume (cm^3) of the specimen and ρ is its density (1.184 g/cm^3).

3.3. Experimental Characterization of Nanofiber Mats

Chapter 3.3 delves into the comprehensive characterization of nanofiber mats, focusing on a detailed analysis through various techniques to assess their structural, mechanical, and thermal properties. Scanning Electron Microscopy (SEM) analysis serves as the cornerstone for examining the microstructural attributes such as nanofiber diameter, orientation, and porosity. This high-resolution imaging allows for an in-depth visualization of the nanofibers, providing critical insights into their arrangement, uniformity, and surface characteristics. The analysis of mechanical properties, including tensile strength, and elasticity, evaluates the nanofiber mats' performance under stress and strain, essential for determining their applicability in various fields. Furthermore, thermal properties are investigated to understand the nanofiber mats' stability and behaviour under different temperature conditions. This encompasses thermal conductivity, thermal stability, and degradation patterns, which are pivotal for applications in environments experiencing wide temperature ranges. Collectively, this chapter aims to furnish a holistic understanding of the nanofiber mats, underpinning their potential uses based on their intrinsic properties.

3.3.1. SEM Analysis

Chapter 3.3.1 delves into the SEM analysis of nanofiber mats, focusing on their diameter, orientation, and porosity. The examination reveals discernible distinctions between oriented and randomly structured nanofiber mats, as depicted in Figures 3.2a and 3.2b. The oriented nanofibers exhibit an average diameter of 580 ± 20 nm, in contrast to the 719 ± 35 nm diameter of nanofibers in the random arrangement. This discrepancy is attributed to the different collection methodologies applied during the electrospinning process. Specifically, the nanofibers retrieved from the rotating drum showcased a narrower diameter, likely a consequence of the drawing effect instigated by the drum's rapid rotation. Conversely, the larger diameter of nanofibers gathered using a flat plate collector could stem from the absence of the drawing effect inherent in the rotating drum method.

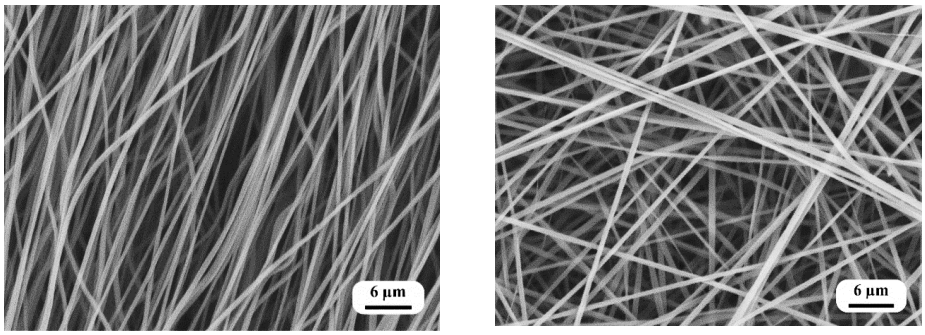

(a) (b)

Figure 3.2 SEM images of the nanofiber mats: (a) oriented nanofibers; and (b) random nanofibers.

Further analysis via Fast Fourier Transform (FFT), shown in Figures 3.3a and 3.3b, quantified the nanofibers' alignment within the mats. The oriented mats, spun at a drum speed of 2100 rpm, displayed an FFT alignment value (normalized) between 0.0 to 0.1, indicating a high degree of fibre alignment predominantly in one direction, with a deviation range of 11 degrees. This uniform alignment is likely due to the constant speed of the drum, which ensures a stable fibre drawing process and results in a consistent diameter range. In contrast, the randomly structured mats presented a smaller fluctuation in the FFT alignment value (normalized), from 0.01 to 0.04, pointing to a more dispersed fibre orientation within the mat, devoid of a pronounced directional preference.

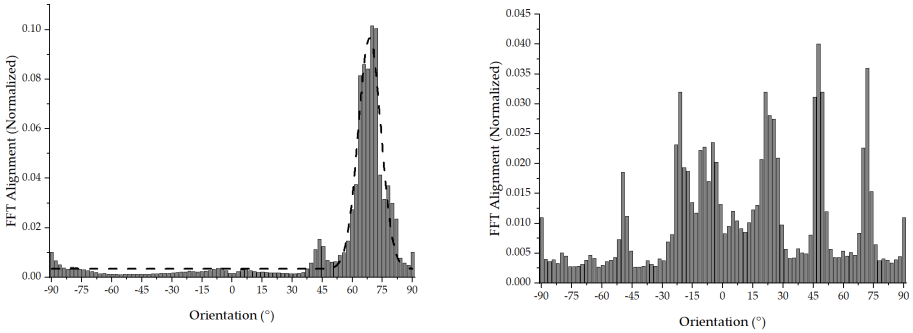

(a) (b)

Figure 3.3 Orientation of the nanofibers: (a) oriented nanofibers; and (b) random nanofibers.

Porosity assessments, conducted using the density comparison method (referenced in Equation 3.1), revealed that the porosity of oriented nanofibers was 75.2 ± 1%, compared to 80.8 ± 1% for random nanofiber mats. The higher porosity in samples collected on a flat plate

is explained by their lower fibre packing density relative to those harvested on the rotating drum, which resulted in more densely aligned and drawn fibres.

3.3.2. Mechanical Properties

Chapter 3.3.2 delves into the mechanical behaviour of PAN nanofiber mats, Figure 3.4 depicts the specimen of the nanofiber mat mounted between the grips of the tensile test machine, along with the paper template.

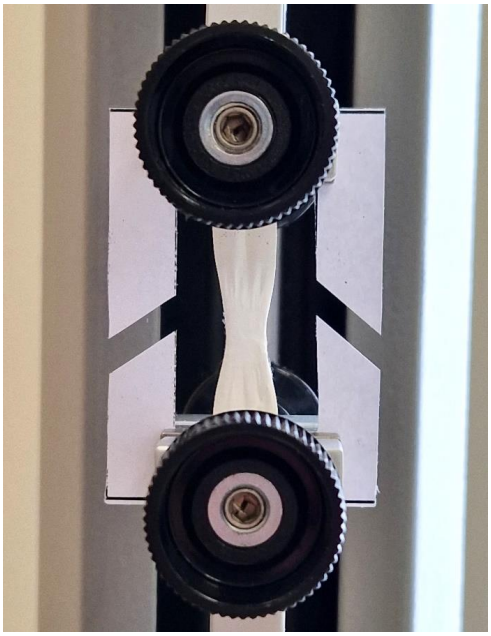

Figure 3.4 Mounting of the nanofiber mat specimen between the grips of the tensile test machine, accompanied by a paper template.

The stress-strain curves as depicted in Figure 3.5 to elucidate the response of oriented nanofiber structures to tensile forces. The oriented nanofiber specimens exhibited an ultimate tensile strength (UTS) of 8.9 ± 0.5 MPa along the fibre orientation, markedly superior to the UTS observed in the perpendicular direction at 1.1 ± 0.1 MPa. This stark contrast in tensile strengths underlines the anisotropic mechanical nature of the oriented nanofiber mats, where fibre alignment significantly influences their tensile properties. In contrast, the UTS values of the randomly structured mats remained consistent across both axes, recording values of 3.9 ± 0.4 MPa and 4.0 ± 0.5 MPa, showcasing their isotropic mechanical behaviour.

Investigating stiffness through Young's modulus measurements, oriented nanofiber mats demonstrated significantly enhanced stiffness in the longitudinal direction, with a modulus of 410 ± 23 MPa, vastly outstripping the transverse measurement of 53 ± 5 MPa. This again highlights the anisotropic characteristics of these mats. Conversely, the Young's modulus of randomly structured mats presented a uniform profile, with measurements of 103 ± 4 MPa and 99 ± 5 MPa, illustrating a more evenly distributed stiffness within the material.

Ductility, as evidenced by elongation at break, showed variance across the two structural orientations and directions. Oriented nanofibers attained elongation at break values of 0.19 ± 0.02 longitudinally and 0.2 ± 0.03 transversely. Meanwhile, randomly structured fibers displayed enhanced ductility, with elongation at break reaching 0.35 ± 0.03 and 0.36 ± 0.04, respectively.

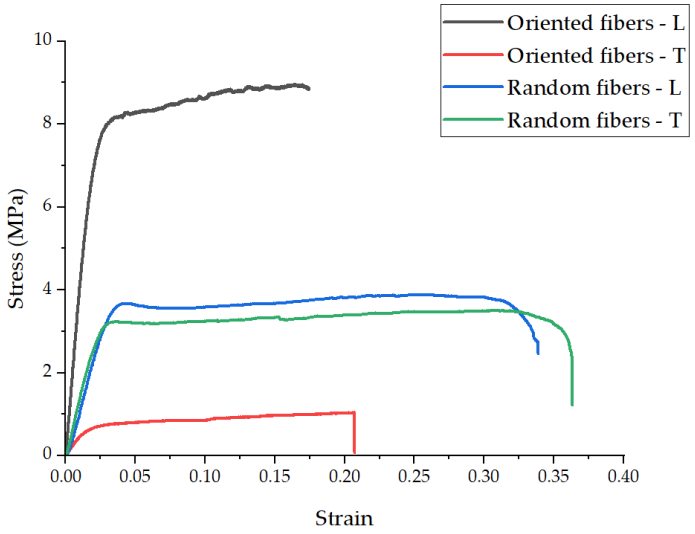

Figure 3.5 Representative stress–strain graphs for oriented and random structures in longitudinal (L) and transverse (T) directions.

The discernible increase in ductility observed in the randomly structured mats can be ascribed to the interlocking of fibers at assorted angles, which facilitates extended elongation prior to failure. Unlike oriented structures where fibers uniformly share the tensile load, leading to collective failure, the random arrangement allows for a varied distribution of load among fibers, contributing to a lower elastic modulus and UTS but increased ductility. This behaviour accentuates the anisotropic mechanical properties of oriented nanofiber mats, as summarized in Table 3.1.

Table 3.1

Summary of the Mechanical Properties of the Nanofiber Mats.

structure of nanofibers	testing direction	thickness, t (μm)	ultimate tensile strength σ_{max} (MPa)	Young's modulus, E (MPa)	elongation at break strain, ε
oriented	longitudinal	84 ± 4	8.9 ± 0.5	410 ± 23	0.19 ± 0.02
	transverse	83 ± 3	1.1 ± 0.1	53 ± 5	0.2 ± 0.03
random	longitudinal	87 ± 5	3.9 ± 0.4	103 ± 4	0.35 ± 0.03
	transverse	85 ± 4	4.0 ± 0.5	99 ± 5	0.36 ± 0.04

These findings underscore the profound impact of fibre orientation on the mechanical attributes of nanofiber mats. Effect of the orientation and structure of the nanofiber directly impact on the strength of the overall structure of the nanofiber mat as observed in prior studies (Beese et al., 2013; Yin et al., 2018). Oriented nanofiber structures exhibit markedly superior mechanical qualities in the direction of fibre alignment, suggesting their suitability for applications demanding elevated tensile strength and rigidity. Conversely, randomly structured mats offer versatile properties ideal for scenarios where isotropic mechanical responses are preferred.

3.3.3. Thermal Properties

Chapter 3.3.3 focuses on the thermal properties of PAN nanofiber mats, utilizing two primary analytical methods: thermogravimetric analysis (TGA) and differential scanning calorimetry (DSC). These methods provide insights into the thermal stability and phase transitions of the nanofiber mats, essential for determining their applicability in various temperature-dependent environments.

Thermogravimetric analysis offers a quantitative measure of the weight change a material undergoes as a function of temperature or time, under a controlled atmosphere. TGA was performed to assess the thermal degradation characteristics of the nanofiber mats. This analysis elucidates the onset of degradation temperature, the rate of weight loss, and the residual mass at high temperatures, providing valuable data on the thermal stability and decomposition kinetics of the PAN nanofibers. The TGA curves typically exhibit distinct regions corresponding to moisture evaporation, polymer degradation, and the decomposition of residual components.

Differential scanning calorimetry, on the other hand, measures the heat flow associated with thermal transitions within the material, such as melting, crystallization, and glass transition temperatures. DSC analysis of the nanofiber mats revealed specific thermal events,

indicating the crystalline and amorphous regions within the PAN polymer matrix. The endothermic and exothermic peaks observed in the DSC thermograms provide detailed insights into the energy required for specific thermal transitions, highlighting the thermal behaviour of the nanofibers in response to temperature changes.

By combining the results from TGA and DSC, a comprehensive understanding of the thermal properties of PAN nanofiber mats is achieved. The analysis not only reveals the thermal stability and degradation profile of the mats but also uncovers important thermal transitions, crucial for optimizing the nanofibers for thermal applications. These findings are pivotal in tailoring the PAN nanofibers' properties for specific uses, including thermal insulation, filtration at elevated temperatures, and composite materials requiring high thermal resistance.

3.3.3.1 Thermogravimetry Analysis (TGA)

In the study of the thermal degradation behaviour of polyacrylonitrile (PAN) and its nanofibers, thermogravimetric analysis (TGA) along with its derivative thermogravimetry (DTG) provides insightful data. The TGA curve for virgin PAN, illustrated in Figure 3.6, features a green line representing the percentage of mass loss across a temperature range, while the red line, the DTG curve, offers detailed insight into the rate of mass loss, facilitating precise determination of critical temperatures.

The analysis of virgin PAN reveals remarkable thermal stability up to 289.5 °C, beyond which degradation begins, as indicated by the onset temperature of 291.6 °C. Between 25°C to 299.8 °C, a mass loss of 14.15% was observed, demonstrating the initiation of thermal degradation. This was followed by a significant mass reduction of 22.78% from 299.8 °C to 374.4 °C. The degradation continues with a 19.70% loss in mass between 374.4°C to 566.0 °C, and a further decline of 3.65% was noted from 566.0 to 799.6 °C. The analysis concludes with a residual mass of 39.42% at 800°C, indicating the amount of non-volatile content remaining after the thermal process.

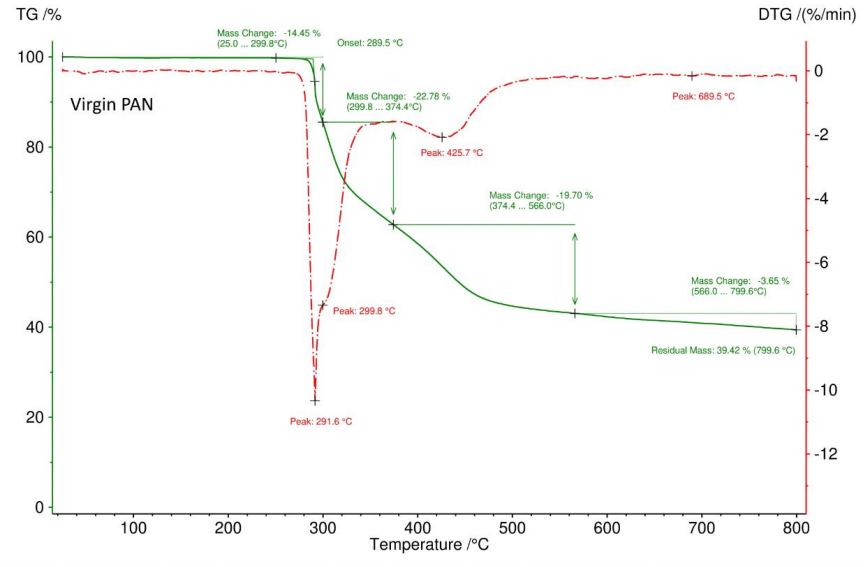

Figure 3.6 TGA and DTG of Virgin PAN

For the PAN nanofibers, depicted in Figure 3.7, the TGA and DTG curves show an early mass reduction at 110.6 °C, attributed to the evaporation of N,N-dimethylformamide (DMF) used as the solvent in the electrospinning process, amounting to approximately 3.08%. The mass loss from 25.0 °C to 158.7 °C registered at 3.08%, and a subsequent reduction of 1.66% was recorded from 158.7 °C to 297.6°C. A notable mass loss of 14.26% occurred between 264.2 °C to 297.6 °C, indicating a critical phase of degradation. The mass loss continued with 22.96% from 297.1 °C to 371.6 °C and 20.23% from 371.6 °C to 552.0 °C. The final phase of mass reduction was 5.61% from 551.3°C to 799.5 °C, leaving a residual mass of 32.63% at the end of the thermal analysis.

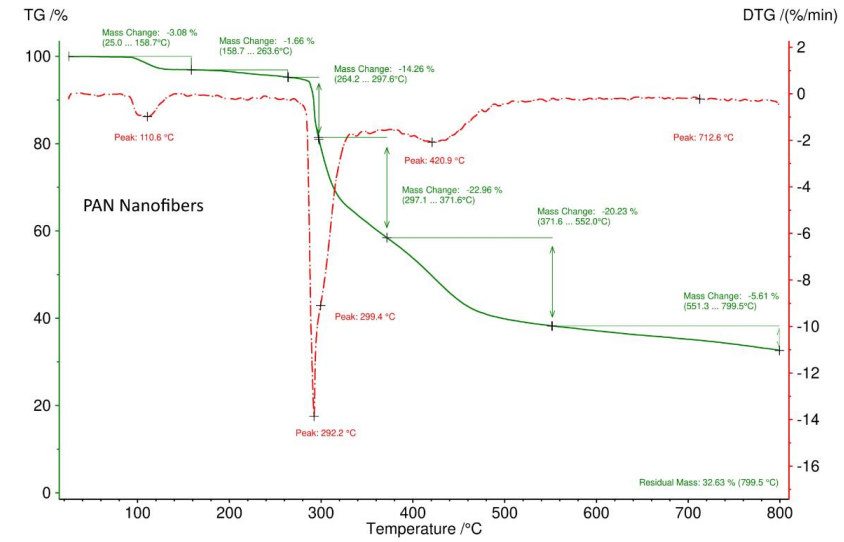

Figure 3.7 TGA and DTG of PAN Nanofiber Mat

This comprehensive TGA and DTG analysis sheds light on the thermal stability and degradation patterns of both virgin PAN and its nanofibers. The results highlight the thermal transitions and degradation kinetics, crucial for understanding the material's performance under high-temperature conditions.

3.3.3.2 Differential Scanning Calorimetry (DSC)

Differential Scanning Calorimetry (DSC) offers insightful data regarding the thermal transitions of materials by measuring the heat flow associated with material phase changes. In this study, the DSC analysis of virgin polyacrylonitrile (PAN) and PAN nanofibers during the thermal cycle provides a detailed examination of their thermal behaviour.

The initial heating phase, illustrated in Figure 3.8, shows that virgin PAN exhibited a heat absorption of 30.06 J/g, while the PAN nanofibers demonstrated a slightly lower heat uptake of 26.88 J/g. This phase revealed two significant peaks in the heat absorption profile, likely corresponding to the solvent evaporation process. This observation aligns with the thermal degradation stages identified in the TGA analysis of PAN nanofibers, underscoring the consistency between the two thermal analytical techniques.

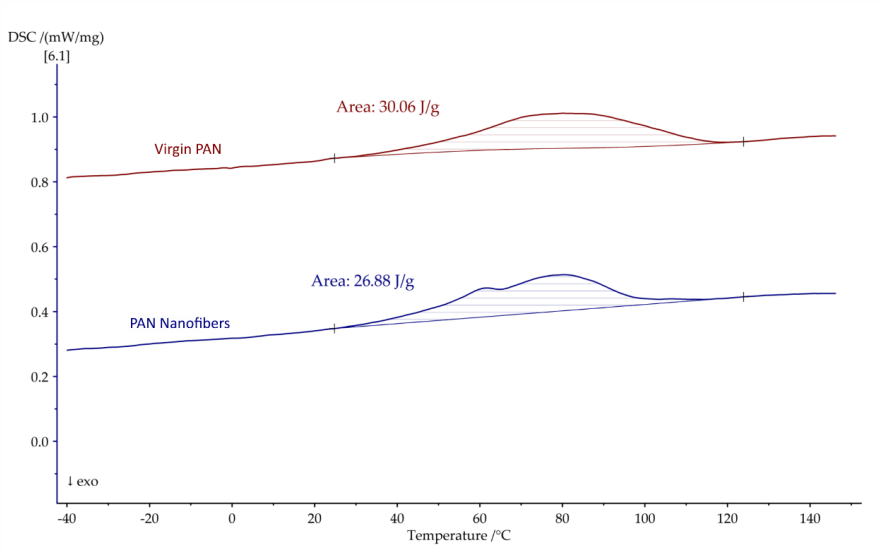

Figure 3.8 1st Heating Cycle of Virgin PAN vs PAN Nanofibers in DSC

Upon cooling, as depicted in Figure 3.9, the glass transition temperature (Tg) for virgin PAN was identified at 97.9 °C, contrasting with a slightly lower Tg of 94.9 °C for PAN nanofibers. This variance suggests a slight reduction in thermal stability, about 3%, possibly due to the altered molecular arrangement or residual solvent effects in the nanofiber structure.

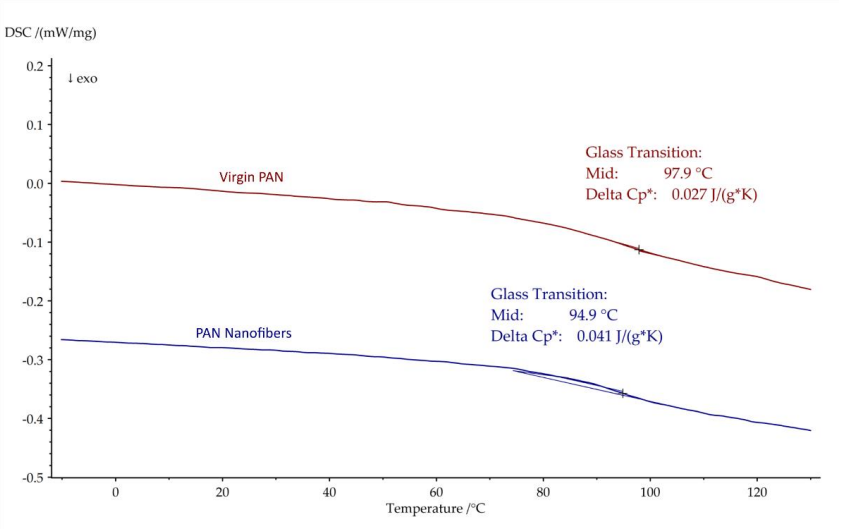

Figure 3.9 1st Cooling Cycle of Virgin PAN vs PAN Nanofibers in DSC

The subsequent heating cycle, captured in Figure 3.10, further refined these observations. The Tg for virgin PAN was recorded at 101.8°C, with the PAN nanofibers displaying a Tg around 96.0°C, marking a reduction of approximately 5%. Moreover, the change in heat capacity (Delta Cp*) between the two materials indicated a significant disparity; virgin PAN showed a Delta Cp* of 0.202 J/(gK), whereas the PAN nanofibers registered a lower value of 0.116 J/(gK), representing a 42% decrease. This notable difference in heat capacity underscores the distinct thermal characteristics imparted by the nanofiber morphology, potentially due to increased surface area, altered crystallinity, or differences in molecular orientation.

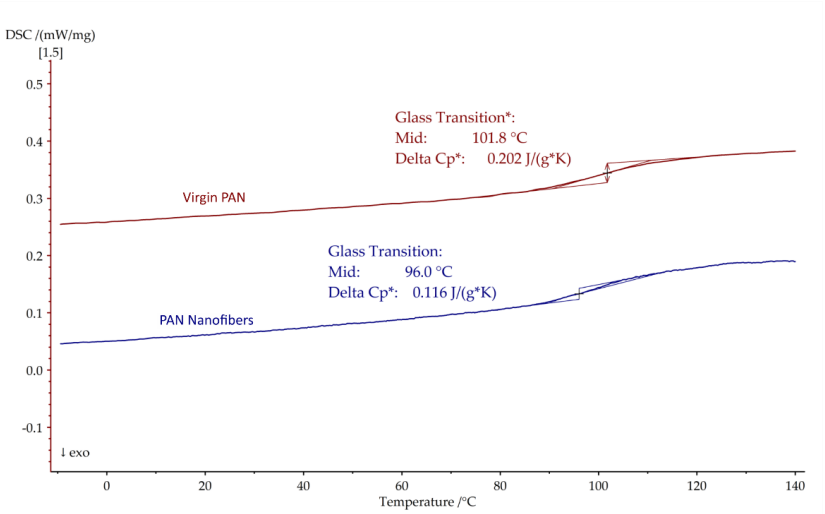

Figure 3.10 2nd Heating Cycle of Virgin PAN vs PAN Nanofibers in DSC

Through the DSC analysis, the nuanced thermal properties of PAN materials, particularly between the bulk and nanofiber form, are elucidated. The observed reductions in glass transition temperatures and heat capacity for PAN nanofibers highlight the influence of nano structuring on thermal behaviour, providing a foundation for further exploration of their applicability in various thermal environments and applications.

3.4. Conclusions of Characteristics of the PAN Nanofiber Mat

The comprehensive characterization of Polyacrylonitrile (PAN) nanofiber mats, as detailed in Chapter 3, provides a foundational understanding of their morphological,

mechanical, and thermal properties. These characteristics are pivotal in assessing the potential applications of PAN nanofiber mats in various fields, including filtration, biomedical applications, and structural composites.

1. SEM Analysis revealed distinct differences in fibre diameter and orientation between nanofibers collected using a flat plate (stationary) and a rotating drum. Nanofibers fabricated with the rotating drum exhibited a narrower diameter and a high degree of alignment, attributed to the drawing effect induced by the rotation. This precise control over fibre morphology underscores the importance of collection methodology in tailoring the properties of nanofiber mats for specific applications.
2. Mechanical Properties assessment showed that oriented nanofiber mats possess superior tensile strength and Young's modulus in the direction of fibre orientation, highlighting their anisotropic nature. In contrast, randomly structured mats exhibited isotropic behaviour, with more uniform mechanical properties in all directions. This directional dependency of mechanical strength in oriented mats opens avenues for designing materials where specific directional strength is required, such as in load-bearing applications.
3. Thermal Properties, analysed through Thermogravimetric Analysis (TGA) and Differential Scanning Calorimetry (DSC), demonstrated the thermal stability and degradation patterns of PAN nanofibers. These findings are crucial for applications where thermal stability is a key factor, such as in high-temperature filtration and thermal insulation materials.
4. The Porosity Analysis, conducted via a density comparison method, highlighted the significant porosity levels in the nanofiber mats, an essential attribute for applications requiring high surface area, such as filtration and tissue engineering scaffolds.

In summary, the fabrication and characterization of PAN nanofiber mats have revealed their complex and versatile nature. The ability to manipulate the fiber diameter, orientation, and porosity through the electrospinning process and collection methodology enables the tailoring of mechanical and thermal properties to meet specific application needs. This adaptability, coupled with their high surface area and porosity, positions PAN nanofiber mats as a promising material for a wide range of applications, from industrial to biomedical fields. The findings from this chapter lay the groundwork for subsequent modifications and applications of PAN nanofiber mats, explored in further chapters of this thesis.

4. A FE MODEL FOR DETERMINING THE MECHANICAL PROPERTIES OF ELECTROSPUN NANOFIBER MAT

In this chapter, I delve into the intricate relationship between the microscale characteristics of individual nanofibers and the macroscale mechanical performance of electrospun nanofiber mats. The investigation highlights the pivotal role of single nanofiber attributes, such as diameter and orientation, in dictating the mechanical behaviour of the mats. A key novelty of this study is the development and application of a finite element method (FEM) model designed to accurately simulate the elastoplastic behaviour of these mats. This model intricately incorporates the impact of various structural parameters on the mechanical properties, offering a nuanced understanding of the material's response under stress.

The rigor of the FEM model is tested through a comparison with experimental data obtained from electrospun polyacrylonitrile (PAN) nanofibers, which vary in their alignment. The model's success in replicating the elastic-plastic tensile behaviour of these nanofiber mats validates its reliability and the credibility of its predictions regarding the mechanical interplay within the mats. By meticulously analysing the influence of nanofiber diameter, fibre orientation, the ratio of length to width, and porosity, this chapter sheds light on the engineering principles underpinning the design of nanofibrous materials tailored for specific mechanical needs.

These insights not only enhance our understanding of the structural complexities of nanofibrous mats but also underscore the importance of comprehensively characterizing individual nanofibers. Recognizing these microscale properties is crucial for advancing material design strategies that leverage the unique mechanical profiles of nanofiber mats for a wide range of applications. Through this approach, the chapter contributes significantly to the field of materials science, particularly in the optimization and design of nanofiber-based materials for enhanced mechanical performance. The content of this chapter is also available for reference in a published format (J. V. Sanchaniya, Lasenko, Gobins, et al., 2024).

4.1. Objective of Developing FE Method

The objective of developing the Finite Element Method (FEM) in this chapter is to enhance our understanding of the intricate stress-strain behaviours of nanofibers, from individual fibers to the cohesive mats they compose. The nanoscopic scale and inherent fragility of these fibers pose significant challenges in accurately determining their mechanical properties using conventional methodologies. Traditional approaches, relying on advanced yet

expensive instruments like atomic force microscopy and micromanipulators, tend to limit evaluations to geometric, morphological, and thermal characteristics. Nonetheless, grasping the tensile stress of single fibers remains paramount for engineering advanced nanofibrous structures, including composites and filtration systems.

The task of discerning individual fibres' mechanical properties within nanofiber mats is further complicated by the mats' complex, highly porous structure. Prior studies have sought to estimate nanofiber mat thickness by evaluating their porosity and comparing specimen mass against known polymer densities. While the mechanical properties of mats composed of randomly oriented fibers are difficult to ascertain, alignment of fibers allows for a more direct assessment of forces, facilitating the determination of mat mechanical properties.

FEM modelling emerges as a crucial tool in the realm of research aimed at analysing fibrous non-woven mats' mechanical properties. This approach, alongside multi-scale modelling techniques such as statistical models, neural networks, molecular dynamics, and FEM, plays a pivotal role in understanding the effects of fibre diameter, material behaviour, and porosity on fibrous mats' mechanical traits (Chavoshnejad et al., 2021; Chavoshnejad & Razavi, 2020; Y. Liu & Dzenis, 2016; Yin et al., 2017, 2018; Yin & Xiong, 2018). FEM, in particular, excels in depicting the elastic-plastic behaviour of fibrous mats by considering the mechanics of embedded microelements.

Recent strides in finite element model development have enabled predictions of the mechanical characteristics of randomly oriented nanofibers by scrutinizing the properties of single nanofibers. This includes studies on the elastic and plastic responses of electrospun fibrous networks to various loadings, demonstrating how macroscopic properties correlate with microstructural evolution. However, a notable gap persists in the literature regarding a thorough comprehension of single nanofibers' elastoplastic behaviour, derived from entire nanofiber mats, and the prediction of whole mats' mechanical behaviour based on these single fibre properties. Additionally, there's a focus gap on mats with oriented, inter-bonded nanofibers as opposed to those with random fibre arrangements.

Addressing this gap, this chapter introduces a novel methodology that leverages aligned nanofibers to predict individual fibres' elastoplastic behaviours. Utilizing PAN nanofibers as a foundation, we have established an experimental basis for modelling development. Subsequently, an FEM model was crafted to accurately predict the elastoplastic behaviour of nanofiber mats, considering the influences of fibre diameter, porosity, orientation, and the length-to-width ratio on their mechanical properties. This model provides a holistic insight into

the behaviour of nanofiber mats under varied conditions, marking a significant advancement in our understanding and capability to engineer nanofibrous materials for specific applications.

4.2. Identifying Mechanical Properties of Single Nanofiber

This subchapter delves into the exploration of the mechanical attributes of single nanofibers, an essential step towards understanding the aggregate mechanical properties of nanofiber mats. This investigation hinges on the construction of stress-strain profiles for individual fibers, especially those that are uniformly aligned. Such alignment facilitates the uniform distribution of tensile load across the fibers, enabling the conceptualisation of the nanofiber mat as a coherent polymeric film. This analogy rests on the assumption of homogenous mechanical properties across the mat's cross-section, down to the nanoscale, ensuring a consistent thickness throughout.

A comprehensive methodological framework was employed to deduce the mechanical properties of single nanofibers within the context of oriented nanofiber mats. This approach leveraged the mechanical behaviour of the mats, gleaned from tensile testing, as a surrogate for discerning the attributes of individual fibers. Critical to this process was the precise measurement of each specimen's mass, underpinning the assumption that the specimen's density aligns with that of pure polyacrylonitrile (PAN).

With precise measurements of the specimens' dimensions - specifically, the span of 30 mm between grips and a width of 10 mm - a recalculated thickness based on PAN's density was determined. This recalibrated thickness was pivotal in mapping out the stress-strain curves for individual nanofibers, thereby encapsulating the elastoplastic dynamics characteristic of each fibre. This meticulous approach unveils a novel pathway to quantify the mechanical properties of single nanofibers, contributing significantly to our understanding of the mechanical comportment of nanofiber mats.

4.3. Geometrical Modelling

In constructing the Finite Element (FE) model, a sophisticated geometric modelling strategy was utilised, centred on devising a parametric representation to meticulously mimic the structure of nanofibers. As depicted in Figure 4.1, certain controlled parameters were instrumental in the geometrical formulation of nanofibers, serving as the cornerstone for the FE model's establishment. The inception of this parametric model involved delineating straight

fibres with a consistent diameter, arranged uniformly over a specified plane, characterised by the domain's known length (D_L) and height (D_H).

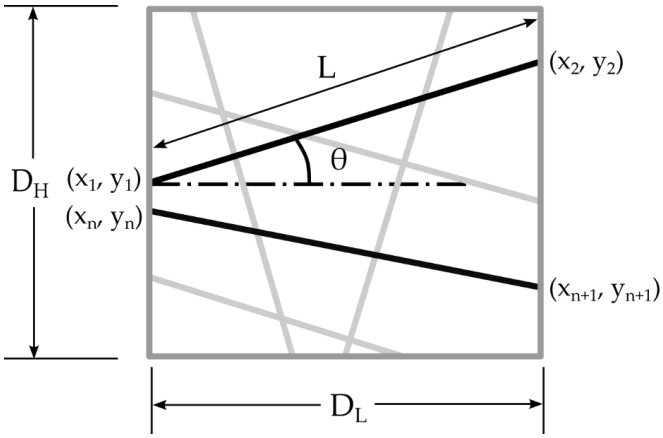

Figure 4.1 Schematic representation of the geometry development process for nanofibers, highlighting the control of fibre orientation and distribution within the domain.

The geometrical development process entailed several pivotal steps:

- Initial fibre creation positioned each fibre's midpoint at the domain area's centre.
- Subsequently, fibres were rotated at random angles, spanning from -90 to +90 degrees, ensuring fibre extension to the domain's limits.
- In the case of oriented nanofibers, the rotation angle was meticulously adjusted to mirror their aligned configuration.

Porosity control within the domain hinged on manipulating the domain area and pinpointing the generated fibres' coordinates. As illustrated in Figure 4.1, for a fibre delineated at angle (θ), the starting and ending coordinates were denoted as (x_1, y_1) and (x_2, y_2), respectively. Employing angle (θ) alongside these coordinates enabled the calculation of the fibre's length (L) within the domain area (D_L x D_H). With the fibre diameter established, this approach facilitated accurate porosity maintenance within the domain.

This geometric model rested upon four fundamental premises:

- Fibres uniformly reached the domain's extremities.
- All fibres shared an identical diameter.
- Fibres maintained a linear form throughout the domain, devoid of bending.
- Intersection points implied inter-bonding amongst fibres within the domain.

The presumption of fibre inter-bonding, informed by preceding research insights (Chavoshnejad et al., 2021; Chavoshnejad & Razavi, 2020), suggested that a significant proportion of inter-bonded fibres yielded more precise mechanical property estimations of nanofiber mats. Consequently, it was posited that fibres were universally inter-bonded. Given this study's emphasis on transverse loading and mechanical property evaluation under such conditions, the fibres' modelling as inter-bonded was paramount. This assumption critically underpinned the accurate depiction of the nanofiber mat's behaviour, particularly under transverse load applications, where fibre inter-bonding significantly influences stress and strain distribution across the material.

An auxiliary Python script was crafted, as referenced in, streamlining the model geometry's efficient and precise construction. This methodology guaranteed that the FE model faithfully represented the nanofiber mat's physical attributes, laying a solid foundation for ensuing mechanical property analyses.

4.4. Boundary Conditions

Subchapter 4.4 expounds on the strategic implementation of boundary conditions essential for the meticulous analysis of the mechanical performance of nanofiber mats when subjected to tensile stresses. These boundary conditions, pivotal in simulating the response to both longitudinal and transverse strains as depicted in Figures 4.2a and 4.2b, are meticulously crafted to monitor the reaction forces elicited by the displacement applied in the longitudinal direction. Specifically, the displacement applied to the fibre ends spans up to 20% of the domain's length, imposing restrictions to negate movement in the Y and Z axes for longitudinal loading, and in the X and Z axes for transverse stress, thereby ensuring a controlled examination of tensile behaviour.

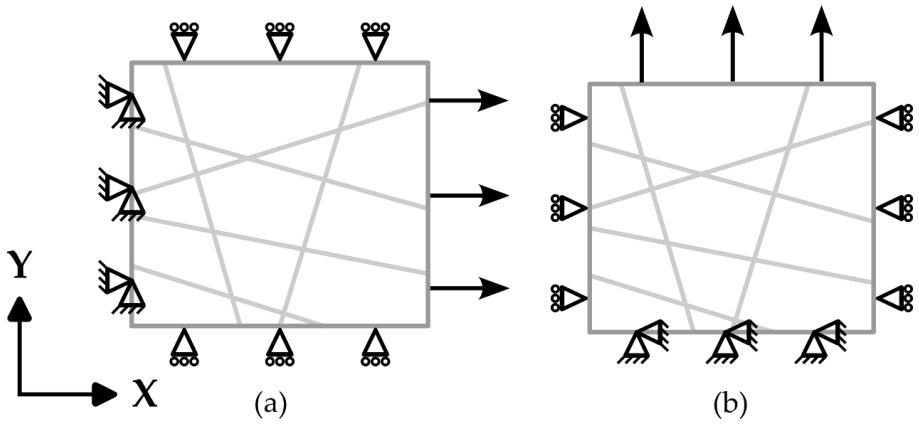

Figure 4.2 Boundary conditions applied in (a) longitudinal, and (b) transverse directions to simulate the normal stress response to displacement.

Further elaboration is provided on the fixation of fibre ends opposite to the displacement direction across all axes, albeit granting rotational freedom around the Z-axis. This nuanced approach allows for the accurate depiction of fibres' angular adjustment in response to applied strains, bolstering the realism of the simulation. The perimeters perpendicular to the displacement trajectory are permitted uninhibited movement parallel to the applied force, ensuring an authentic simulation environment.

For the finite element analysis, fibres are represented using linear beam elements (B31) within the Abaqus software, a choice dictated by the elements' capacity to accommodate shear deformation and finite axial strains. This selection underscores the adaptability of these elements in modelling the slender, delicate structure of nanofiber mats, offering a high-fidelity representation of their mechanical properties.

Subsequent to the imposition of boundary conditions, the resultant reaction force of each fibre in relation to the X-axis is aggregated, and the collective reaction force is normalized by the domain's cross-sectional area. The following relationship forms the basis for calculating the stress within the nanofiber mat, providing a clear and quantifiable measure of the material’s response to applied dis-placement.

$$\sigma_x = \frac{\sum F_x}{A_D}, \qquad \ldots (4.1)$$

where σ_x is the normal stress in X-axis, F_x is the reaction force (μN) acting at each end of the fibers, and A_D is the cross-sectional area of the domain. This relationship forms the basis

for calculating the stress within the nanofiber mat, providing a clear and quantifiable measure of the material's response to applied displacement.

Acknowledging the inherent variability in fibres' orientation and porosity, and consequently, in the resultant structures from set parameters, this chapter advocates for conducting multiple simulations to counteract this unpredictability. This rigorous methodological approach, involving at least five simulations per parameter combination, ensures a robust and reliable analysis. By encompassing a spectrum of potential structural configurations, the derived mechanical properties offer a comprehensive reflection of the nanofiber mats' behaviour under diverse conditions. Through the aggregation and averaging of these simulation outcomes, the chapter contributes significantly to our understanding of the mechanical dynamics governing nanofiber mats, offering invaluable insights into their application potential.

4.5. Material Model

The values used in the FEM results section are derived from the mechanical properties of individual nanofibers, providing a foundational understanding of the material's behaviour under stress on the basis of three key parts: namely, addressing the elastic behaviour, plastic behaviour, and damage model of the nanofiber mat material. The elastic behaviour of the material is described in Equation 4.2, which relates stress (σ) in the material to strain (ε) through Young's modulus (E), where ε_y is the yield strain:

$$\sigma = E \cdot \varepsilon \; for \; \varepsilon \leq \varepsilon_y \qquad \ldots (4.2)$$

The non-linear behavior of the elastic–plastic transition is described in Equation 4.3:

$$\varepsilon = \frac{\sigma}{E} + (\frac{\sigma}{K})^n, \qquad \ldots (4.3)$$

where *K* is the strength coefficient and *n* are the hardening exponent.

For the damage model, which predicts the energy that must be absorbed by the individual nanofiber to fail under stress, Equation 5 is used, which is based on the concept of fracture energy and linear plastic displacement:

$$G_f = \frac{1}{2}\sigma_f \cdot \Delta_f \qquad \ldots (4.4)$$

where G_f is the fracture energy (μN/μm) representing the energy absorbed by the individual nanofiber until failure, σ_f is the stress at failure, and Δ_f is the linear plastic displacement at failure.

Together, these equations form the basis for the material model used in the study, enabling comprehensive analysis of the mechanical behaviour of nanofiber mats from elastic response through plastic deformation to ultimate failure.

4.6. Experimental Predicted Mechanical Properties of Single Nanofiber

The exploration into the mechanical characteristics of nanofiber mats has advanced to encompass the analysis of the stress-strain responses anticipated for individual nanofibers, especially after contemplating the porosity impact within the mats.

Figure 4.3 elucidates the modeled elastoplastic behaviour of a singular nanofiber, achieving this through the theoretical exclusion of porosity's effects from the nanofiber mats. This methodology facilitates a more focused evaluation of the nanofibers' intrinsic mechanical characteristics, detached from the structural idiosyncrasies of the mats.

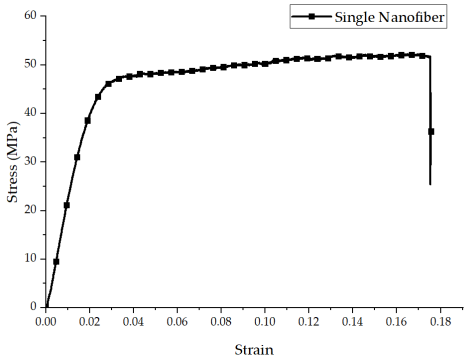

Figure 4.3 Representative stress–strain graph for a single nanofiber.

This scrutiny unveiled that the elastic modulus of an individual nanofiber far exceeds that noted in the aggregated mats, recorded at 2100 ± 110 MPa. This marked elevation underscores the intrinsic rigidity and resilience of singular nanofibers, which might be tempered in a collective material format due to porosity and fiber distribution variances. Moreover, the ultimate tensile strength (UTS) of a single nanofiber was identified at 51.9 ± 5 MPa. This figure, inferred from the elongation at break data of oriented nanofibers, mirrors the formidable tensile potential of the fibers, with the elongation at break strain consistently noted at 0.19 ± 0.02.

Employing the mechanical attributes of the singular nanofiber to validate the finite element (FE) model facilitated the prediction of the nanofiber mat's mechanical conduct. This strategy assured that both theoretical and computational frameworks accurately embody the

inherent properties of the nanofibers, enabling a more refined simulation of the nanofiber mats' response to applied stresses. By juxtaposing the properties of singular fibers against the collective behaviour of the mats, this methodology erects a solid foundation for comprehending and foreseeing the utility of nanofiber-based constructs in real-world scenarios, underscoring the pivotal role of individual fibre characteristics in material design and application efficacy.

4.7. Convergence and Validation of Developed FE Model

To assure the accuracy and reliability of the Finite Element (FE) Model, its initial construct was based upon data derived from empirical observations. This prototype model encapsulated a domain of dimensions 100 µm by 100 µm and was set to a porosity level of 75%. The fibres within this model were aligned within a confined angular scope of 11 degrees, oscillating between +5.5 and -5.5 degrees, each fibre uniform in diameter at 580 nm and varying in length from 70 µm up to 100.47 µm, contingent upon their angular orientation relative to the X-axis. The nanofibers' elastic modulus was fixed at 2100 MPa, with a Poisson's ratio of 0.4, laying down the fundamental material characteristics for simulation purposes. A longitudinal displacement of 20 µm, equating to 20% of the domain's length, was administered, setting the requisite fracture energy for fibre severance at 13 µN/µm. Throughout the simulations conducted in Abaqus, micrometres (µm) were consistently employed as the unit of measure. Figure 4.4 delineates the normal stress along the x-axis in an oriented nanofiber mat subjected to displacement.

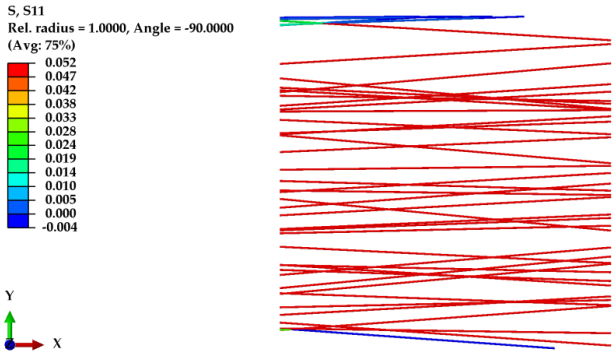

Figure 4.4 Normal stress along the X-axis for oriented nanofiber mat under displacement.

Mesh refinement's influence on the developed FE Model is depicted in Figure 4.5, utilising identical geometry and parameters albeit with an increased element count, approximately 2.5-times. This graph place alongside the normal stress-strain reactions of systems comprising 842 elements (illustrated through a solid black line) against those with 2093 elements (depicted by a dashed red line). The findings indicate that the augmentation in element count does not markedly alter the stress-strain dynamics of the oriented fibres, attributed to the calculation of reaction force in relation to the domain's cross-sectional area.

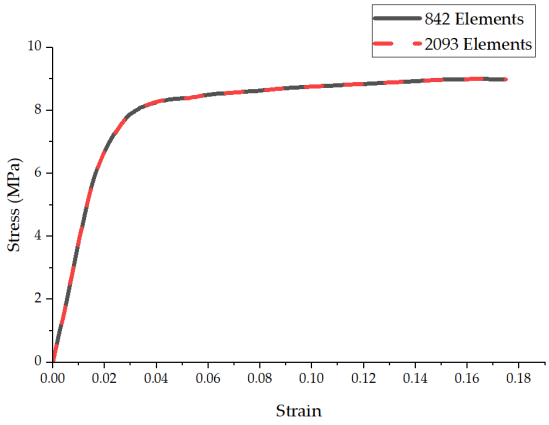

Figure 4.5 Mesh refinement of the FE model for oriented nanofibers.

To emulate the random fibre structure and corroborate experimental findings, a similar domain dimension of 100 μm by 100 μm was adopted, this instance incorporating an 80% porosity with fibres of 720 nm diameter, and lengths spanning from 30 μm to 141.44 μm, dependent on their angular disposition relative to both the X and Y axes. Fibres were scattered randomly within the domain, with displacements applied along both the X and Y axes for comparative analysis. Figure 4.6 and Figure 4.7 exhibit the normal stress and von Mises stress respectively, in the randomly structured nanofiber mats under displacement.

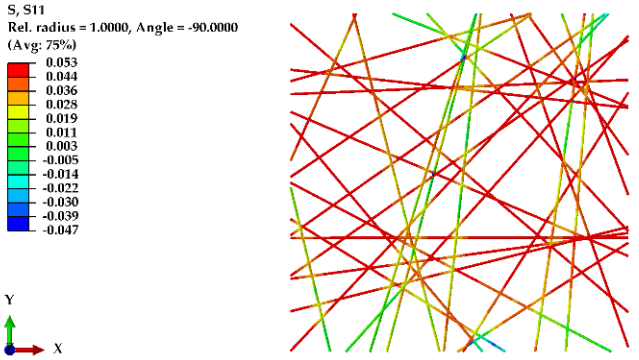

Figure 4.6 Normal stress along the X-axis in random structure of nanofibers under X-axis displacement.

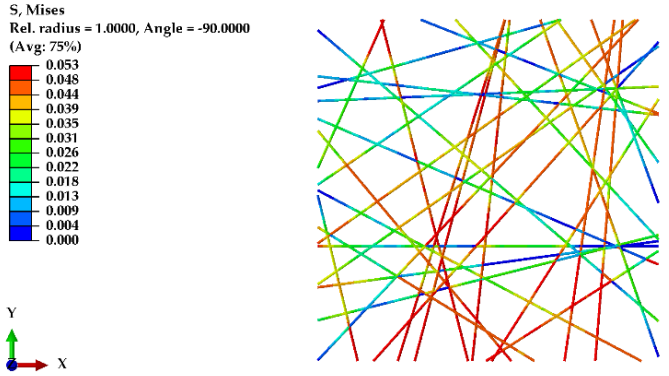

Figure 4.7 von Mises stress in random fibers under Y-axis displacement.

Figure 4.8 synthesises the FE model's prognostications concerning the mechanical behaviours of nanofiber mats with both oriented and randomly structured fibres, where grey region represents experimental results and red line represents the results obtained from the FE model. Regarding the random structure, empirical data suggested analogous mechanical responses across both transverse and longitudinal orientations. The FE model successfully mirrored this finding, indicating almost indistinguishable stress reactions for both axes in the random configuration.

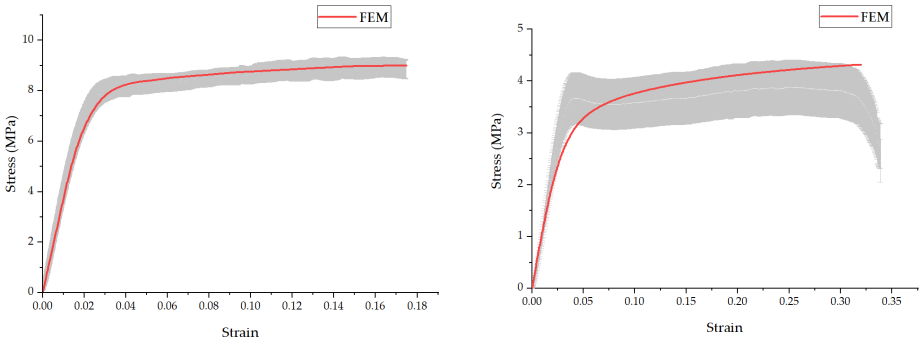

(a) (b)

Figure 4.8 Comparison of FE model predictions for (a) oriented and (b) random structured nanofiber mats, highlighting its accuracy in simulating mechanical behaviours.

In the transverse orientation, the integrity of the oriented fibres predominantly hinges on the requisite strength to disrupt the inter-fibre bonds, as the absence of fibres in this direction precludes transverse reaction forces. This limitation confines the model's predictive accuracy to scenarios wherein some fibres align with the loading direction, underscoring a pivotal facet of the model's utility in gauging the mechanical attributes of nanofiber mats across various orientations.

The examination of random nanofiber mats unearthed a notable elastic region peak, attributable to a handful of fibres in alignment. Upon reaching their tensile thresholds, these fibres rupture, relegating the load to adjacent fibres of varying orientations. Within the FE model's framework, these initially aligned fibres, upon encountering their failure thresholds, are deemed compromised and no longer contribute to load bearing, with the burden subsequently reallocated to angular fibres.

This accounts for the FE model's depiction of a seamless progression from the elastic to the plastic phase, accurately reflecting the complex mechanical responses of nanofiber mats under duress. Contrary to direct empirical outcomes, where a pronounced peak in the stress-strain graph signifies the initial aligned fibres' failure, the FE model delineates a more nuanced transition from elastic deformation to plastic flow, congruent with findings from several studies. This model’s capacity to mimic the incremental degradation and failure of individual fibres, alongside the stress redistribution among surviving fibres, elucidates discrepancies that physical experiments might not readily capture.

4.8. Effect of Structural Parameters on Strength of the Nanofiber Mat

This section delves into the exploration of how structural parameters such as fibre diameter, orientation, porosity, and the length-to-width (L:W) ratio distinctly influence the mechanical integrity, specifically focusing on the elastic modulus and ultimate tensile strength (UTS) of nanofiber mats. Adopting a methodical approach, the study manipulated one variable at a time while maintaining the constancy of other factors to discern their individual contributions. The predefined domain for this analysis spanned 100 µm by 100 µm, with all material characteristics reflecting those experimentally observed in single nanofibers.

In the case of oriented fibers, the study ensured alignment within a precise angular alignment of 10 degrees. Conversely, for the random fibre configurations, no such constraints were imposed, allowing for an unrestricted fibre orientation distribution. The porosity level across all experiments was standardized at 75%, aiming to replicate a common structural characteristic found in electrospun nanofiber mats. Furthermore, the nominal diameter of the nanofibers was set at 600 nm, a value representative of the common dimensions encountered in the fabrication of such mats.

The intricate interplay between these structural parameters and the mechanical properties of nanofiber mats is critical for tailoring these materials for specific application needs. By systematically varying each parameter, this study aims to shed light on the structural determinants of mechanical performance in nanofiber mats, thereby enabling the design and fabrication of nanofiber-based materials with optimized mechanical properties. The findings from this analysis are anticipated to contribute significantly to the body of knowledge on nanofiber mats, paving the way for their enhanced application in fields where specific mechanical characteristics are paramount.

4.8.1. Effect of Nanofiber Diameter

An in-depth exploration was undertaken to assess the impact of nanofiber diameter on the mechanical attributes of nanofiber mats, spanning diameters from 150 nm to 900 nm, within both oriented (O) and randomly structured (R) configurations. The analysis, as illustrated in Figure 4.9, divulges those oriented nanofibers possessing a minimal diameter of 150 nm exhibited an elastic modulus of 374 ± 3 MPa alongside a UTS of 8.6 ± 0.2 MPa. Conversely, when the diameter was augmented to 900 nm, a slight diminution was observed, with the elastic modulus dropping to 337 ± 7.8 MPa and the UTS decreasing to 8.1 ± 0.1 MPa. This observed decrement in mechanical strength as the diameter increases is attributed to the augmented likelihood of thicker fibres engaging with the domain's upper or lower confines, consequently exempting them from contributing to the structural integrity of the mat. This effect is

significantly less pronounced in fibres of lesser diameter, owing to the reduced probability of such fibres extending to the domain's extremities.

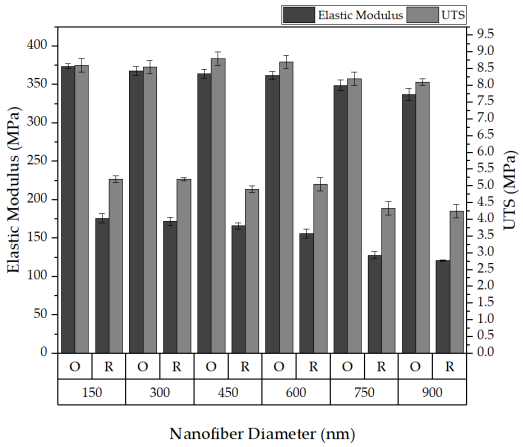

Figure 4.9 Effect of the nanofiber diameter on elastic modulus and UTS.

4.8.2. Effect of Orientation

The study delved into the impact of fibre orientation on the mechanical properties of nanofiber mats, with orientations scrutinised at 10 degrees, 30 degrees, and 45 degrees. As depicted in Figure 4.10, fibres aligned within a narrow 10-degree window showcased an elastic modulus of 385 ± 8 MPa and an ultimate tensile strength (UTS) of 9.16 ± 0.3 MPa. Conversely, at a broader 45-degree orientation, a marked decrease in mechanical strength was observed, with the elastic modulus dropping to 216 ± 12 MPa and the UTS reducing to 5.5 ± 0.5 MPa. These findings underscore the pivotal influence of fibre orientation on the overall mechanical integrity of nanofiber mats, demonstrating that tighter alignment correlates with enhanced mechanical properties.

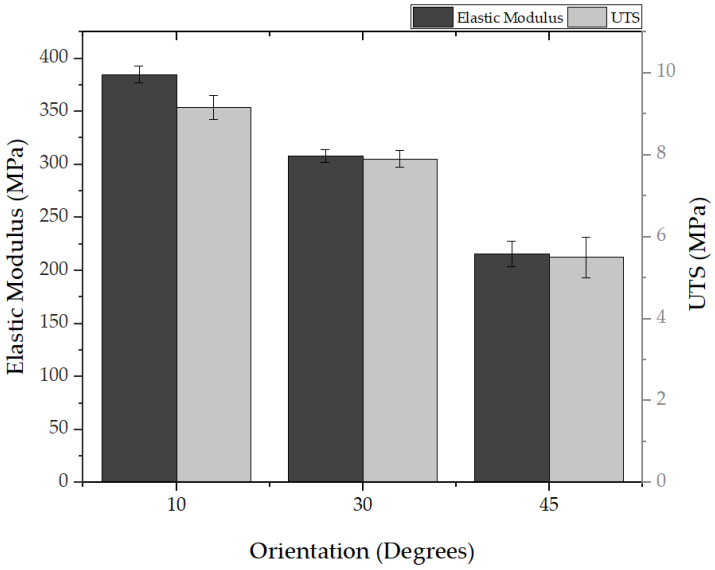

Figure 4.10 Effect of orientation on the elasticity and UTS.

4.8.3. Effect of Porosity

The study further delved into the impact of porosity levels on the mechanical characteristics of nanofiber mats, exploring porosities of 50%, 70%, and 90%. As depicted in Figure 4.11, at a porosity of 50%, the elastic modulus and ultimate tensile strength (UTS) for oriented fibres significantly exceeded those of the random structure, registering at 743 ± 12 MPa and 18.1 ± 2 MPa, respectively, compared to 340 ± 8 MPa and 9.1 ± 0.8 MPa for the latter. These findings indicate that a higher porosity level correlates with diminished mechanical properties across both fibre configurations.

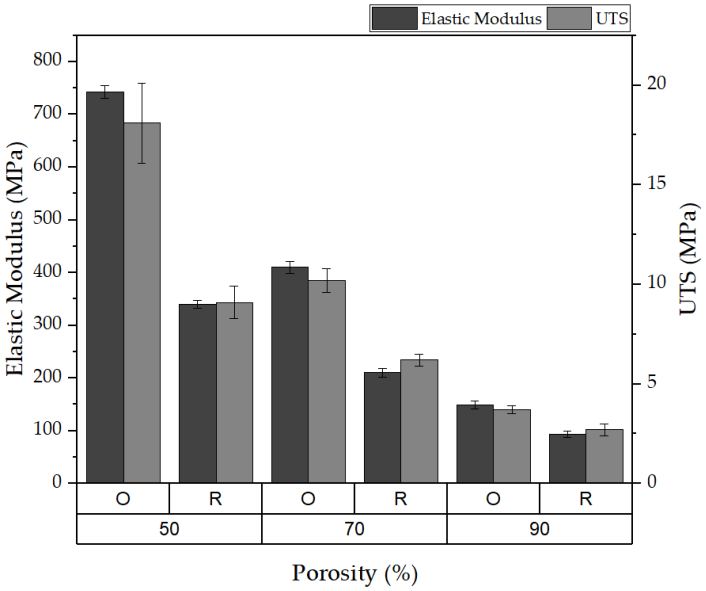

Figure 4.11 Effect of porosity on elasticity and UTS.

The investigation confirmed the anticipated relationship between porosity and the mechanical strength of nanofiber mats: mats with reduced porosity, signifying a denser arrangement of fibres, exhibited superior rigidity and tensile strength relative to their counterparts with increased porosity (M. Zhang et al., 2019). A particularly noteworthy observation was the almost linear decline in mat stiffness corresponding to the rise in porosity, highlighting the crucial role of fibre density in influencing the mechanical behaviour of nanofiber mats.

4.8.4. Effect of the L:W ratio

The study extended to assess the influence of the length-to-width (L:W) ratio on nanofiber mats by varying the domain's length from 200 µm to 300 µm, while keeping the height constant. Figure 4.12 elucidates those alterations in the L:W ratio significantly influenced the mechanical characteristics of mats with random fibre orientations, manifesting anisotropic tendencies as the ratio shifted. Conversely, mats comprised of oriented fibers exhibited stable mechanical properties, undisturbed by variations in the L:W ratio.

When exploring the L:W ratio, a discernible trend emerged showing a decline in elastic modulus with an elevation in the L:W ratio for mats with a random fibre distribution. This trend underscores that an augmented domain length relative to its width weakens the mat's structural

resilience in terms of elasticity. Such a phenomenon is likely due to a greater propensity for non-homogeneous stress distribution and localized deformation within elongated configurations.

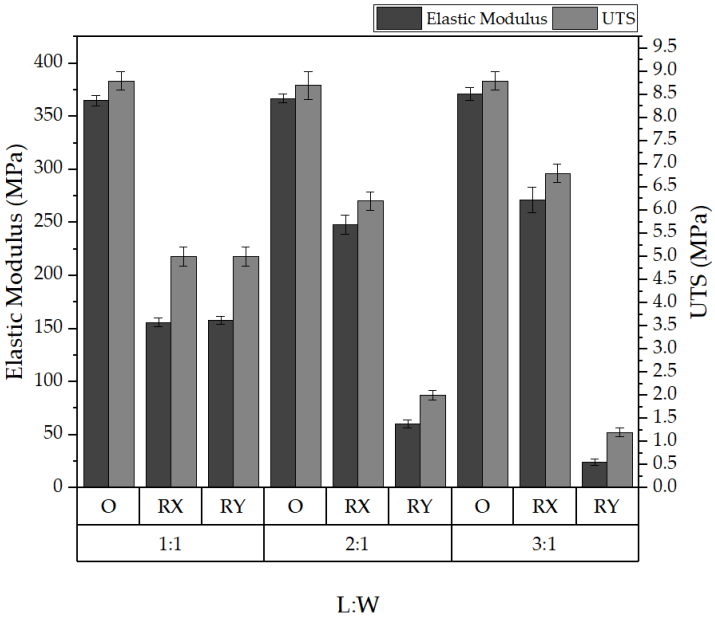

Figure 4.12 Effect of the L:W ratio on elastic modulus and UTS.

This extensive investigation underscores the profound impact that structural attributes—namely, fibre diameter, orientation, porosity, and the L:W ratio—have on the mechanical performance of nanofiber mats. It revealed that while randomly arranged fibers display anisotropic mechanical behaviours in response to varying L:W ratios, oriented fibers maintain their mechanical integrity, underlining the critical role of structural configuration in tailoring nanofiber-based materials for specific end-use applications.

However, this study's reliance on computational modelling brings with it inherent limitations. One such limitation is the assumption of a 100% perfect bonding condition, disregarding potential debonding occurrences amongst intersecting fibers. Real-world scenarios often see variations in bonding strength, with insufficient bonding leading to fractures that critically alter the mat's mechanical properties (Choi et al., 2004; Stockdale et al., 2020). The presumption of perfect interfibre bonding in this analysis does not encompass the variability in bonding effectiveness and its potential repercussions on the mat's structural stability.

Moreover, the model overlooks frictional interactions between unbonded, contacting fibers. In practice, slippage among fibers can significantly influence the distribution of load and the mechanical response of mats under stress (N. Chen et al., 2016; Ridruejo et al., 2011). By omitting frictional considerations, the model simplifies fibre interactions but fails to capture the intricate dynamics of fibre movement and interactions under applied loads.

Another noted limitation is the exclusive use of straight fibers within the model, neglecting the impact of fibre curliness or curvature on the mats' mechanical attributes. Previous studies have highlighted the significance of fibre geometric characteristics, including curvature, in defining the overall mechanical efficacy of fibre mats. Therefore, the exclusion of fibre curvature from the model potentially restricts the precision of the mechanical behaviour predictions.

4.9. Conclusions of developed FE Model

The development and validation of a Finite Element (FE) model specifically crafted to explore the mechanical behaviours of electrospun nanofiber mats has been elucidated in this chapter. A standout feature of this model is its incorporation of individual nanofibers' mechanical properties, such as elastic modulus and ultimate tensile strength, to predict the mats' elastoplastic response under varying conditions. By adjusting structural parameters including nanofiber diameter, orientation, porosity, and the length-to-width ratio, the model offers comprehensive insights into their impact on the mats' mechanical properties.

1. A key achievement of this model is its accuracy in simulating the complex mechanical interactions within nanofiber mats, validated by the alignment of simulation outcomes with experimental findings. This precision in forecasting the mats' elastic-plastic tensile behaviour underscores the model's efficacy in predicting the performance of nanofiber-based materials in practical scenarios.
2. The analysis conducted reveals a nuanced understanding of how structural parameters influence the mechanical properties of the mats. For instance, a decrease in mechanical properties with increasing nanofiber diameter suggests that thinner fibers enhance the load-bearing capacity more effectively. Similarly, the orientation of fibers significantly affects the mats' mechanical properties, with oriented fibers displaying superior mechanical strength and stiffness compared to their randomly arranged counterparts. Furthermore, the model's findings on porosity and the

length-to-width ratio highlight the critical role of structural design in optimizing nanofiber-based materials for specific applications.

3. The assumptions underlying the model's development, such as perfect bonding among fibers, simplify the intricate fibre interactions within nanofiber mats. However, these assumptions may overlook the potential effects of debonding or friction among fibers, as well as the influence of fibre curvature, which could refine the understanding of the mats' mechanical properties. In conclusion, the FE model presented serves as a valuable tool for investigating the mechanical characteristics of nanofiber mats, offering significant insights for the design and optimization of nanofiber-based materials. The identification of limitations suggests avenues for future enhancements to the model, potentially including considerations of inter-fibre friction, variability in bonding strength, and the effects of fibre curvature for more detailed and accurate predictions of nanofiber mat behaviour.

5. EXPERIMENT OF THE EFFECT OF ANNEALING ON PAN NANOFIBER MATS

In the realm of electrospinning, numerous methods have been explored to improve the mechanical properties of nanofiber membranes. These methods include cross-linking, annealing, hot stretching, hot pressing, solvent welding, and drawing, each offering unique advantages. Among these, annealing stands out as a prevalent technique, primarily due to its efficacy in enhancing the strength of polymers. However, the influence of annealing extends beyond merely bolstering mechanical characteristics. This process also significantly affects the morphology and thermal properties of nanofiber membranes. In this chapter, I have delved into a comprehensive discussion on the multifaceted impacts of annealing, examining how it alters the structural and thermal dynamics of nanofiber membranes, thereby contributing to their overall performance and application potential. The content of this chapter is also available for reference in a published format (J. V. Sanchaniya, Lasenko, Kanukuntala, et al., 2023).

5.1. Objective of Annealing on PAN Nanofiber Mats

Polyacrylonitrile (PAN), a key player in the realm of semicrystalline synthetic polymers, exhibits unique characteristics that make it indispensable in various applications. Notably, its hydrophobic nature and limited solubility in most solvents—excluding specific polar aprotic solvents and mineral salts—define its usage (Musale & Kumar, 2000; Scharnagl & Buschatz, 2001). PAN's thermoplastic properties are particularly intriguing; it tends to decompose before melting when heated at rates below 80 °C/min, with initial degradation commencing at 250 °C and a degradation temperature of 317 °C (Gupta et al., 1998; Nataraj et al., 2012). These properties render PAN an essential material for electrospinning, leading to the production of PAN nanofibers, which serve as the foundation for continuous carbon nanofibers through stabilization and carbonation processes (L. Feng et al., 2014), and find applications in filtration (H. Zhang et al., 2010) and catalysis (Guo et al., 2011; P. Zhang et al., 2011).

PAN nanofibers, owing to their extensive surface area and electrostatic properties, are highly efficient in filtering applications. They play a crucial role in air and water filtration, biofluid purification, and the removal of toxic substances from contaminated water (Duan et al., 2019; Zhou et al., 2022). Their ability to effectively capture airborne particles, including dust and microorganisms during air filtration, and to remove pollutants in water filtration demonstrates their versatility (Jamil et al., 2021; Lee et al., 2018). Additionally, their

biocompatibility and ecological safety make them ideal for medical and biological applications, such as in dialysis machines, wound dressings, and tissue engineering scaffolds (Radu et al., 2023).

However, a challenge arises from the random orientation and varying diameters of fibers in electrospun mats, which can limit their mechanical performance in practical applications. The strength of the nanofibers, often insufficient for certain uses, is a key area of focus (Lasenko et al., 2023; J. V. Sanchaniya et al., 2022). The use of rotating drum collectors to produce oriented nanofibers can enhance their strength. Understanding the mechanical properties of these oriented nanofibers, especially in the longitudinal and transverse directions, is crucial. After testing, the effect of annealing on the transverse direction of the nanofiber mat with oriented fibers is particularly noteworthy.

The strength of electrospun nanofibers is influenced by factors such as the type of polymer, the rate of crystallization, and the level of crystallinity. The strength and deformation mechanisms in nonwoven materials depend on the fibers and their interconnections (Backer & Petterson, 1960). Given the challenges posed by random fibre alignment, insufficient fibre adhesion, and excessive porosity, enhancing the mechanical properties of electrospun nanofiber mats is essential for expanding their potential applications (Z. M. Huang et al., 2003). Various techniques, including cross-linking, annealing (Z. Wang et al., 2014), hot stretching (Z. Song et al., 2010), hot pressing (Z. Wang et al., 2020), solvent welding (Sallakhniknezhad et al., 2021), and drawing (Xu et al., 2020), have been explored to improve these properties. Notably, the incorporation of nanoparticles during the fabrication of electrospun fibers can increase the mechanical properties of polymeric nanofiber mats by 35–65% (Albetran, 2021; A. Li et al., 2022; Mondal et al., 2022; Wijerathne et al., 2023; Xiang & Frey, 2016). Nanosized materials like carbon nanotubes and graphite oxide nanoplatelets reinforce the strength of individual nanofibers, akin to the addition of short fibers in strengthening structures (Habeeb et al., 2023).

Previous research has demonstrated the effectiveness of annealing in enhancing the tensile strength and Young's modulus of nanofibers. For instance, annealing electrospun poly(L-lactic acid) (PLLA) at 75 °C for 24 hours resulted in an increase in Young's modulus from 4.7 GPa to 11.1 GPa (Tan & Lim, 2006). Similarly, annealing chitosan–gelatine (CG) membranes at various temperatures in a vacuum oven improved both Young's modulus and tensile strength (Ramaswamy et al., 2011). Another study investigating the thermal treatment of poly(L-lactic acid) doped with multiwalled carbon nanotubes at temperatures near Tg and

Tm highlighted the importance of selecting appropriate annealing temperatures (Es-Saheb & Elzatahry, 2014).

The objective of this chapter is to enrich the existing knowledge base on oriented PAN electrospun nanofibers by examining the effects of annealing at various temperatures. While prior studies have explored this area, there has been limited focus on the specific impacts of annealing on oriented PAN nanofiber mats produced via electrospinning and collected using rotating drum collectors. This study aims to address this research gap by conducting a detailed analysis of the changes in morphology, mechanical properties, and thermal behaviour of PAN nanofibers subjected to different annealing conditions, thereby offering valuable insights into their behaviour and potential applications.

5.2. Materials and Methodology of Annealing on Oriented PAN Nanofibers

To investigate the effects of annealing on oriented polyacrylonitrile (PAN) nanofibers, we commenced with the production of electrospun nanofibers. Following the protocol outlined in Chapter 3, PAN powder was combined with N,N-dimethylformamide to create the electrospinning solution. The annealing process, a crucial part of this study, was conducted using a Nabertherm LH 30/13 furnace, sourced from Nabertherm GmbH, Lilienthal, Germany.

Each nanofiber mat, referenced in Figure 5.1d, underwent a precise annealing regimen. Initially placed in the furnace at ambient room temperature, the mats were systematically heated to specific target temperatures of 70 °C, 140 °C, 210 °C, and 280 °C. This heating process was conducted at a controlled rate of 10 °C/min. Upon reaching the target temperature, the mats were maintained at that constant temperature for a duration of 5 minutes, ensuring uniform heat treatment. Subsequent to this, the mats were allowed to cool back to room temperature at the same rate of 10 °C/min. post-annealing, all samples were stored under controlled conditions at 22 ± 1 °C and a relative humidity of less than 60% for 48 hours to stabilize. The complete methodology, encapsulating the spinning and annealing of nanofibers, is succinctly summarized in Figure 5.1.

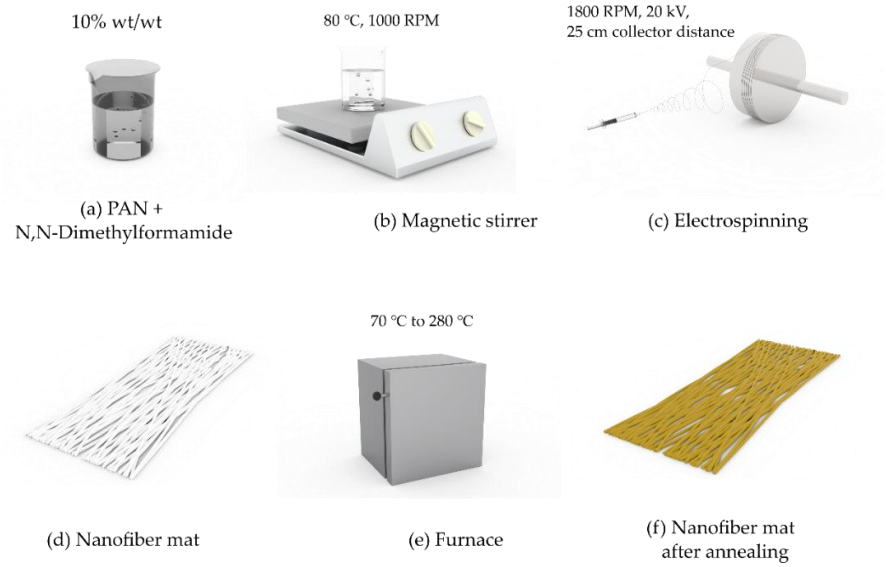

Figure 5.1 The fabrication process of nanofibers and annealing: (a) preparation of the PAN and N, N-dimethylformamide mixture; (b) magnetic stirring of the mixture at 80 °C and 1000 rpm; (c) fabrication of an electrospun nanofiber mat; (d) nanofiber mats; (e) annealing nanofiber mats inside the furnace; (f) annealed nanofiber mats.

For a comparative analysis of the morphology and tensile strength along the longitudinal direction (aligned with the orientation of the nanofibers), it was meticulously sectioned a single electrospun nanofiber mat, measuring 440 mm by 50 mm, into six equal parts. Each segment was then subjected to tensile testing to evaluate the strength in the longitudinal direction. To assess the strength in the transverse direction (perpendicular to the fibre orientation), an identically produced nanofiber mat was utilized.

The evaluation of morphology, mechanical testing, and thermal properties was conducted as detailed in Chapter 3. This comprehensive analysis included a range of techniques to assess the alterations in the nanofibers post-annealing, thereby providing a thorough understanding of the changes in their structural, mechanical, and thermal characteristics due to the annealing process.

5.3. Morphology Analysis

Figure 5.2 provides a visual comparison of PAN nanofiber mats before and after the annealing process. It was observed that untreated mats and those annealed at lower temperatures (70 °C and 140 °C) retained their original white coloration. However, as the

annealing temperature increased, notable colour changes were observed. Mats annealed at 210 °C exhibited a pale-yellow hue, while those treated at 280 °C turned golden, indicative of the onset of degradation. At 350 °C, the nanofibers appeared thoroughly degraded, turning a distinct black colour and becoming too frail for further thermal or tensile testing. This colour transition from light yellow to brown during annealing was also noted in our previous studies (Lasenko et al., 2022).

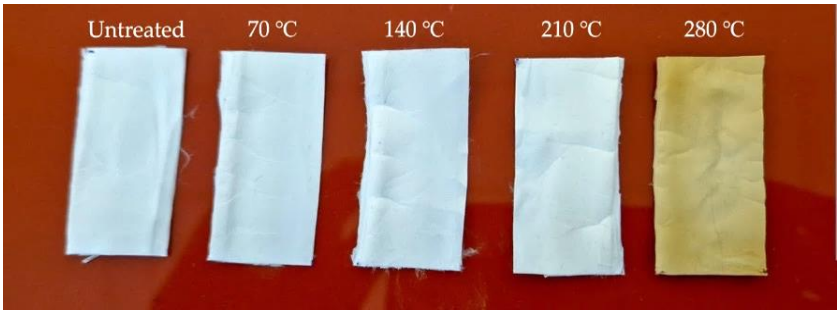

Figure 5.2 Samples of PAN nanofiber mats after annealing

In Figure 5.3, shows the morphology of PAN nanofibers. Figure 5.3a presents a scanning electron microscopy (SEM) image of an untreated nanofiber mat. Fast Fourier transform (FFT) analysis on this image (Figure 5.3b) provided insights into the alignment of the PAN nanofibers post-annealing. Despite the drum rotating at 1800 rpm during electrospinning, the FFT alignment values fluctuated minimally, mostly remaining within the 0.0 to 0.085 range, indicating that most nanofibers were aligned in a single direction. This consistency in alignment, influenced by the constant rotational speed of the drum, also contributed to a uniform diameter of the nanofibers. The anisotropy observed is a critical factor in determining the mechanical properties of the mats; mats with randomly aligned fibers exhibit lower strength compared to those with unidirectionally aligned fibers. Furthermore, a higher rotational speed of the drum collector (over 1000 rpm) resulted in better alignment of the nanofibers compared to lower speeds (Kim, 2008).

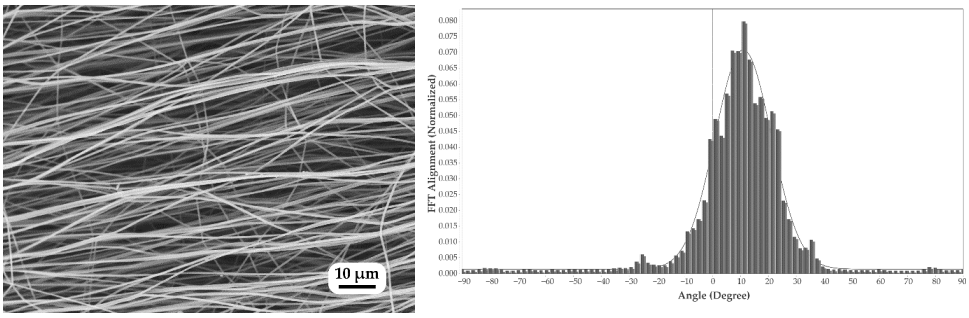

(a) (b)

Figure 5.3 Morphology of nanofibers: (a) untreated nanofibers and (b) orientation of untreated nanofibers.

Figure 5.4 presents SEM images comparing control samples of PAN nanofibers before and after annealing at 140 ℃. It was noted that the average diameter of untreated electrospun PAN nanofibers was 532 ± 28 nm. Annealing at 70 °C resulted in a minor change in diameter, measuring 526 ± 32 nm. However, a significant reduction to 434 ± 21 nm was observed when annealed at 140 °C. This diameter remained relatively stable with further increases in annealing temperature, showing no significant change until degradation commenced at 350 °C.

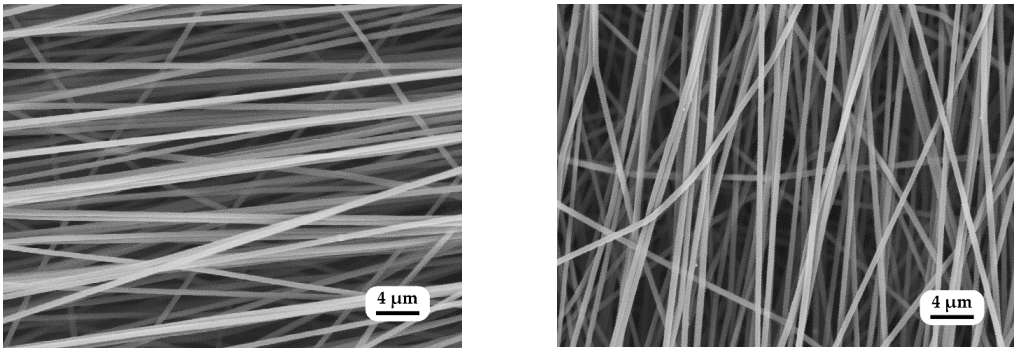

(a) (b)

Figure 5.4 SEM image of nanofiber mats and changes in the diameter of the nanofibers: (a) untreated and (b) annealed at 140 °C.

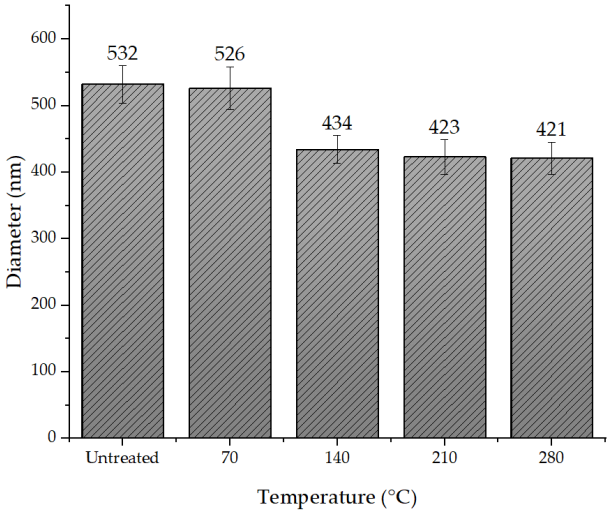

Figure 5.5 Relationship between the nanofiber diameter and annealing.

The relationship between nanofiber diameter and annealing temperature is depicted in Figure 5.5. Statistical analysis, particularly the calculation of p-values, revealed a significant difference in the diameter of nanofiber mats annealed at 70 °C and 140 °C, with a threshold significance level set at 0.05.

The study found that the diameter of PAN nanofibers generally decreased by approximately 20% when annealed at 140 °C, a trend consistent with findings from other research groups. As the annealing temperature increased, the diameter continued to reduce until it stabilized at 210 °C, beyond which no significant change was observed until the onset of degradation at 350 °C. This reduction in diameter and consequent increase in packing density is attributed to several factors (Liang et al., 2013; Sheng et al., 2016).

Firstly, the initial electrospinning process involves dissolving PAN in a solvent, which likely evaporates upon heating, causing fibre contraction (Tan & Lim, 2006). Secondly, PAN, being a thermoplastic polymer, undergoes degradation under high temperatures, leading to a reduction in fibre diameter as the polymer chains break down and occupy less space (Barua & Saha, 2017). Finally, with increasing temperature, polymer chains contract and transition from a solid to a more flexible, liquid-like state, further decreasing fibre diameter. The extent of diameter reduction is influenced by various processing conditions, including temperature, heating rate, and duration.

5.4. Experimental Mechanical Properties of Annealed PAN Nanofibers

In this section, the mechanical properties of annealed polyacrylonitrile (PAN) nanofibers are explored, focusing on their stress-strain behaviour. Figure 5.6a,b presents the stress (σ)–strain (ε) curves for untreated and annealed PAN nanofiber mats in both the longitudinal and transverse directions. Additionally, Table 5.1 compiles the average values derived from these tests.

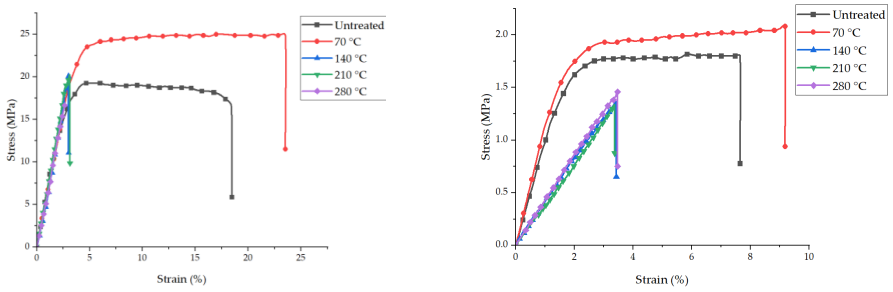

(a) (b)

Figure 5.6 Representative stress–strain graphs of oriented PAN nanofiber mats: (a) longitudinal direction; (b) transverse direction.

Table 5.1
Average mechanical properties of oriented PAN nanofiber mats in longitudinal and transverse directions.

	Annealed PAN Nanofiber Mats	**Thickness, t (μm)**	**Tensile Strength σ at Break (MPa)**	**Young's Modulus, E (MPa)**	**Elongation at Break, ε at Break (%)**
Longitudinal	Untreated	156 ± 7	19.1 ± 3	610 ± 30	18.2 ± 2
	70 °C	154 ± 5	25.2 ± 2	650 ± 21	23.6 ± 2
	140 °C	121 ± 5	19.5 ± 1	598 ± 26	3.1 ± 0.3
	210 °C	119 ± 4	19.7 ± 1	595 ± 24	3.1 ± 0.2
	280 °C	114 ± 4	16.8 ± 1	596 ± 23	3.0 ± 0.1
Transverse	Untreated	153 ± 9	1.7 ± 0.1	97 ± 6	7.6 ± 1
	70 °C	154 ± 6	2.1 ± 0.1	115 ± 8	9.2 ± 1
	140 °C	125 ± 5	1.7 ± 0.1	44 ± 3	3.3 ± 0.2
	210 °C	117 ± 4	1.3 ± 0.1	42 ± 3	3.3 ± 0.2
	280 °C	113 ± 5	1.4 ± 0.1	45 ± 2	3.4 ± 0.1

During the tensile testing, it is ensured that the clamping pressure was sufficient to prevent failure at the grips. The stress-strain graphs highlighted an intriguing finding: the strength of the PAN nanofiber mat annealed at 70 °C was higher than that of the untreated mat.

Specifically, the untreated mat exhibited a tensile strength of 19.1 ± 3 MPa and a Young's modulus of 610 ± 30 MPa. Following annealing at 70 °C, there was a notable increase in both tensile strength (to 154 ± 5 MPa) and Young's modulus (to 25.2 ± 2 MPa), along with an elongation at break from 18.2 ± 2% to 23.6 ± 2%.

However, for all PAN nanofiber mats annealed above the glass transition temperature of 90 °C, a consistent decrease in tensile strength, Young's modulus, and elongation at break was observed. For instance, a mat annealed at 140 °C showed a tensile strength of 19.5 ± 1 MPa, Young's modulus of 598 ± 26 MPa, and an elongation at break of 3.1 ± 0.2%. At higher temperatures (210 °C and 280 °C), the tensile strength values were 19.7 ± 1 MPa and 16.8 ± 1 MPa, respectively, with Young's modulus values of 595 ± 24 MPa and 596 ± 23 MPa.

Statistical analysis revealed that the changes in mechanical properties of the nanofibers when untreated and annealed at 70 °C were significant. The thickness of the nanofiber mat annealed at 140 °C decreased markedly from 154 ± 5 µm to 121 ± 5 µm. A similar trend was observed in the transverse direction: tensile strength at 70 °C increased by 23%, elongation at break by 21%, and elastic modulus by 18%.

For nanofibers collected using a rotating drum collector at speeds exceeding 1000 rpm, an increase in tensile strength was attributed to improved orientation (W. J. Li et al., 2007; Pham et al., 2021). Young's modulus and tensile strength increased as the diameter of the fibers decreased below 700 nm, aligning with studies suggesting that mechanical properties of nanofibers exponentially increase as fibre diameter approaches this critical value (Arinstein et al., 2007; Wong et al., 2008; Yao et al., 2014). The average diameter of PAN electrospun nanofibers in our study was 532 ± 28 nm, with tensile strength and Young's modulus recorded at 19.1 ± 3 MPa and 610 ± 30 MPa, respectively (Table 4.1), corroborating our previous results with oriented PAN nanofibers.

Annealing, a process of heating and cooling materials to alter their physical and mechanical characteristics, affects polymers by modifying their crystallinity. It can enhance the modulus and tensile strength of undrawn materials. However, changes in mechanical properties of annealed polymers are sometimes inversely proportional to the annealing temperature, with significant changes often observed near the glass transition temperature (L. Huang et al., 2013). The improvement in mechanical performance may result from enhanced crystallinity (Srithep et al., 2013). In our results, annealing at 70 °C led to an increase in tensile strength (from 19.1 ± 3 MPa to 25.2 ± 2 MPa) and a rise in Young's modulus (from 610 ± 30 MPa to 650 ± 21 MPa), along with a 20% reduction in nanofiber diameter at 140 °C.

Heating can align polymer chains in nanofibers, leading to higher chain orientation and improved tensile strength. However, our findings indicated that annealing PAN nanofibers at temperatures exceeding the glass transition temperature (Tg), particularly at 140 °C and above, resulted in a significant reduction in mechanical properties. This decline could be attributed to the volatilization of the solvent used in electrospinning at temperatures over 100 °C. During annealing, high temperatures cause solvent evaporation within the nanofiber mat, leading to structural and morphological changes. This solvent evaporation induces nanofiber contraction and rearrangement, resulting in higher packing density and decreased intermolecular interactions.

Furthermore, exposure to oxygen during annealing can induce oxidation reactions, altering the chemical structure and properties of the fibers. Oxidation can degrade polymer chains, decreasing the mechanical integrity of the nanofibers. The introduction of oxygen may break down polymer chains, weakening the forces responsible for the mechanical characteristics of the nanofiber mat.

In summary, heating PAN nanofibers at 70 °C enhances their mechanical properties by improving chain orientation and material density, resulting in increased tensile strength, elongation, and Young's modulus. Conversely, annealing above the glass transition temperature or up to the solvent evaporation point can degrade the mechanical properties of the nanofiber mat.

5.5. Experimental Thermal Properties of Annealed PAN Nanofibers

This section delves into the thermal behaviour of polyacrylonitrile (PAN) nanofibers, both untreated and annealed, through thermogravimetric analysis (TGA) and differential scanning calorimetry (DSC).

Figure 5.7 presents the TGA graphs for PAN powder, untreated nanofiber mats, and annealed nanofiber mats, illustrating their thermal degradation patterns. A notable, sharp decline in weight, indicating a mass loss of up to 30%, was consistently observed at approximately 290 °C across all samples. This mass loss points to the rapid degradation of PAN. Specifically, the PAN powder showed degradation at 291.6 °C, while nanofiber mats annealed up to 210 °C degraded around the same temperature. Interestingly, the nanofiber mat annealed at 280 °C exhibited a higher degradation temperature of 301.8 °C.

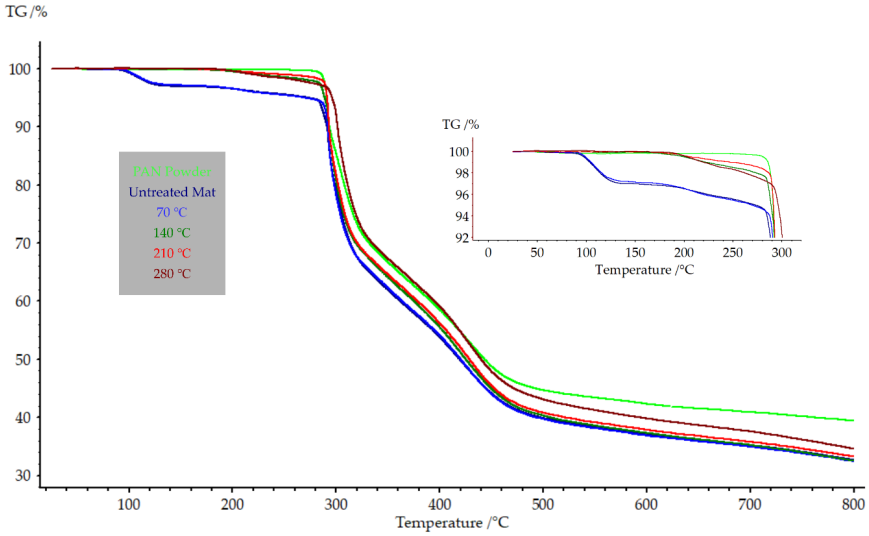

Figure 5.7 TGA of PAN nanofiber mats annealed at different temperatures.

Both the untreated and the 70 °C annealed nanofiber mats displayed a common initial mass loss at 100 °C, likely attributable to solvent evaporation. This evaporation process began at 100 °C and completed by 120 °C. Post solvent evaporation, the mass of the nanofiber mats remained constant until complete degradation occurred.

The DSC results, illustrated in Figure 5.8 for the first heating cycle, provide insights into the glass transition temperatures of PAN. During this cycle, heat absorption observed was attributed to evaporation, indicating that the heat absorption noted did not reflect the glass transition temperature. The PAN powder absorbed 30.43 J/g of heat. The untreated nanofiber mat and the mat annealed at 70 °C showed significant heat absorptions of 26.1 J/g and 25.79 J/g, respectively. In contrast, nanofiber mats annealed above 120 °C, where solvent evaporation had occurred, exhibited lower heat absorption: 7.35 J/g, 6.288 J/g, and 6.19 J/g for mats annealed at 140 °C, 210 °C, and 280 °C, respectively.

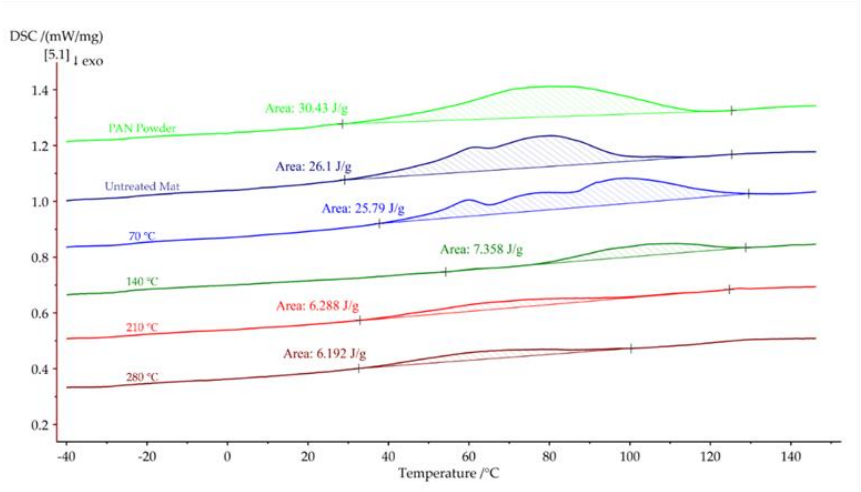

Figure 5.8 First DSC heating cycles of PAN nanofiber mats annealed at different temperatures.

The second heating cycle (Figure 5.9) reveals the glass transition temperatures. PAN powder exhibited a glass transition temperature at 96.8 °C. The untreated and 70 °C annealed nanofiber mats showed similar glass transition temperatures at 97.0 °C and 96.7 °C, respectively. However, mats annealed above the glass transition temperature displayed a marked decrease in this temperature: 90.1 °C, 92.3 °C, and 91.0 °C for mats annealed at 140 °C, 210 °C, and 280 °C, respectively.

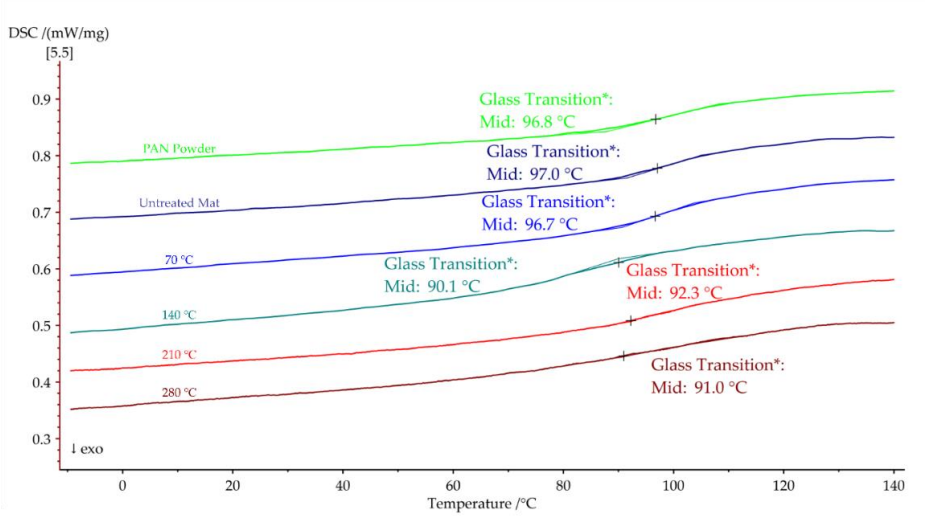

Figure 5.9 Second DSC heating cycles of PAN nanofiber mats annealed at different temperatures.

Table 5.2 summarizes the relationship between annealing temperature, glass transition temperature, and degradation temperature. It indicates a decrease of approximately 3.5% in the glass transition temperature and an increase of about 6% in the degradation temperature as the annealing temperature rises, compared to untreated PAN nanofiber mats.

Table 5.2

Thermal properties of the nanofiber mat annealed at different temperatures.

Properties	Untreated		Annealed			
	PAN Powder	Nanofiber Mat	70 ℃	140 ℃	210 ℃	280 ℃
TGA (℃)	291.6	292.2	292.6	292.7	292.8	301.8
Heat absorbed during first DSC heating cycle (J/g)	30.43	26.1	25.79	7.358	6.288	6.192
Tg during second DSC heating cycle (℃)	96.8	97.0	96.7	90.1	92.3	91.0

The decrease in the glass transition temperature (Tg) with increasing annealing temperatures, from 70 °C to 280 °C (96.7 °C to 91.0 °C), can be linked to a reduction in fiber diameter due to annealing. Slight degradation of PAN, possibly due to cross-linking reactions, also contributes to this change, especially since thermal treatments were conducted at temperatures high enough to induce chemical modifications in PAN macromolecules. At the glass transition temperature, the material's state changes from flexible and rubbery to stiff. This change explains the reduced elongation observed in annealed nanofiber mats.

In conclusion, TGA analyses reveal a significant weight reduction around 290 °C, signaling PAN degradation. The degradation temperature was affected by the annealing temperature, with higher annealing temperatures leading to higher degradation temperatures. DSC results from the first heating cycle indicated heat absorption unrelated to the glass transition temperature. However, the glass transition temperature was clearly observed in both PAN powder and nanofiber mats during the second heating cycle. The glass transition temperature was found to decrease with increasing annealing temperatures.

5.6. Conclusions of Effect of Annealing on PAN Nanofiber Mats

This section presented an in-depth analysis of the thermal and mechanical properties of untreated and annealed polyacrylonitrile (PAN) nanofiber mats. The key findings from the

thermogravimetric analysis (TGA), differential scanning calorimetry (DSC), and tensile testing are summarized as follows:

1. Tensile Testing: Stress (σ)-strain(ε) curves (Figure 4.6a,b) indicated that the annealed PAN nanofiber mat at 70 °C had greater strength than the untreated mat. The tensile strength and Young's modulus of untreated mats were 19.1 ± 3 MPa and 610 ± 30 MPa, respectively. These values increased significantly for the 70 °C annealed mats. However, mats annealed above the glass transition temperature showed a decrease in tensile strength, Young's modulus, and elongation at break.
2. Influence of Annealing Temperature: Annealing temperatures ranging from 70 °C to 280 °C caused a decrease in the glass transition temperature (Tg) from 96.7 °C to 91.0 °C. This decrease is likely due to a reduction in fibre diameter and slight degradation of PAN due to cross-linking reactions. Higher annealing temperatures led to higher degradation temperatures and reduced mechanical properties, attributed to changes in PAN's chemical structure and increased packing density due to solvent evaporation.
3. Thermogravimetric Analysis (TGA): TGA graphs (Figure 5.7) demonstrated a sharp decline in weight at approximately 290 °C across all samples, indicating rapid degradation of PAN. Untreated nanofiber mats and those annealed up to 210 °C showed degradation around 291.6 °C, while mats annealed at 280 °C degraded at 301.8 °C. Initial mass loss at 100 °C in untreated and 70 °C annealed mats was attributed to solvent evaporation.
4. Differential Scanning Calorimetry (DSC): DSC results (Figures 5.8 and 5.9) revealed that heat absorption during the first heating cycle was due to evaporation rather than glass transition. The second heating cycle identified the glass transition temperature of PAN powder at 96.8 °C, with untreated and 70 °C annealed mats showing similar temperatures. Mats annealed above 120 °C displayed lower heat absorption, and those annealed above the glass transition temperature showed a significant decrease in this temperature.

In summary, the study demonstrated that annealing significantly influences the thermal and mechanical properties of PAN nanofibers. While annealing at 70 °C improved the mechanical strength of the nanofibers, higher annealing temperatures resulted in a decrease in both the glass transition and mechanical properties. These findings highlight the delicate balance between annealing conditions and the resultant properties of PAN nanofibers, offering valuable insights for their application in various fields.

6. INVESTIGATION OF PVA BONDED PAN NANOFIBER MATS

Chapter 6 delves into the exploration of bonded PAN nanofiber mats, with a focus on improving the transverse mechanical properties of oriented polyacrylonitrile (PAN) nanofibers. Recognized for their superior longitudinal tensile strength, the challenge lay in augmenting these properties without detrimentally affecting their intrinsic porosity critical for efficient filtration applications. The study investigates the integration of polyvinyl alcohol (PVA) into PAN nanofiber mats through a dip-coating technique, applying varying PVA concentrations (0.5%, 1%, and 2%) to the PAN matrix. This method aimed to achieve a homogeneous PVA distribution within the nanofiber mat, capitalizing on the combined benefits of PAN fibers and PVA to elevate the composite material's overall functionality.

A suite of analytical techniques was deployed to thoroughly assess the impact of PVA doping on the nanocomposite's characteristics. Scanning electron microscopy (SEM) provided detailed morphological observations, while mechanical tests in both the transverse and longitudinal directions quantified the strength enhancements. Thermogravimetric analysis (TGA) and differential scanning calorimetry (DSC) offered insights into the thermal stability and behaviour of the composite, respectively. Complementing these experimental approaches, finite element method (FEM) analysis was applied to numerically simulate the nanocomposite's behaviour under stress.

The findings from this comprehensive investigation indicated that even minimal PVA solution concentrations could maintain the nanofiber mats' porosity while significantly bolstering their mechanical strength. The FEM simulations corroborated the experimental data, affirming the efficiency of PVA incorporation in enriching the PAN nanofiber mats' mechanical attributes without compromising their essential porosity. This chapter not only validates the hypothesis of using PVA doping to enhance the structural integrity of PAN nanofiber mats but also underscores the potential of such composites in advanced filtration and other application domains requiring a balance between strength and permeability. The content of this chapter is also available for reference in a published format (J. V. Sanchaniya, Lasenko, Vijayan, et al., 2024).

6.1. Objective of Bonded PAN Nanofiber mats with PVA Solution

The primary aim of incorporating Polyvinyl Alcohol (PVA) into Polyacrylonitrile (PAN) nanofiber mats through a dip-coating technique is to fortify the transverse mechanical

properties of the mats. This initiative seeks to bolster the inherent longitudinal tensile strength characteristic of oriented PAN nanofibers without adversely affecting their porosity, which is pivotal for effective filtration applications. This study embarks on a comprehensive investigation into the implications of embedding PAN nanofiber composites with PVA at varied concentrations, namely 0.5%, 1%, and 2%, introduced into the PAN matrix via dip-coating. This methodology aims to ensure a homogeneous dispersion of PVA within the nanofiber mat, capitalizing on the synergistic interplay between PAN fibers and PVA to augment the composite's overall mechanical performance.

To thoroughly evaluate the composite's enhancements, an array of comprehensive analysis techniques was employed. These included scanning electron microscopy (SEM) for morphological insights, mechanical testing in both transverse and longitudinal orientations, thermogravimetric analysis (TGA) for assessing thermal stability, and differential scanning calorimetry (DSC) for thermal behaviour examination. Additionally, finite element method (FEM) analysis was executed to numerically simulate the nanocomposite's behaviour. The findings underscored that a minimal PVA concentration effectively maintains porosity while notably improving mechanical strength. Furthermore, the numerical simulations corroborated the experimental outcomes, substantiating the efficacy of PVA embedding in enhancing PAN nanofiber mats' mechanical properties without compromising their functional porosity.

6.2. Materials and Methodology

To fabricate doped polyacrylonitrile (PAN) nanofiber mats enhanced with polyvinyl alcohol (PVA), the initial phase encompassed producing electrospun nanofibers. This procedure employed PAN powder dissolved in N, N-dimethylformamide (DMF) to create the nanofibers, combined with a PVA solution prepared in distilled water for the doping process. The selection of materials for this investigation prioritized purity and molecular weight to guarantee uniformity and dependability in both the electrospinning and doping phases. PAN, selected for its average molecular weight of approximately 150,000 and identified by CAS number 25014-41-9, served as the primary polymer. DMF, chosen for its role as a solvent due to its high purity level of 99.8% and CAS number of 68-12-2, facilitated the dissolution of PAN. PVA, with an average molecular weight ranging from 89,000 to 98,000 and a hydrolysis degree exceeding 99%, was selected for doping, denoted by CAS number 9002-89-5. These chemicals, procured from Sigma-Aldrich Chemicals (Merck KGaA, Steinheim, Germany),

were chosen for their superior quality and standardization, laying a solid foundation for the creation of the enhanced PAN nanofiber mats.

6.2.1. Experimental Process of Bonding PAN Nanofiber mats with PVA Solution

In the experimental journey to enhance the transverse mechanical properties of polyacrylonitrile (PAN) nanofiber mats without compromising their intrinsic porosity, a meticulous procedure was adopted, as delineated in Chapter 3. This involved synthesizing PAN nanofibers through an electrospinning process utilizing a rotating drum collector. A 10% (w/w) PAN powder solution in N,N-dimethylformamide (DMF) was electrospun under carefully controlled conditions. The subsequent step entailed doping these nanofibers with polyvinyl alcohol (PVA) through a dip-coating method, employing PVA solutions of varying concentrations (0.5%, 1%, and 2% w/w) to ensure a homogenous distribution of PVA within the nanofiber mat.

This delicate process of doping PAN nanofiber mats with PVA involved immersing cut PAN nanofiber mats into the PVA solutions, followed by a drying period to evaporate the solvent, thereby embedding PVA uniformly within the mat. The preparation, electrospinning conditions, and the dip-coating methodology are visually encapsulated in Figure 6.1, providing a step-by-step illustration of the fabrication process aimed at producing enhanced nanofiber mats capable of improved performance in various applications.

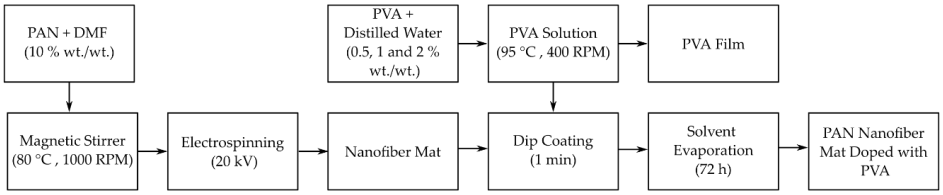

Figure 6.1 Fabrication process of PVA-doped PAN nanofiber mats.

Furthermore, an additional procedural step involved forming a thin film of PVA by carefully pouring the residual PVA solution into a Petri dish, facilitating a direct comparison between the thermal and mechanical properties of the pure PVA film and the PVA-doped PAN nanocomposite mats. This comparative analysis is pivotal, offering insights into the compatibility and interaction between PAN and PVA, and underlining the efficacy of PVA doping in augmenting the properties of PAN nanofiber mats.

This detailed experimental methodology, from the preparation of the PAN solution through to the final dip-coating in PVA, underscores the methodical approach undertaken to develop PVA-doped PAN nanofiber mats that synergistically harness the strengths of both PAN and PVA. This approach aims to create composites with superior structural integrity and functionality, thereby paving the way for the advancement of nanofiber-based materials tailored for specific applications.

The morphological, porosity, mechanical, and thermal properties of these composites were subsequently analysed, adhering to the protocols outlined in Chapter 3, ensuring a thorough understanding of the enhanced performance capabilities of the doped nanofiber mats.

6.2.2. Development of FE Model

The development of a Finite Element (FE) model for PVA-doped PAN nanofiber mats was meticulously undertaken, leveraging methodologies previously established in chapter 5. This advanced model integrates essential geometric parameters to precisely depict the structural nuances of the nanofibers post-PVA doping, as illustrated in Figure 6.2. Key parameters such as domain length (D_L) and height (D_H) were defined to demarcate the spatial extents of the nanofiber mat model accurately. Detailed attention was paid to determining the length (L) of the nanofibers, their diameter, and the coordinates marking each fibre's endpoints (x_1, y_1, and x_2, y_2), thereby capturing the mat's designed porosity. An innovative aspect of this model is the depiction of the mass increase in the nanofiber mat following PVA doping, represented by the relative area of PVA (A_P) to the domain area, demonstrating the dopant's concentration within the mat.

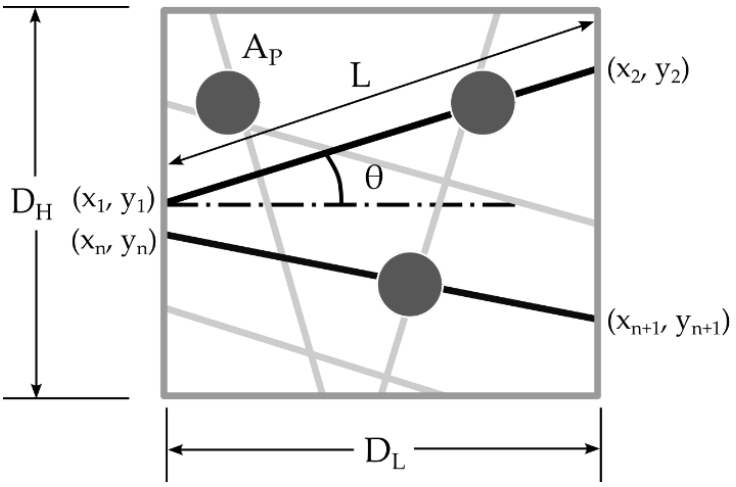

Figure 6.2 Schematic representation of the geometric parameters of nanofibers doped with PVA within an established domain.

In establishing the FE model, assumptions were harmonized with those in Chapter 5, particularly regarding the distribution of PVA at fibre intersections. This approach is pivotal for accurately simulating the PVA doping's impact on the nanofiber mat's mechanical attributes, as it concentrates on enhancing inter-fibre bonding without compromising the undoped mat sections' structural integrity.

The model is configured to simulate the tensile behaviour of nanofiber mats. Boundary conditions detailed in Figure 6.3 were meticulously applied to emulate their response to displacement, focusing on the reaction force (RF) along the X axis. Displacements (U1, U2, U3) were strategically imposed to reflect real-life stretching behaviours under tensile load, with particular constraints ensuring a faithful simulation of the material's deformation characteristics. The utilization of linear beam elements (B31) and shell elements (S4R) in Abaqus FEA software (2022) facilitates a nuanced representation of the nanofibers and the PVA dopant, respectively, ensuring a high fidelity model of the nanocomposite material.

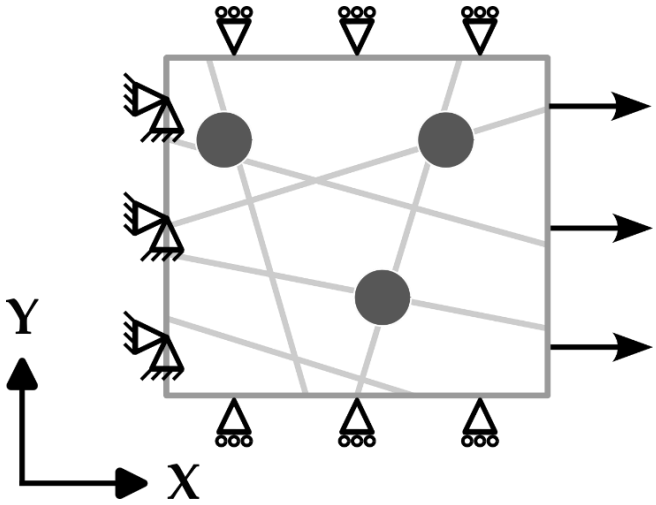

Figure 6.3 Boundary conditions applied to observe the normal stress response of the samples to displacement.

To counteract potential variability in fibre orientations, porosity levels, and dopant sizes, a rigorous simulation protocol was adopted. By executing a minimum of five simulations for each parameter configuration, the study guarantees the robustness and reliability of the

elastic response data, thus reinforcing the FE model's predictive accuracy regarding the doped nanofiber mats' tensile performance.

Moreover, the model employs tie joints to interconnect the beam and shell elements, mirroring the dynamic interaction between nanofibers and the dopant under mechanical stress. This connection technique not only enhances the model's realism but also provides insights into the rotational movements at the joints, which could significantly influence the material's mechanical response under tensile loading (Farukh et al., 2014). Through this comprehensive and detailed FE modelling approach, the study offers profound insights into the mechanical properties and performance of PVA-doped PAN nanofiber mats, underpinning future advancements in nanofiber-based composite materials.

6.3. SEM Analysis of PAN-PVA Composites

The Scanning Electron Microscopy (SEM) analysis of PVA-doped PAN nanofiber mats unveils the intricate impact of the dip-coating process on their morphology, as vividly captured in Figure 6.4. This figure showcases the nanofiber mats subjected to a 2.0% PVA solution treatment, revealing three noteworthy morphological transformations: the formation of localized PVA agglomerations within the nanofiber mat, the emergence of thin PVA films bridging the gaps between PAN nanofibers, and a uniform PVA coating enveloping the surface of the PAN nanofibers. These morphological alterations are pivotal, enhancing the structural robustness of the mats by fostering additional interaction points between fibers, thereby augmenting the composite's mechanical attributes significantly.

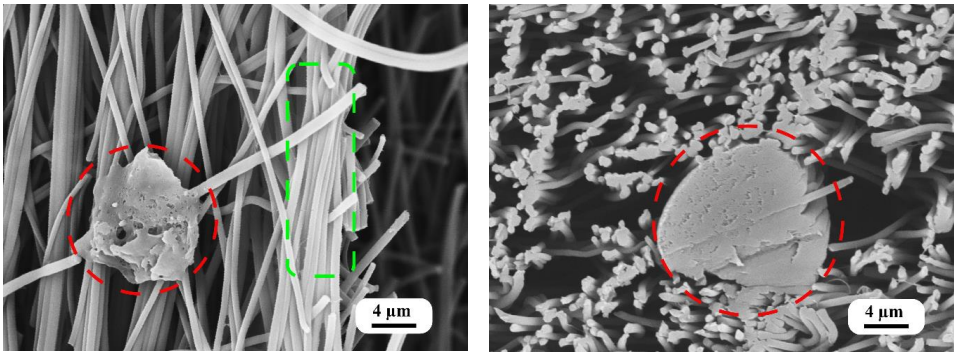

(a) (b)

Figure 6.4 SEM images of a PAN nanofiber mat doped with a 2.0% PVA solution: (a) localized agglomerations of PVA within the nanofiber mat (red) and coating on fibers (green); (b) cross-sectional image of the localized agglomerations of PVA.

The occurrence of localized PVA agglomerations and the enveloping PVA coating on the fibers mark a strategic morphological evolution within the fibre mat, likely enhancing load distribution and fostering stronger inter-fibre bonding. Furthermore, the presence of nanoscale PVA films interspersed among the nanofibers is presumed to evenly distribute mechanical stresses throughout the mat, elevating its strength and durability.

The morphological transformations observed post dip-coating corroborate our anticipations, attesting to the process's proficiency in instigating thin coatings, films, and PVA agglomerations within a PAN nanofiber matrix. These findings are in harmony with earlier documented observations by researchers (Niu et al., 2014; Tang & Yan, 2017), which had prognosticated the dip coating's potential to intricately alter both the surface and the internal configuration of nanofiber mats.

A meticulous examination revealed the nanofibers' diameter to be 609 nm ± 43 nm, an indicator of the electrospinning process's efficacy in maintaining uniformity and precision. This dimensional consistency mirrors the results of a preceding study cited in chapter 3, which employed identical electrospinning parameters. Such uniformity in fibre diameter is essential for applications demanding specific surface area and porosity features, as these characteristics significantly influence the composite material's mechanical performance and filtration efficiency.

This SEM analysis elucidates the complex interplay between PVA and PAN within the nanofiber mats, validating the dip-coating process's effectiveness in refining the composite's structural properties. The examination of these morphological nuances underscores the PVA-doped PAN nanofiber mats' potential suitability for applications necessitating materials with enhanced mechanical strength and structural integrity, paving the way for their deployment in advanced technological applications.

Furthermore, an insightful porosity analysis conducted through density comparison underscores a systematic reduction in porosity upon PVA doping, delineated across varying PVA concentrations. The inherent porosity of the pure PAN nanofiber mat stood at 72 ± 0.5%, a figure ideal for applications like filtration and tissue engineering, where an open structure and high surface area are paramount. Nevertheless, with incremental PVA doping, a discernible decline in porosity was recorded, plunging to 63 ± 0.7% at a 2% PVA concentration, as tabulated in Table 6.1. This porosity reduction, attributed to the densification effects of PVA incorporation and solvent evaporation during PVA solidification, suggests a trade-off between mechanical strength enhancement and potential impacts on filtration efficiency or tissue scaffold permeability.

Table 6.1
Summary of the calculated porosities of the pure and dip-coated PAN nanofiber mats.

Samples	Porosity (%)
PAN Nanofiber mat	72 ± 0.5
PAN + 0.5 % PVA	69 ± 0.5
PAN + 1 % PVA	67 ± 0.4
PAN + 2 % PVA	63 ± 0.7

The observed trends illuminate the nuanced relationship between PVA concentration and nanofiber mat porosity, emphasizing the necessity to finely balance material properties to suit specific application needs. This SEM analysis not only reaffirms the structural modifications induced by PVA doping but also sets a precedent for tailoring nanocomposite materials to achieve bespoke performance characteristics, marking a significant stride in the field of nanofiber research.

6.4. Mechanical Properties of PAN-PVA Composites

The meticulous evaluation of the mechanical properties of PVA-doped PAN nanofiber mats, as delineated in Figures 6.5a and b, provides a comprehensive insight into the enhancements achieved through the incorporation of PVA at various concentrations. The independent PVA films showcased a robust elastic modulus of 1254 ± 57 MPa, an ultimate tensile strength of 34 ± 2.4 MPa, and an exceptional plasticity with an elongation at break of 0.38 ± 0.03. Notably, the thickness consistency observed across both undoped and PVA-doped PAN nanofiber mats indicates that the incorporation of a low percentage of dopant meticulously maintained the mats' structural dimensions.

The pristine PAN nanofiber mat exhibited an elastic modulus of 383 ± 34 MPa and an ultimate tensile strength of 9.9 ± 0.8 MPa, alongside an elongation at break of 0.18 ± 0.02 in the longitudinal direction. Conversely, in the transverse direction, a reduced elastic modulus of 47 ± 6 MPa and a lower ultimate tensile strength of 1.13 ± 0.15 MPa were observed, with a slightly increased elongation at break of 0.21 ± 0.02.

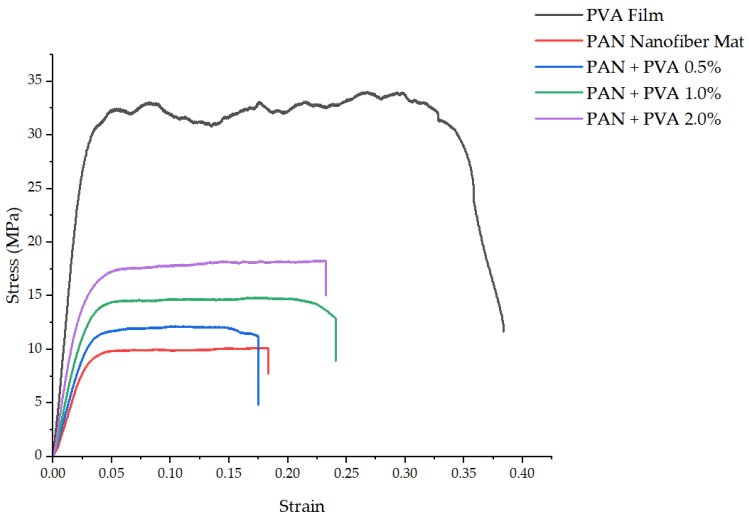

(a)

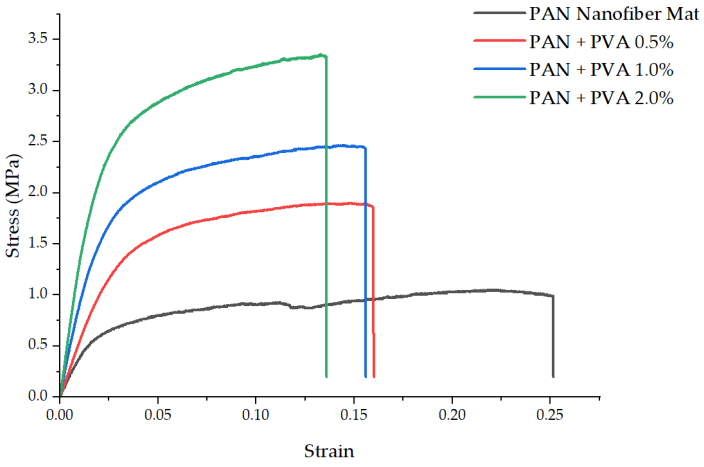

(b)

Figure 6.5 Representative stress–strain graphs: (a) longitudinal direction, (b) transverse direction.

The introduction of PVA into the PAN nanofiber mats led to discernible improvements in their mechanical attributes across both directions. In the longitudinal direction, the elastic modulus saw increments to 475 ± 42 MPa, 538 ± 29 MPa, and 683 MPa with the addition of 0.5%, 1%, and 2% PVA, respectively. The transverse direction mirrored this enhancement, exhibiting increases in the elastic modulus to 65 ± 4 MPa, 81 ± 6 MPa, and 122 ± 12 MPa for the respective PVA concentrations. Correspondingly, the ultimate tensile strength in the

longitudinal direction ascended to 12.1 ± 1.1 MPa, 14.9 ± 1 MPa, and 18.25 MPa for 0.5%, 1%, and 2% PVA, respectively, and in the transverse direction, it elevated to 1.87 ± 0.11 MPa, 2.5 ± 0.1 MPa, and 3.4 ± 0.24 MPa for the respective concentrations of PVA. These mechanical property enhancements are succinctly summarized in Table 6.2.

Table 6.2
Summary of the mechanical properties of the PVA film, PAN nanofiber mat, and PAN nanofiber mats doped with PVA.

Sample	**testing direction**	**thickness, t (μm)**	**ultimate tensile strength, σ_{max} (MPa)**	**Young's modulus, E (MPa)**	**elongation at break strain, ε**
PVA film	-	53 ± 4	34 ± 2.4	1254 ± 57	0.38 ± 0.03
PAN nanofiber mat	longitudinal	95 ± 7	9.9 ± 0.8	383 ± 34	0.18 ± 0.02
	transverse	97 ± 6	1.13 ± 0.15	47 ± 6	0.21 ± 0.02
PAN + 0.5 % PVA	longitudinal	96 ± 5	12.1 ± 1.1	475 ± 42	0.18 ± 0.02
	transverse	98 ± 5	1.87 ± 0.11	65 ± 4	0.16 ± 0.02
PAN + 1 % PVA	longitudinal	96 ± 6	14.9 ± 1	538 ± 29	0.23 ± 0.02
	transverse	95 ± 7	2.5 ± 0.1	81 ± 6	0.16 ± 0.02
PAN + 2 % PVA	longitudinal	97 ± 4	18.25 ± 1.4	683 ± 27	0.23 ± 0.02
	transverse	101 ± 6	3.4 ± 0.24	122 ± 12	0.14 ± 0.01

The congruence of the mechanical properties of the independent PVA films with existing literature (Guzman-Puyol et al., 2015; Jain et al., 2017; Kashyap et al., 2016; Sonker et al., 2016), and the consistency of the PAN nanofiber mat properties with those previously established by the authors, underscore the reliability of the experimental setup and parameters employed. The marked enhancement observed in the doped nanofiber mats highlights the structural reinforcement imparted by PVA, both as an inter-fibre adhesive and a fibrous coating. The notable increase of 84.34% in ultimate tensile strength and 78.33% in elastic modulus in the longitudinal direction, upon the addition of a 2% PVA dopant, is particularly remarkable. Even more pronounced improvements were observed in the transverse direction, with the ultimate tensile strength and elastic modulus increasing by 200% and 159.5%, respectively.

These enhancements in mechanical properties, especially pronounced in the transverse direction, underscore PVA's critical role in augmenting the interfiber bonds within the mat. The improved load-bearing capacity and the shift in failure mode from fibre debonding to shear, attributable to PVA incorporation, significantly elevate the nanofiber mat's mechanical strength and structural resilience, highlighting the potential of PVA doping in engineering nanofiber mats with superior mechanical performance.

6.5. Thermal Properties of PAN-PVA Composites

The thermogravimetric analysis (TGA) and derivative thermogravimetry (DTG) investigations, as depicted in Figure 6.6, offer pivotal insights into the thermal stability and degradation tendencies of pure PAN nanofiber mats compared with PVA films under variable temperature conditions. The DTG graph elucidates a significant peak reduction at 293.3°C for the PAN nanofiber mat and at 277.0°C for the PVA film, delineating each material's primary degradation temperature. Moreover, initial mass losses recorded up to 150°C were 2.43% for the PAN nanofiber mat and 4.53% for the PVA film, indicative of solvent evaporation or moisture loss from the samples. This initial reduction for the PAN nanofiber mat aligns with previous authorial findings in chapter 3, attributed to the evaporation of residual solvents, a pattern mirrored in the PVA film, consistent with literature (Thomas et al., 2018; Tsioptsias et al., 2023), where PVA exhibited analogous behaviour.

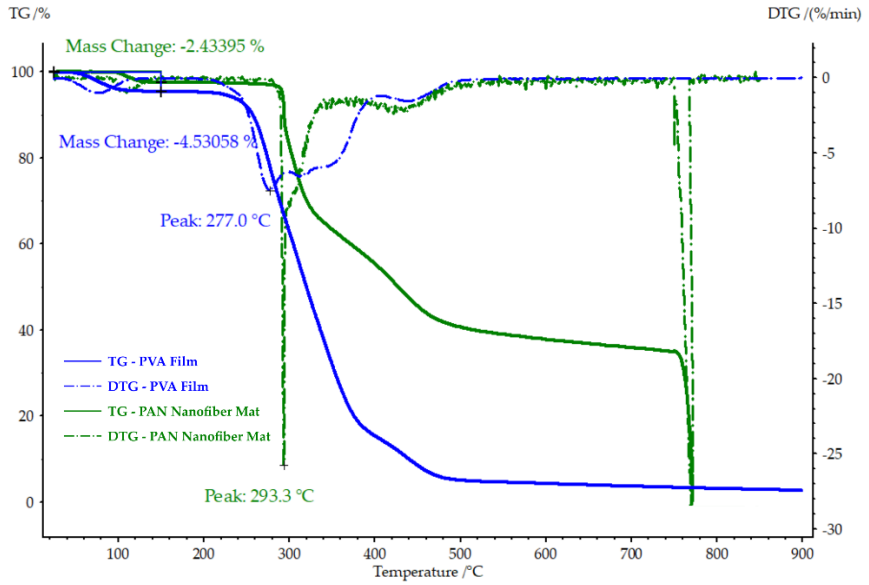

Figure 6.6 TGA and DTG of the pure PAN nanofiber mat and PVA film, highlighting their thermal degradation points and initial mass loss due to solvent evaporation.

Figure 6.7 underscores the TGA and DTG analyses for PAN nanofiber mats infused with varying PVA concentrations. Remarkably, an increment in PVA concentration heralds a decrease in peak degradation temperature, suggesting an alteration in the composite's thermal stability. At a 0.5% PVA concentration, the peak degradation temperature closely matched that

of the undoped PAN nanofiber mat. However, at 1% and 2% PVA concentrations, a discernible reduction to 288.2°C and 288.0°C, respectively, was noted. Concurrently, early mass loss up to 150°C escalated with PVA concentration, marking a progression from 1.27% at 0.5% PVA to 1.67% and 1.7% at 1% and 2% PVA, respectively.

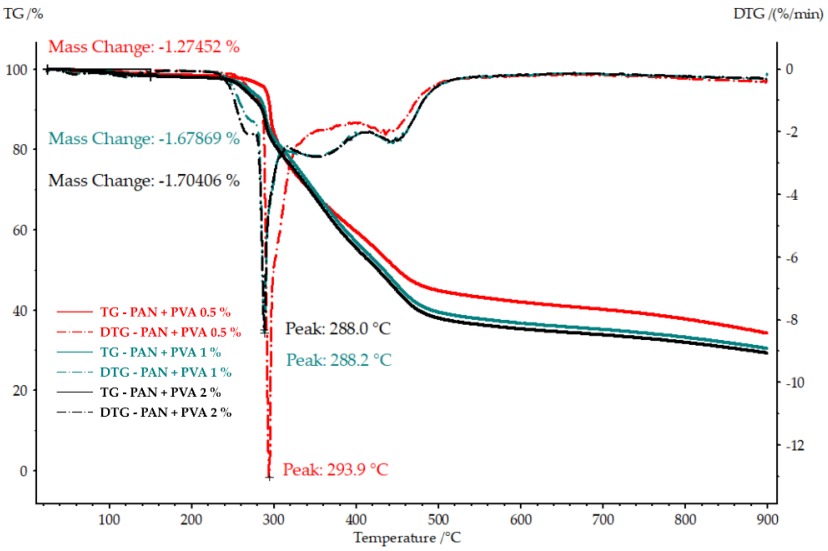

Figure 6.7 TGA and DTG of the PAN nanofiber mats doped with different concentrations of PVA, illustrating the effect of the PVA concentration on their thermal degradation and early mass loss.

These observations intimate that an augmented PVA presence in the nanocomposite impacts both its thermal stability and early mass loss characteristics, potentially due to PVA's inherently lower thermal stability relative to PAN, affecting the nanofiber mats' overall thermal resilience. Figure 6.8 and 6.9 delineate the first DSC heating cycles for both the pure PAN nanofiber mat and the PVA-infused variants, revealing an increase in heat absorption with rising PVA concentration, likely resultant from the combined effects of solvent evaporation and the enthalpy relaxation of PVA.

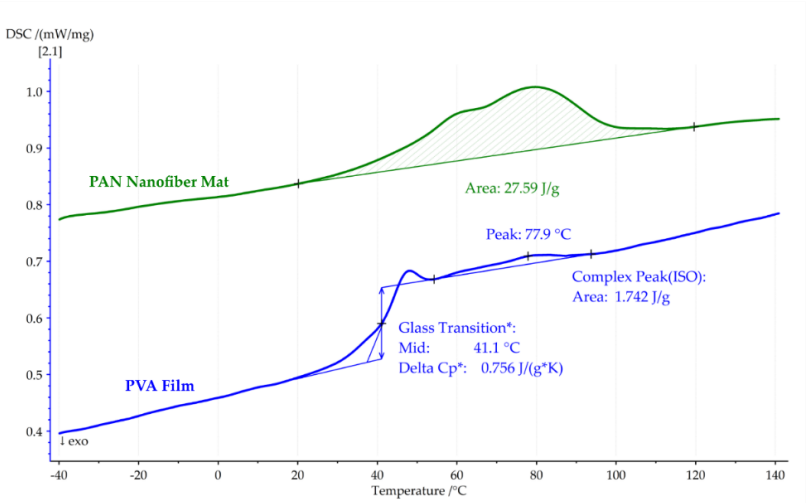

Figure 6.8 First DSC heating cycle of the pure PAN nanofiber mat and PVA film, showcasing their heat flow and glass transition temperatures.

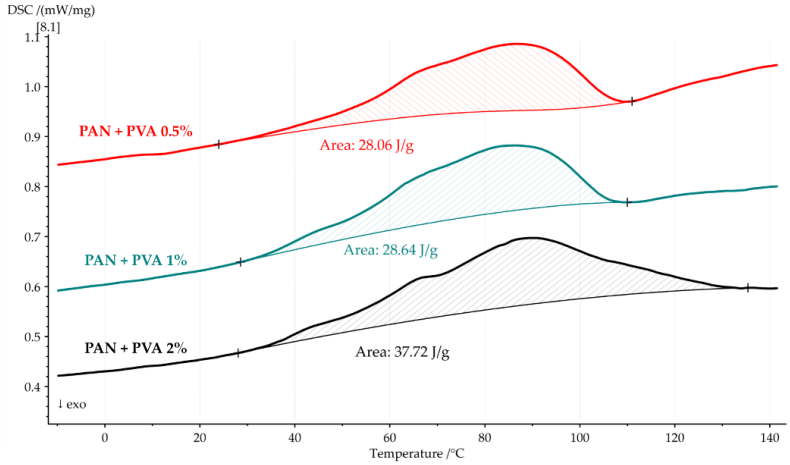

Figure 6.9 First DSC heating cycle of PAN nanofiber mats doped with PVA, showing their increased heat absorption with higher PVA concentrations.

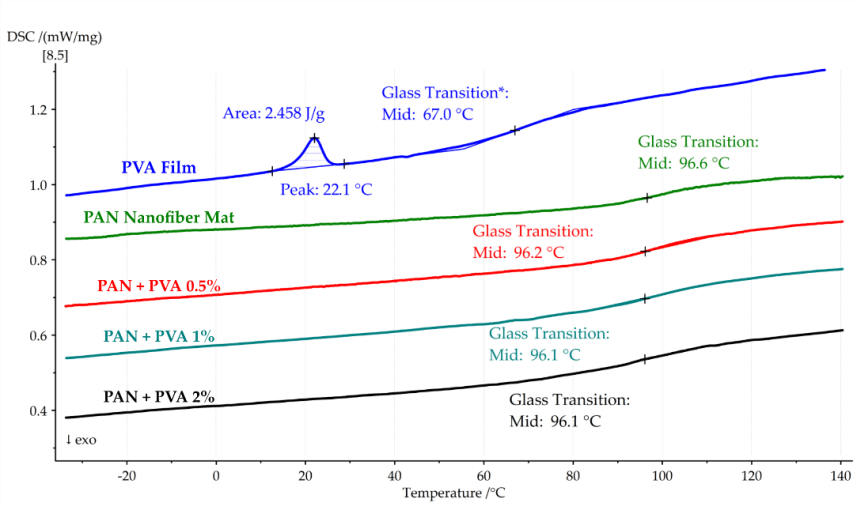

Figure 6.10 Second DSC heating cycle of the PAN nanofiber mat, the PVA film, and the PAN nanofiber mats doped with PVA, indicating their glass transition temperatures.

In the second DSC heating cycle, as presented in Figure 6.10, the glass transition temperatures of the doped nanocomposites closely mirrored those of the pure PAN nanofiber mat, suggesting that PVA's inclusion does not significantly alter the composites' Tg. Table 6.3 encapsulates a summary of the thermal properties of both the pure and PVA-doped PAN nanofiber mats, cataloguing their heat flows and glass transition temperatures.

Table 6.3
Summary of the thermal properties of the pure PAN nanofiber mat, PVA film, and PAN nanofiber mats doped with PVA, detailing their heat flows and glass transition temperatures.

Properties	**Materials**				
	PAN	**PVA film**	**PAN + 0.5% PVA**	**PAN + 1% PVA**	**PAN + 2% PVA**
DTG peak (°C)	293.3	277.0	293.9	288.2	288.0
Mass loss up to 150 °C (%)	2.43	4.53	1.27	1.67	1.7
Heat absorbed during the first DSC heating cycle (J/g)	27.59	1.742	28.06	28.64	37.32
Tg during the first DSC heating cycle (°C)	-	41.1	-	-	-
Tg during the second DSC heating cycle (°C)	96.6	67.0	96.2	96.1	96.1

This detailed thermal characterization elucidates the impact of PVA doping on the thermal behavior of PAN nanofiber mats. Increasing PVA concentration not only affects the

thermal degradation profile and mass loss behavior but also enhances heat absorption, indicative of a strengthened interaction between the PAN nanofibers and PVA. Such insights are invaluable for tailoring the thermal properties of PAN-PVA composites for applications demanding high thermal stability, offering a profound understanding of these materials' thermal dynamics and laying a foundational basis for their utilization in thermally stringent applications.

6.6. Simulation of PAN-PVA Composites

The development of the Finite Element (FE) model for PAN-PVA composites meticulously integrates the mechanical characteristics of individual PAN nanofibers, as extensively elucidated in Chapter 4, alongside the experimentally derived mechanical properties of PVA. This integration facilitated a nuanced evaluation of the composite's elastic response, with a particular emphasis on the decreased porosity indicative of the dopant's volume within the PAN nanofiber mats. Table 6.4 succinctly encapsulates the critical structural parameters and material properties, offering a detailed framework for replicating or extending the study's findings.

Table 6.4
Summary of the material properties of a single nanofiber and the structural parameters used to develop the FE model.

Structural parameters and material properties	**Characteristics/Value**
Elastic material model	Hooke’s law
Domain size (µm)	100 × 100
Orientation (°)	+5.5 to -5.5 (11)
Fiber diameter (nm)	610
Fiber length (µm)	10-100.47
Porosity (%)	72
Volume of PVA (%)	9
Doped PVA arrangement	Random
Diameter of PVA dopant (µm)	5 to 10
Elastic modulus fibre (MPa)	2050
Elastic modulus dopant (MPa)	1254
Poison’s ratio (ν)	0.4
Element size (µm)	1

Figure 6.11 vividly illustrates the normal stress distribution along the X axis under loading, highlighting the dopant's role in augmenting the nanofiber mat's structural integrity. This enhancement in rigidity underscores the composite's fortified resilience against stress.

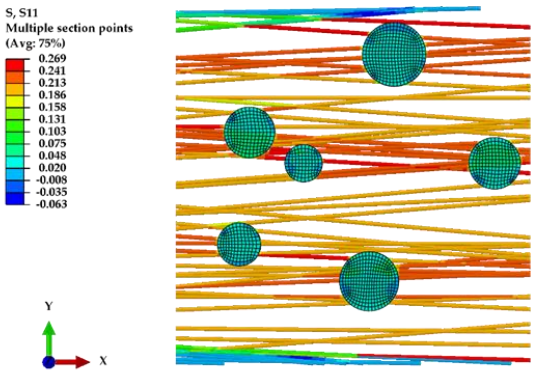

Figure 6.11 Normal stress on X axis for nanofiber mat doped with 2% PVA.

The juxtaposition of the FE model's calculated elastic responses against the spectrum of experimental data, as delineated in Figure 6.12, underscores the model's fidelity. Notably, the elastic modulus for the undoped PAN nanofiber mat, as per the FE model, was determined to be 395 MPa ± 19 MPa. In contrast, PVA-doped mats demonstrated elevated elastic moduli of 487 ± 18 MPa, 550 ± 21 MPa, and 697 ± 17 MPa for the respective dopant concentrations of 0.5%, 1%, and 2%. These findings not only corroborate the model's precision but also affirm the structural reinforcement conferred by PVA doping.

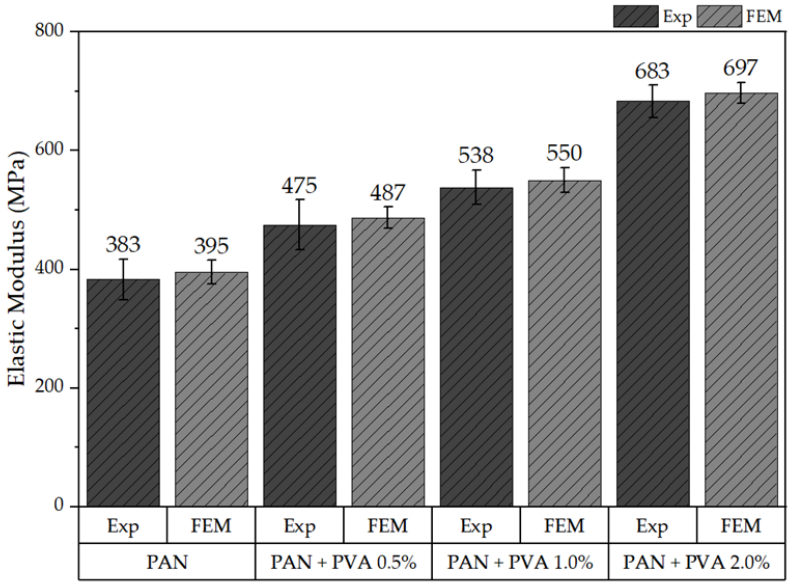

Figure 6.12 Comparison of the elastic moduli obtained from the experiments and the FE model.

Despite the strides made in this inquiry, it is crucial to acknowledge the computational modeling's limitations. The assumption regarding the PVA dopant's volume fraction, while instrumental in mirroring the experimental elasticity outcomes, may not extend with equal accuracy to predicting plastic behaviour. This limitation is particularly pertinent given the dopant's potential to form thin films along the fibers, thus intricately influencing the composite's mechanical behaviour. Such intricacies spotlight the challenges inherent in modelling material behaviours where dopant distribution and matrix interaction significantly shape the composite's structural properties.

Future research avenues could potentially hone in on these dynamics, aiming to refine the FE model to more comprehensively capture the complex interplay between elasticity, plasticity, and dopant concentration within composite nanofiber mats. Such endeavours could illuminate the path towards a deeper understanding of the structural and mechanical nuances of PAN-PVA composites, thereby broadening the scope for their application in various fields.

6.7. Conclusions of PVA Bonded PAN Nanofiber Mats

This chapter delves into the intricacies of doping PAN nanofiber mats with PVA, presenting a nuanced examination of the resultant mechanical, thermal, and structural modifications. This segment of the thesis shows experimental outcomes with computational predictions to elucidate the multifaceted enhancements achieved through PVA integration.

1. The augmentation of mechanical properties stands as a cornerstone of this exploration, evidencing a significant bolstering in both the elastic modulus and ultimate tensile strength of the doped mats. This reinforcement, particularly noted in the transverse direction, underscores the pivotal role of PVA in solidifying inter-fiber connections and amplifying the composite’s overall resilience. The congruence between the experimental findings and the FE model's simulations underscores the latter's validity, spotlighting computational modeling as an instrumental foresight tool in the development of nanofiber-based composites.
2. The thermal analysis component, encompassing thermogravimetric and differential scanning calorimetry assessments, sheds light on the nuanced interaction between the PVA content and the composite's thermal dynamics. A discernible decrement in thermal stability with an uptick in PVA concentration hints at the delicate balance between dopant quantity and thermal resilience, implicating potential application-specific

ramifications. Moreover, the observed escalation in heat absorption in tandem with PVA concentration suggests a deepening synergy between PAN nanofibers and PVA, pivotal for the material's thermal behaviour.

3. Structural and morphological insights gleaned from SEM analysis reveal the profound impact of PVA doping on the nanofiber mats' architecture, including the emergence of PVA agglomerations and coatings on fibre surfaces. These morphological shifts, essential for the mechanical fortification of the mats, also bring to light the issue of decreased porosity with increased PVA concentration. This alteration, while potentially limiting in applications requiring high permeability, also opens avenues for mechanical property optimization through precise dopant adjustments.

The chapter acknowledges the limitations inherent in current computational approaches, particularly in modeling plastic behaviour and the dopant-matrix interplay, setting the stage for future explorations aimed at refining these predictive models. Such advancements could further delineate the impact of dopant concentration on composite materials, enriching the toolkit available for tailoring nanocomposite materials to specific application needs.

In essence, this presents a holistic investigation into the effects of PVA doping on PAN nanofiber mats, unveiling significant enhancements across mechanical and thermal properties, alongside critical structural modifications. The fusion of experimental analysis with computational modeling not only validates the observed property enhancements but also heralds a new era of material design, where computational insights guide the empirical tailoring of nanocomposite materials for diverse applications. This approach not only propels the understanding of PAN-PVA composites forward but also illuminates the path toward their optimized application in various domains.

7. NON-CRIMPING TEXTILES REINFORCED WITH PAN NANOFIBERS

In the dynamic landscape of modern textiles, the surge in demand for human-adaptive smart (electronic) skins is noteworthy (You et al., 2018), particularly in the domain of flexible wearable electronic sensors and devices. Such devices span an array of applications including wearable health monitors (Jin et al., 2019; Meena et al., 2023), diagnostic instruments, and multifunctional robotic skins (Georgopoulou et al., 2021). A critical requirement for these innovations is their ability to emulate human skin's functionalities. This includes the conversion of physical stimuli into electrical signals and the precise monitoring of various physical parameters like pressure, strain, flexion, movement, deformation, spatial pressure distribution, and even contactless sensing capabilities such as detecting finger proximity (Kang et al., 2017; Sharma et al., 2021).

However, conventional fabrics pose significant limitations in these advanced applications. Their inherent three-dimensional, wavy structure leads to a crimping effect, diminishing their efficiency in both physical and mechanical aspects (Zhao et al., 2023). This challenge extends beyond the healthcare sector to encompass smart textiles integrated with nanoparticle-reinforced fabric yarns (Qiu et al., 2020), which tend to lose a significant portion of their efficiency when stretched.

Nanofibers have emerged as a promising solution, particularly in medical fields for applications like wound dressings (Ambekar & Kandasubramanian, 2019; Homaeigohar & Boccaccini, 2020; Munir et al., 2023), drug delivery (Arun et al., 2021), and tissue engineering scaffolds (Hanumantharao & Rao, 2019; Nemati et al., 2019). Their high surface-to-volume ratio, lightweight nature, and flexibility are noteworthy advantages. Yet, the primary drawback of nanofiber mats lies in their relatively low strength when the fibers are randomly oriented. In laminated composite materials and fibre-reinforced composites, the fibres' orientation, length, and diameter are crucial determinants of the elastic response (Lasenko et al., 2023).

This backdrop has led to the exploration of nanofiber-laminated textile composites, combining the strengths of PAN nanofibers and traditional textiles. The goal is to create enhanced smart, functional, and antimicrobial textiles that overcome the limitations of conventional fabrics. These composites aim to retain elasticity in the crimped regions under low strain rates, akin to nanofibers, while also offering greater durability than nanofiber mats alone. The successful development of these composites could revolutionize human-adaptive

smart skins, enabling more efficient and reliable monitoring of physical parameters with the desired flexibility and durability.

7.1. Objective of Non-Crimping Laminated Textiles

Research on textiles reinforced with nanofibers has predominantly focused on various properties of the resultant composites, with limited studies delving into changes in their mechanical properties. For instance, Jalalah et al.'s study, which closely aligns with our current research, involved creating nanofiber/textile composites using PA6 nanofibers through a needleless electrospinning process. However, they did not observe changes in the stress–strain behaviour of the composite in the elastic region, possibly due to the non-uniform orientation of aggregated nanofibers (Jalalah et al., 2022).

In contrast, Xiaolu et al. developed a stretchable electronic capacitive fabric skin incorporating nanofiber-coated yarns (You et al., 2018). This innovative fabric demonstrated the potential for quick response sensing (less than 50 ms) and applications in voice recognition and non-contact airflow monitoring. Jin et al. focused on creating durable, skin-tight electronic textiles using PVDF nanofibers, assessing the cyclic stability of the composite material (Jin et al., 2019). Guan et al. developed woven triboelectric nanogenerators from electrospun nanofibers, aiming for energy harvesting and self-powered sensing, while Qiu et al. highlighted the durable antibacterial properties of textiles embedded with nanofibers (Guan et al., 2021; Qiu et al., 2020). Chen et al.'s creation of URETEK3216LV laminated composite fabric and Kucukalo-Ozturk et al.'s development of a nanofiber-laminated composite for acoustic applications are other notable studies (J. Chen et al., 2017; Kucukali-Ozturk et al., 2017).

Other research, like that of Hahn et al., reviewed methods for creating stitch-free and non-crimping textiles but did not incorporate nanofibers (Hahn et al., 2018). Bhudolia et al. explored the impact of stitches on non-crimping composite fabrics (Bhudolia et al., 2019). Our previous work with direct electrospun PA6 nanofibers laminated textiles revealed a lack of significant adhesion between the textile and the nanofiber mat, leading to delamination post-tensile strength testing. To address this, solvent-free textile glue to enhance adhesion between the electrospun nanofiber mat and the textile was employed, without adversely affecting either component.

This chapter introduces a novel method for creating crimp-free textiles using direct electrospun nanofibers on textiles and examines their mechanical properties. The findings of this study have the potential to contribute significantly to the development of new, high-

performance materials that are both lightweight and strong, thus advancing textile technology and inspiring further research in this evolving field. The content of this chapter is also available for reference in a published format(J. V. Sanchaniya, Lasenko, Kanukuntla, et al., 2023) .

7.2. Materials and Methodology of PAN Nanofibers as Reinforcement

In this research, our focus was to fabricate laminated textile composites reinforced with electrospun PAN nanofibers. The production process of these nanofibers has been elaborated in detail in Chapter 3. For the base textile, we selected a special plain interlacing fabric (model T561) composed of a linen warp of 28 Tex, a cotton weft of 20 Tex, and amber fibers of 7.8 Tex, having a density of 115 ± 6 g/m^2. This fabric was procured from AB Linas, Lithuania. To bond the layers, solvent-free fabric glue (Art. 639820) from Gutermann GmbH, Germany, was used.

The laminated textile composite preparation involved cutting the fabric to match the dimensions of the rotating drum (45 cm × 5 cm), with careful orientation along the weft. This fabric was then adhered to a rotating drum collector (RC-5000, Shenzhen Tongli Tech Co, Ltd., China). The fabric glue application (~208 g/m^2) followed a manual lay-up method, gauged by the mass difference of the glue before and after application. For separate testing of the PAN nanofiber mat, a 5 cm × 5 cm square of aluminium foil was placed on the glue to collect nanofibers without glue interference.

Electrospinning was conducted in a controlled environment (+22 ± 1 °C) using a Fisherbrand™ single-syringe pump and a needle-based electrospinning machine. The setup for preparing the laminated textile composites is depicted in Figure 7.1.

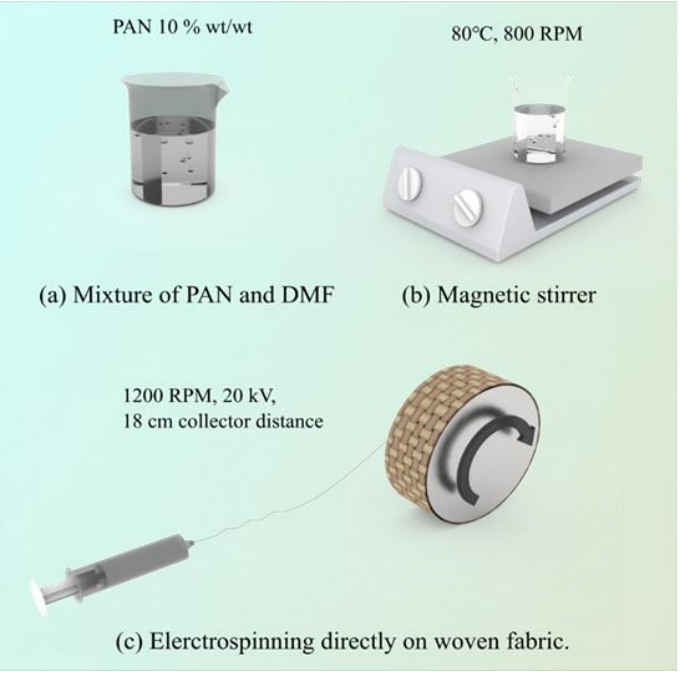

Figure 7.1 The fabrication process of PAN nanofiber-laminated composite fabrics: (a) mixture of PAN and DMF; (b) magnetic stirrer; (c) electrospinning directly on woven fabric.

Morphology analysis was consistent with the procedures outlined in Chapter 3. The plain fabric and PAN nanofiber-laminated composites underwent tensile testing as per ASTM D2261 standards, with a specimen size of 75 mm × 25 mm (Figure 7.2a), using a Mecmesin Multi-Test 2.5-i tensile testing machine. The testing conditions adhered to ISO 139:1973 standards. The thickness of the test specimens was recorded using a digital micrometre, with measurements taken at three different points to determine the average thickness. For independent analysis, nanofiber mats collected using aluminium foil were tested following the ASTM D882-18 standard (Figure 7.2b).

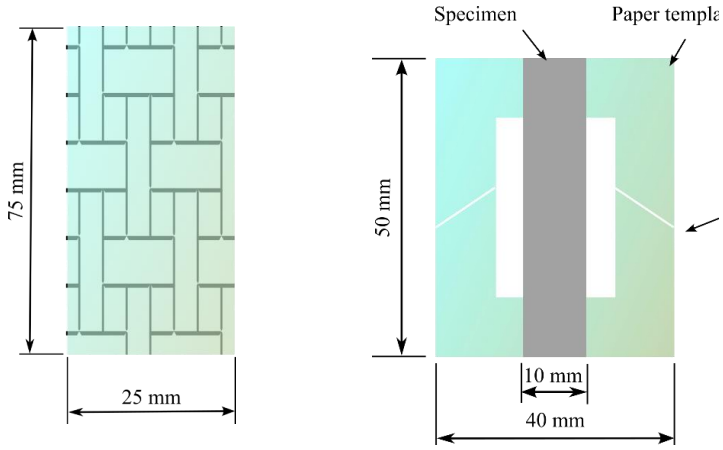

(a) (b)

Figure 7.2 Dimensions of the specimens: (a) plain fabric and the composite PAN nanofiber-laminated fabric; (b) specimen of the nanofiber mat with a paper template.

To analyse the elastic properties of the prepared nanofiber-laminated composite fabrics, several micromechanical models were employed:

Rule of Mixtures (ROM): This fundamental model was used to evaluate Young's modulus of the nanofiber-laminated composite fabric (Equation 7.1) (Magazzù & Marcuello, 2023). It predicts the linear relationship between the fabric and the nanofiber mat, considering the volume fraction of the fabric and the increase in thickness due to the nanofibers.

$$E_C = E_{FA} V_{FA} + E_{NF} (1 - V_{FA}) \tag{7.1}$$

Cox–Krenchel Model: Based on the classical shear-lag theory, this popular model (Equation 7.2) assumes elastic response from fibre and matrix, no axial loads on fibres' ends, and an ideal fibre-matrix interface. It calculates the elastic modulus considering the fibre orientation factor and aspect ratio.

$$E_C = \eta_0 E_{NF} V_{NF} \left(1 - \frac{\tanh(ns)}{ns}\right) + E_{FA} (1 - V_{NF}) E_{FA} \tag{7.2}$$

$$n = \sqrt{2E_{FA} / [E_{NF}(1 + V_{FA}) \ln \frac{1}{V_{NF}}]} \tag{7.3}$$

where EC is the elastic modulus of the nanofiber-laminated composite fabrics; E_{NF} and E_{FA} are the experimental moduli of the PAN nanofiber mat and fabric, respectively, with the fibre orientation factor η_0 = 3/8, assuming an in-plane isotropic orientation of the fibers in a

random short-fibre polymer composite; and s is the fibre aspect ratio, where the average length of the fibers L can be used to calculate s = L/D, where D is the fibres' diameter

Tsai–Pagano Model: This model (Equation 7.4) (Agarwal et al., 2017) calculates the longitudinal and transverse modulus of the nanofiber-laminated textile composite, assuming unidirectional composite with cylindrical fibers and a random in-plane fibre orientation.

$$E_C = \frac{3}{8} E_L + \frac{5}{8} E_T \tag{7.4}$$

$$E_L = E_{NF} V_{NF} + E_{FA}(1 - V_{NF}) \tag{7.5}$$

$$E_T = \frac{E_{NF} E_{FA}}{E_{NF}(1-V_{NF}) + E_{NA} V_{FA}} \tag{7.6}$$

where E_L and E_T are the longitudinal and transverse modulus of the nanofiber-laminated textile composite, respectively, which were computed longitudinally and transversely in the direction of the fibers, assuming a unidirectional composite with cylindrical fibers.

Halpin–Tsai Model: A mathematical model predicting the elasticity of composite materials (Equation 7.7), it considers the geometry and orientation of the filler, as well as the elastic properties of both filler and matrix.

$$E_C = \frac{E_{FA}(1 + \zeta \eta V_{NF})}{1 - \eta V_{NF}} \tag{7.7}$$

$$\eta = \frac{E_{NF} - E_{FA}}{E_{NF} + \zeta E_{FA}} \tag{7.8}$$

In Equations (7.7) and (7.8), η is a function and ζ denotes an empirical parameter or a curve-fitting parameter which is used to calculate the value that matches the experimental data. In this study, the empirical parameter ζ = 1 was selected, as this is used for a single composite (Ayres et al., 2008; Landel & Nielsen, 1993).

Through these models, we aim to comprehensively understand the reinforcing effect of PAN nanofibers in the textile composites, contributing to the advancement of smart textile technology.

7.3. Structural Characterization

The structural characterization of the nanofiber-laminated composite fabric, created by electrospinning nanofibers onto a rotating drum collector covered with woven fabric, revealed several key features indicative of its precise lamination and uniform fibre distribution.

The composite fabric exhibited a consistent thickness across its surface, devoid of any visible voids or signs of separation between the nanofiber mat and the underlying fabric. This uniformity is a testament to the effective phase morphology and integration achieved during the electrospinning process. The reinforced fabric maintained a generally flat profile, facilitating its handling and ease of cutting into rectangular specimens for subsequent tensile testing.

Figure 7.3 showcases an SEM image from the fabric-side view of the nanofiber-laminated composite. This image revealed the presence of two distinct types of yarn within the weft: amber fibre and cotton fibre. The amber fibers exhibited an average diameter of 25 ± 2 µm, while the cotton fibers were slightly narrower, measuring 15 ± 1 µm in diameter. In the warp direction, which utilized linen yarns, the filaments were even finer, with a diameter of 12 ± 1 µm.

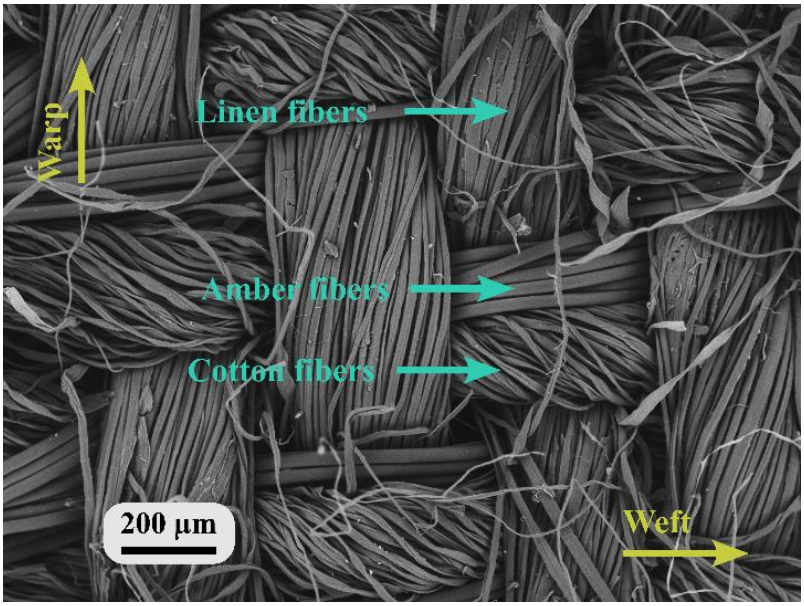

Figure 7.3 Nanofiber-laminated composite textile (view: outer side).

Figure 7.4a offers an enhanced SEM image of the nanofiber mat on the fabric, showcasing the orientation of the nanofibers. Notably, there was an absence of droplet formation within the nanofiber mat, indicating a consistent flow of the PAN solution and successful formation of nanofibers during electrospinning. Figure 7.4b focuses on the edge of the nanofiber-laminated composite fabric, where the interface between the nanofiber mat and the fabric is distinctly visible. Here, the nanofibers formed ring-shaped layers around the fibers

of the yarn, creating a radial zone that signified the connection point between the nanofiber mat and the yarn fibers.

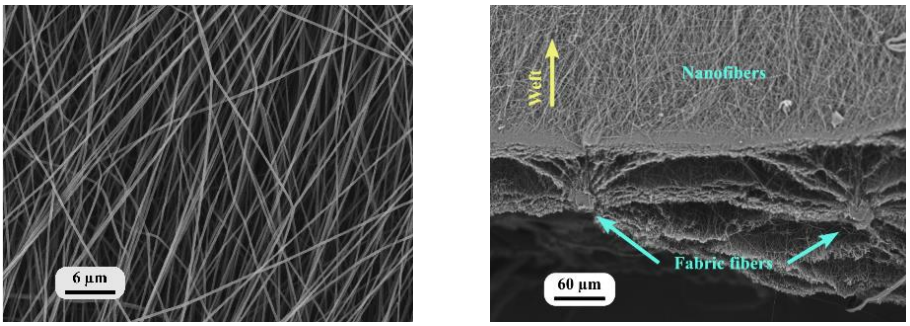

(a) (b)

Figure 7.4 Nanofiber-laminated composite fabrics: (a) view from the PAN nanofiber side; (b) cross-sectional view.

The distribution of the nanofibers' diameter is presented in Figure 7.5a. The distribution exhibited a skew of less than 0.5, indicating the appropriateness of a Gaussian distribution model. The average diameter of these nanofibers was found to be 432 ± 57 nm. Further analysis of the alignment of PAN nanofibers laminated onto the fabric is shown in Figure 7.5b. When the drum rotated at 1200 rpm, the FFT alignment values ranged from 0.0 to 0.65, suggesting that the majority of the nanofibers were oriented between 0° and 30°. This orientation was facilitated by the constant rotational speed of the drum, which not only stabilized the drawing process but also ensured a uniform range of diameters.

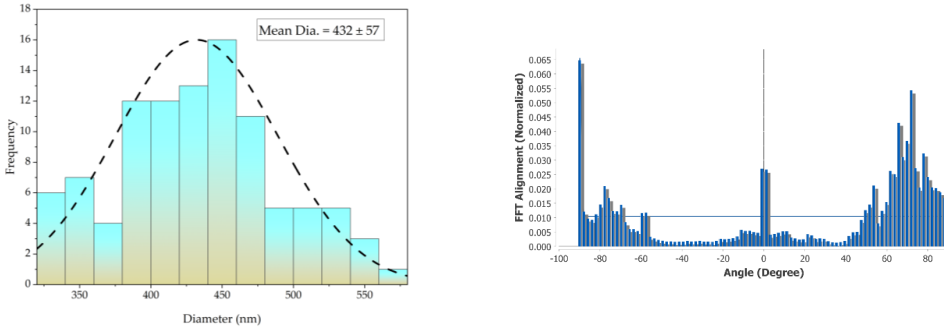

(a) (b)

Figure 7.5 Characteristics of nanofibers in the nanofiber-laminated composite fabric: (a) distribution of the nanofibers' diameter; (b) orientation of the PAN nanofibers.

The structural analysis of the nanofiber-laminated composite fabric highlights its potential for applications requiring high durability, uniformity, and precise nanofiber

alignment. The successful integration of the nanofiber mat with the woven fabric, without compromising the individual characteristics of either component, opens avenues for innovative uses in smart textiles, wearable electronics, and other advanced materials that require both flexibility and strength.

7.4. Mechanical Properties of Laminated Textiles

This chapter focuses on the mechanical properties of PAN nanofiber mats, plain fabric, and nanofiber-laminated composites, with an emphasis on their stress-strain relationships and elastic behaviour.

Figure 7.6a displays the stress (σ) versus strain (ε) curves for the PAN nanofiber mat, plain fabric, and the laminated composites. Notably, no failures occurred at the grips during tensile testing due to the effective gripping force. An enlarged view of these curves within a 5% deformation range (Figure 7.6b) reveals that the elastic modulus of the laminated composite fabric was higher than that of the plain fabric alone. This enhancement is attributed to the reinforcement provided by the nanofibers.

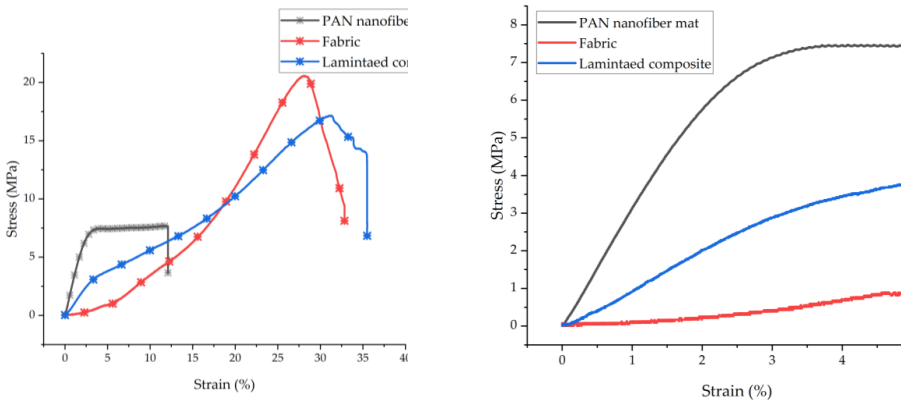

(a) (b)

Figure 7.6 (a) Representative stress–strain graph of the nanofiber mat, the fabric, and the laminated composite fabrics; (b) enlargement of the stress–strain curve in the low range of deformation (0–5%).

The stress-strain curve for the fabric illustrates a crimping region where the fabric deforms without effectively carrying a load. In contrast, the nanofiber-laminated composite shows a crimp-free behaviour in its elastic region, indicating a more uniform load distribution under stress.

The initial thickness of the plain fabric was measured at 301 ± 12 µm, which increased to 565 ± 13 µm post-electrospinning. The PAN nanofibers had a thickness of 147.8 ± 7 µm. This discrepancy is partly attributed to the fabric glue, which added approximately 50 ± 2 µm to the total thickness. Nanofibers collected on interleaved aluminium foil showed some loss of nanofibers as well.

Regarding tensile strength, the PAN nanofiber mat recorded a strength of 10.2 ± 2 MPa. The ultimate tensile strength for the fabric was 18.9 ± 2 MPa, compared to 17.2 ± 1 MPa for the nanofiber-laminated composite. Young's modulus for the fabric in the linear region was 72.9 MPa, increasing to 128 ± 12.5 MPa for the laminated composite, indicating a 75.5% increase. The PAN nanofiber mat exhibited the highest elastic modulus at 333.4 ± 32 MPa.

The elongation before breaking was 18 ± 4% for the PAN nanofiber mat, 31.2 ± 2% for the fabric, and 37.5 ± 2% for the nanofiber-laminated fabric. The increase in elongation at breaking for the laminated fabric was approximately 20%. These measurements, along with thickness, tensile strength, and elastic moduli, are summarized in Table 7.1.

Table 7.1

Tensile properties of the PAN nanofiber mat, the fabric, and the laminated composite.

Materials	Thickness, t (µm)	Ultimate Tensile Strength, σ (MPa)	Young's Modulus, E (MPa)	Elongation at Breaking, ε (%)
Fabric	301 ± 12	18.9 ± 2	72.9 ± 3	31.2 ± 2
PAN nanofiber mat	147.8 ± 7	10.2 ± 2	333.4 ± 32	18 ± 4
Laminated composite	565 ± 13	17.2 ± 1	128 ± 12.5	37.5 ± 2

The reinforcement of the fabric with nanofibers was achieved through electrospinning onto the fabric using a high-velocity rotating drum collector. This method enhanced the alignment of the nanofibers, contributing to the composite's strength. The perfect adhesion between the fabric fibers and electrospun nanofibers, as evidenced in Figure 7.4b, is attributed to intermolecular forces and surface interactions, including electrostatic attraction and mechanical interlocking.

Figure 7.7 visually represents the stress-strain behaviour of both plain fabric and the nanofiber-laminated composite fabric. The plain fabric exhibited a transition in the crimping region under loading, aligning the woven structure of the yarns. The nanofiber-reinforced

fabric, however, displayed a non-linear region due to the delamination and constant elongation of the PAN nanofibers under stress, leading to plastic deformation.

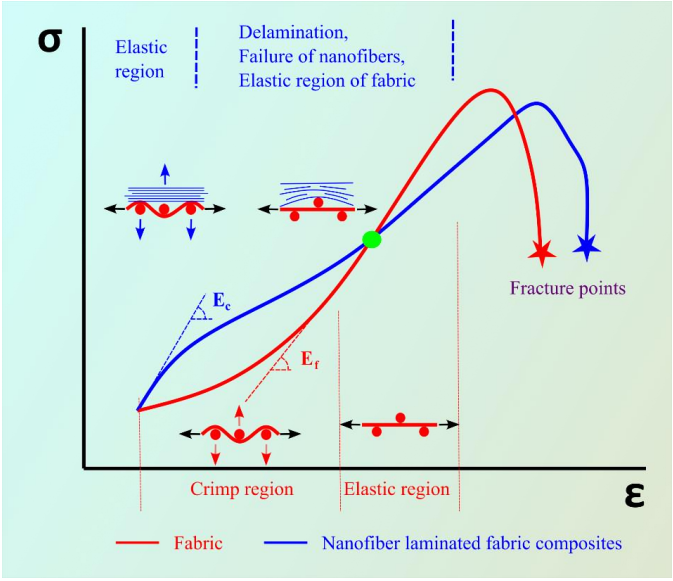

Figure 7.7 Typical stress–strain curve of the fabric and the nanofiber-laminated composite fabric.

The experimental elastic modulus was compared with theoretical predictions from various micromechanical models (Figure 7.8). The ROM model overestimated the elastic modulus, while the Cox–Krenchel model underestimated it. In contrast, the Tsai–Pagano and Halpin–Tsai models provided more accurate predictions, closely matching the experimental results.

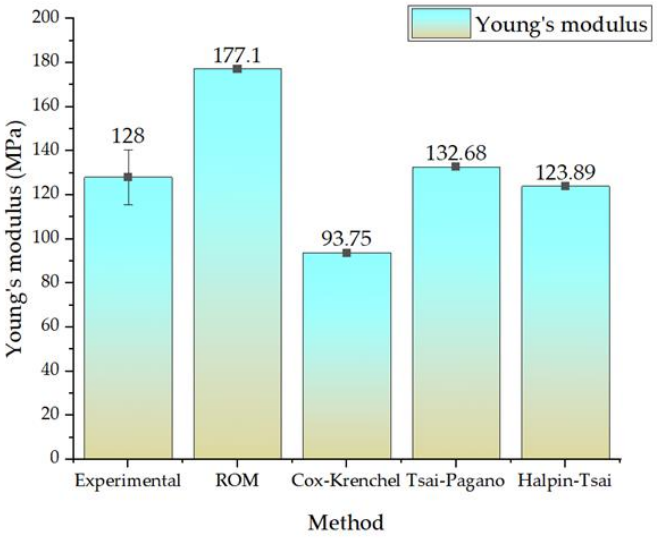

Figure 7.8 Comparison of micromechanical models and the experimental results.

These observations underscore the significance of fibre orientation and composite geometry in determining the mechanical properties of nanofiber-laminated textiles. The more precise predictions of the Tsai–Pagano and Halpin–Tsai models highlight their suitability in accounting for the orientation and geometry of the composite materials.

The discrepancies observed in the elastic modulus estimations by different micromechanical models can be attributed to their underlying assumptions about the behaviour and orientation of materials within the composite. The Rule of Mixtures (ROM) model, for instance, tends to overestimate the elastic modulus as it assumes an average behaviour of two independent materials, disregarding their specific geometry and orientation. In our study, this assumption did not hold true since the nanofibers were oriented between 0° and 30° (as shown in Figure 7.5b) and not randomly distributed, leading to a contradiction with the ROM model's basic premise.

Conversely, the Cox–Krenchel model, which accounts for random fibre orientation, underpredicted the results in our experimental setup. This discrepancy occurred because the model's assumptions did not align with the actual orientation of the nanofibers in our composite, which were not randomly oriented.

In contrast, the Tsai–Pagano and Halpin–Tsai models provided more accurate predictions of the elastic modulus, aligning closely with the experimental results. The deviations observed were 4.68 MPa and 4.11 MPa, respectively, both within a 5% range of the

experimental values. These models successfully incorporate the orientation and geometry of the composite material, offering a more realistic estimation of its mechanical properties. This approach aligns with findings from a previous study [40], where the Tsai–Pagano model aptly predicted the elastic modulus for composites with nanofibers, whereas the ROM model overestimated and the Cox–Krenchel model underestimated the results.

The Tsai–Pagano model, in particular, offered a nuanced prediction by considering both the random in-plane fibers and the transverse elastic modulus. It provided a more precise estimation of the elastic modulus for the nanofiber-laminated composite material, taking into account these specific factors. Similarly, the Halpin–Tsai model, by accounting for both the orientation and geometry of the composite, predicted the elastic modulus within a margin that was acceptably close to the experimental results (within a 5% range). These models' ability to incorporate critical variables such as fibre orientation and composite geometry renders them more reliable than the ROM model for predicting the elastic modulus of nanofiber-laminated composite materials.

7.5. SEM Analysis after Tensile Test of Laminated Textiles

In this chapter, we employed Scanning Electron Microscopy (SEM) to meticulously examine the morphological characteristics of the fractured tensile cross-sections of both the woven fabric and the nanofiber-laminated composite fabric. This analysis aimed to unravel the underlying mechanisms of their fracturing behaviour.

Figure 7.9 offers a visual representation of the fractured surfaces of both materials. The SEM images provided a detailed view of the fracturing patterns, highlighting the differences in fracture mechanisms between the two types of fabrics. The woven fabric's fractured surface predominantly exhibited broken fibers, aligning with a brittle fracture mechanism. The deformation was confined within the same plane, indicating a lack of multi-planar stress distribution. This behaviour is typical of traditional woven fabrics, where the failure occurs primarily along the fibre breaking points.

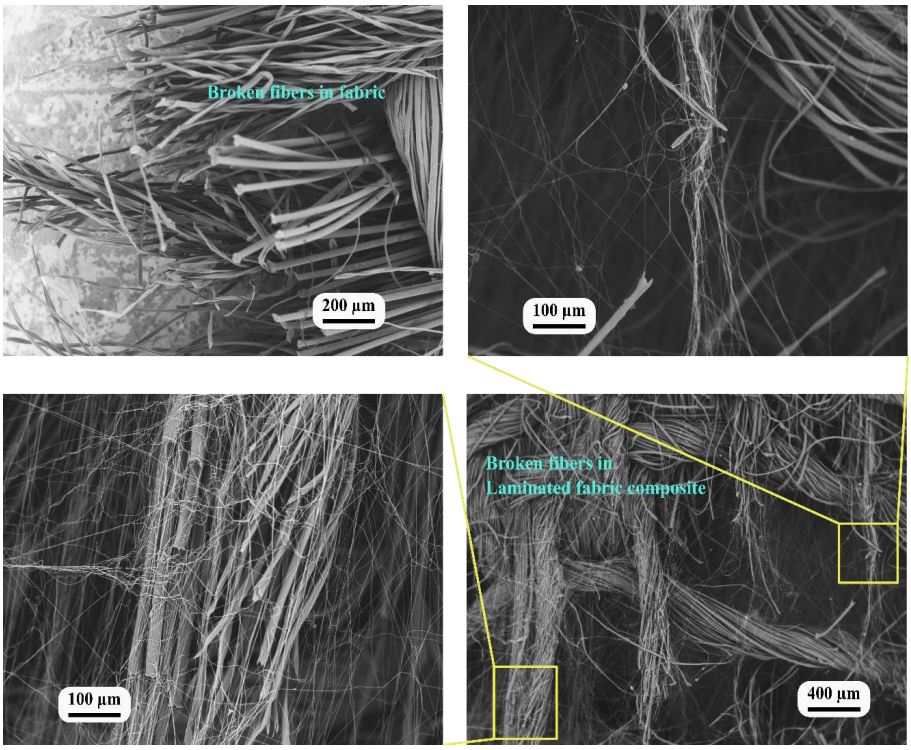

Figure 7.9 SEM image of test specimens of the fabric and the nanofiber-laminated composite fabric.

In stark contrast, the fractured surface of the nanofiber-laminated composite fabric showed a more complex pattern. It revealed individual fibers fracturing at different levels and across multiple planes. Several factors contribute to this behaviour. The role of fabric glue, which promoted the direct adhesion of nanofibers to the yarn's microfibers, was evident (as shown in Figure 7.4b). SEM images (Figure 7.7) suggested that the notable increase in elongation could be attributed to this adhesion, with some nanofibers maintaining their connection to the microfiber ends post-fracture due to strong interfacial forces (Marcuello et al., 2023).

SEM analysis provided clear visual evidence of the interactions between nanofibers and the microfibers within the yarn structure. The presence of connected nanofibers post-fracture indicated that the bonds between nanofibers and microfibers remained intact, contributing to the composite material's enhanced elongation and overall mechanical properties.

Figure 7.10 focuses on SEM images near the clamps and the ends of the warp fibers, shedding light on the fracture behaviour and shear stress presence within the laminated

composite and woven fabric. Post-fracture, the SEM images revealed that the nanofiber-laminated composite fabric and the woven fabric separated, indicative of in-plane shear stress causing delamination. This stress resulted from the mismatched elastic regions between the layers, leading to their separation.

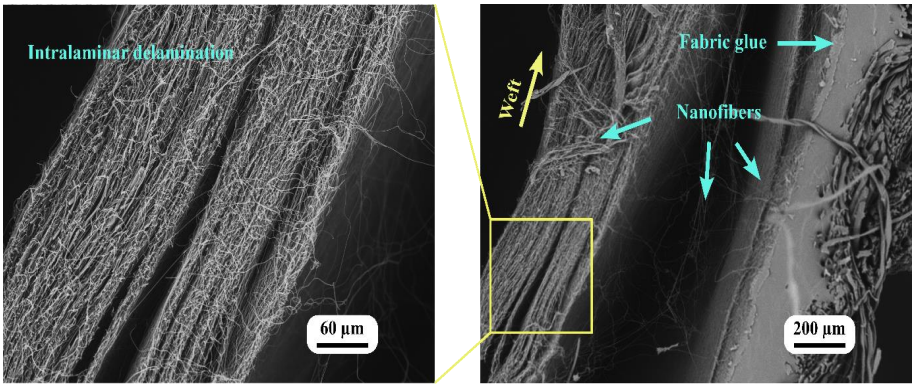

Figure 7.10 SEM image of a broken specimen of nanofiber-laminated composite fabric (near the grip).

Shear stress was not only observed between the layers but also within the nanofiber mat itself. The SEM analysis showed the mat separating into distinct layers, underscoring the orthotropic nature of the material, composed of individual, distinct layers. This behaviour further confirmed the presence of shear stress within the microlayers of the nanofiber mat.

Interestingly, one of the microlayers remained attached to the fabric glue, while the second layer of nanofibers delaminated. This finding suggests that the direct electrospinning technique used to apply nanofibers onto the fabric surface resulted in strong adhesion between the nanofibers and the fabric glue. This adhesion was crucial for transferring the load in the crimping region and maintained even after delamination. The preservation of this bond between the first electrospun microlayer and the adhesive glue (Figure 7.10) is testament to the effective load transfer mechanism established.

The adhesion between the nanofibers and the fabric adhesive is pivotal for the structural integrity and mechanical performance of the nanofiber-laminated composite fabric. This adhesion facilitates efficient load transfer between the nanofibers and the fabric, enabling them to function cohesively as a composite material. Moreover, it contributes to the enhanced mechanical properties observed, such as increased elongation and improved elasticity, as discussed in previous sections.

7.6. Conclusions of Laminated Textiles Reinforced with Electrospun Nanofibers

Chapter 7 provided a comprehensive analysis of the structural and mechanical properties of laminated textile composites reinforced with PAN nanofibers, highlighting their potential applications in smart textiles and electronic skins.

1. The structural characterization of the nanofiber-laminated composites revealed precise lamination and uniform distribution of nanofibers. SEM analysis showed the distinct yarn types in the fabric, indicating a successful integration of amber and cotton fibers with linen warp. The average diameters of these fibers were meticulously measured, showcasing the composite's complex structural integrity.
2. Mechanical testing revealed that the elastic modulus of the nanofiber-laminated composites was significantly higher than that of the plain fabric, indicating enhanced mechanical strength. The stress-strain curves demonstrated the elimination of the crimping effect typically observed in plain fabrics, contributing to the composites' improved load-bearing capabilities. The increase in the thickness of the fabric post-electrospinning, tensile strength, and elongation at breaking were all indicative of the reinforced nature of the laminated composites.
3. Post-tensile testing, SEM analysis of the fractured cross-sections of both the woven fabric and the nanofiber-laminated composites offered insights into their fracturing behaviours. The woven fabric exhibited a brittle fracture mechanism, while the nanofiber-laminated composites showed multi-planar fracturing, attributed to the effective adhesion between the nanofibers and the microfibers of the yarn. This adhesion was critical in enhancing the elongation and mechanical properties of the composite material.
4. SEM analysis also revealed in-plane shear stress between the layers of the laminated composite fabric, leading to delamination. This observation was crucial in understanding the interaction between the nanofiber mat and the fabric, particularly in terms of load transfer and stress distribution.
5. The strong adhesion between the nanofibers and the fabric, essential for the composite's structural integrity, was evident. The use of different micromechanical models to predict the elastic modulus of the laminated composites showed that the Tsai–Pagano and Halpin–Tsai models provided the most accurate predictions, considering the orientation and geometry of the composite material.

The findings from Chapter 7 underscore the effectiveness of using PAN nanofibers as reinforcement in textile composites. The enhanced mechanical properties, combined with the improved structural integrity due to effective adhesion, make these composites promising candidates for advanced applications in smart textiles and electronic skins. This study paves the way for further exploration into the use of nanofiber-reinforced composites in various industries, potentially leading to innovative solutions in wearable technology and beyond.

CONCLUSIONS

This doctoral thesis is embarked on a comprehensive journey through the intricate world of nanofiber technology, with a specific focus on polyacrylonitrile (PAN) nanofiber mats. The essence of this research lies in its holistic approach, spanning from the foundational principles of nanofiber fabrication to the innovative enhancement of their mechanical and thermal properties, culminating in the exploration of their applications in reinforcing non-crimping textiles. This final section aims to encapsulate the significant strides made in understanding and optimising PAN nanofiber mats, reflecting on the key findings, contributions to the field of nanotechnology, broader implications of this research, and outlining a pathway for future investigations. By delving into the specifics of each chapter and integrating these insights into a cohesive narrative, we highlight the pivotal role of this thesis in advancing nanofiber technology and setting new benchmarks for future scholarly endeavours.

Chapter conclusions:

1. Introduction: The thesis introduces the pioneering field of nanofiber technology, emphasising its significance due to the unique properties of nanomaterials. It sets the stage for the study by highlighting the potential of polyacrylonitrile (PAN) nanofiber mats in various applications, driven by their exceptional mechanical, thermal, and filtration capabilities. The introduction delineates the research gap and the necessity for a deeper investigation into the fabrication techniques, properties, and applications of PAN nanofibers.
2. Literature Review: This chapter provides an exhaustive review of the current state of nanofiber technology. It covers the evolution of nanofibers, focussing on fabrication techniques with a special emphasis on electrospinning, and exploring the mechanical and thermal properties critical to their performance. The review identifies the existing research gaps, particularly in the area of PAN nanofibers, and sets a clear direction for the study.
3. Fabrication of PAN nanofiber mats: The third chapter delves into the experimental procedures for fabricating PAN nanofiber mats. Examine different methods of electrospinning, assessing their impact on fibre orientation and mat structure. This chapter provides foundational work for understanding how fabrication techniques influence the physical properties of nanofiber mats. The nanofiber mat with the

orientated structure has 128% higher UTS and 298% (~4 times) higher Young's modulus compared to the random structure.

4. A FE Model for Determining the Mechanical Properties: Here, the development and validation of a Finite Element (FE) model for predicting the mechanical properties of electrospun nanofiber mats are presented. The model's accuracy in simulating the behaviour of nanofibers under different conditions represents a significant step forward in the analytical capabilities in nanofiber research.
5. Effect of Annealing on PAN Nanofiber Mats: This chapter investigates the effects of annealing on the properties of PAN nanofiber mats. It provides critical insights into how thermal treatments can enhance the strength and stability of nanofibers, offering a pathway to improve their application potential. Annealing has a significant impact on PAN nanofibers when annealed at various temperatures, the diameter of nanofibers decreased by 20%. Annealing at 70 ° C increased UTS by 32% and Young's modulus by 6.5%. However, annealing above 100 °C resulted in a decrease in tensile strength and Young's modulus. In the transverse direction, the enhanced UTS increased by 23.5 % and Young's modulus increased by 18.5%.
6. Investigation of PVA Bonded PAN Nanofiber Mats: The sixth chapter explores a novel approach to enhance the mechanical properties of PAN nanofibers through PVA bonding. This innovative strategy addresses the challenge of maintaining the structural integrity of nanofiber mats while enhancing their strength. Adding PVA with 2% to the PAN nanofiber porosity was slightly reduced by 12.5%, with 1 % PVA solution it was reduced to 6.9% and with 0.5% PVA solution it reduced to 4.1%. The thermal stability remained constant with the PVA dopant, with a slight change with 0.5%. The composite prepared with added 2% PVA solution showed increased Young's modulus by 78.3% and UTS by 84.3% in the longitudinal direction whereas in the transverse direction it was 159.5% and 200%, respectively. The nanofiber composite mat made with 2.0% PVA has 563% higher Young's modulus in the longitudinal direction, and 22% higher Young's modulus in the transverse direction compared to the Young's modulus of the random nanofiber structure.
7. Non-Crimping Textiles Reinforced with PAN Nanofibers: The final experimental chapter focusses on the application of PAN nanofibers in reinforcing non-crimping textiles. Highlights the potential of PAN nanofibers in the creation of composite materials with superior mechanical properties.

   Comprehensive Conclusion:

Summary of Key Findings: The thesis significantly advances the field of nanofiber technology by elucidating the impact of fabrication techniques, annealing, and novel bonding methods on the properties of PAN nanofiber mats. It demonstrates the pivotal role of fibre alignment and thermal treatment in enhancing nanofiber performance.

Contribution to Nanofiber Technology: Through experimental investigations and FE modelling, the study provides new insights into the optimization of nanofiber mats for various applications. The findings provide a detailed understanding of the relationship between processing conditions and the physical properties of nanofibers.

Implications of Research: The implications of this research are far-reaching and provide a foundation for the development of stronger, more durable nanofiber-based materials. The improved understanding of PAN nanofibers' properties opens up new avenues for their use in filtration, biomedical, and structural applications.

Recommendations for Future Work: Future research should focus on exploring the effects of different nanofiber compositions and further refining the FE model for broader applications. Investigating the long-term durability of PAN nanofiber mats under various environmental conditions would also be valuable.

Final Thoughts and Closing Remarks: This doctoral thesis marks a significant milestone in nanofiber technology, pushing the boundaries of material science and engineering. Research not only fills a critical gap in the literature, but also sets the stage for future innovations that could revolutionise multiple industries. The journey from understanding the basic properties of PAN nanofibers to exploring their potential applications underscores the transformative power of nanotechnology and its promise for the future.

REFERENCES

1. Agarwal, B. D., Broutman, L. J., & Chandrasekhara, K. (2017). Analysis and performance of fiber composites. In *Materials Science and Engineering: A* (Vol. 151, Issue 1). JohnWiley & Sons: Hoboken.
2. Albetran, H. M. (2021). Investigation of the Morphological, Structural, and Vibrational Behaviour of Graphite Nanoplatelets. *Journal of Nanomaterials*, *2021*. https://doi.org/10.1155/2021/5546509
3. Aliheidari, N., Aliahmad, N., Agarwal, M., & Dalir, H. (2019). Electrospun nanofibers for label-free sensor applications. *Sensors (Switzerland)*, *19*(16). https://doi.org/10.3390/s19163587
4. Ambekar, R. S., & Kandasubramanian, B. (2019). Advancements in nanofibers for wound dressing: A review. *European Polymer Journal*, *117*(March), 304–336. https://doi.org/10.1016/j.eurpolymj.2019.05.020
5. Anusiya, G., & Jaiganesh, R. (2022). A review on fabrication methods of nanofibers and a special focus on application of cellulose nanofibers. *Carbohydrate Polymer Technologies and Applications*, *4*(November), 100262. https://doi.org/10.1016/j.carpta.2022.100262
6. Araujo, S., Delpouve, N., Delbreilh, L., Papkov, D., Dzenis, Y., & Dargent, E. (2019). Dielectric and calorimetric signatures of chain orientation in strong and tough ultrafine electrospun polyacrylonitrile. *Polymer*, *178*(July), 121638. https://doi.org/10.1016/j.polymer.2019.121638
7. Arinstein, A., Burman, M., Gendelman, O., & Zussman, E. (2007). Effect of supramolecular structure on polymer nanofibre elasticity. *Nature Nanotechnology*, *2*(1), 59–62. https://doi.org/10.1038/nnano.2006.172
8. Arun, A., Malrautu, P., Laha, A., & Ramakrishna, S. (2021). Gelatin nanofibers in drug delivery systems and tissue engineering. *Engineered Science*, *16*, 71–81. https://doi.org/10.30919/es8d527
9. Ayres, C. E., Jha, B. S., Meredith, H., Bowman, J. R., Bowlin, G. L., Henderson, S. C., & Simpson, D. G. (2008). Measuring fiber alignment in electrospun scaffolds: A user's guide to the 2D fast Fourier transform approach. *Journal of Biomaterials Science, Polymer Edition*, *19*(5), 603–621. https://doi.org/10.1163/156856208784089643
10. Backer, S., & Petterson, D. R. (1960). Some Principles of Nonwoven Fabrics1. *Textile Research Journal*, *30*(9), 704–711. https://doi.org/10.1177/004051756003000912
11. Balogh, A., Farkas, B., Verreck, G., Mensch, J., Borbás, E., Nagy, B., Marosi, G., & Nagy, Z. K. (2016). AC and DC electrospinning of hydroxypropylmethylcellulose with polyethylene oxides as secondary polymer for improved drug dissolution. *International Journal of Pharmaceutics*, *505*(1–2), 159–166. https://doi.org/10.1016/j.ijpharm.2016.03.024
12. Barua, B., & Saha, M. C. (2017). Influence of Humidity, Temperature, and

Annealing on Microstructure and Tensile Properties of Electrospun Polyacrylonitrile Nanofibers. *POLYMER ENGINEERING AND SCIENCE*, 1–10. https://doi.org/doi.org/10.1002/pen.24657
13. Beese, A. M., Papkov, D., Li, S., Dzenis, Y., & Espinosa, H. D. (2013). In situ transmission electron microscope tensile testing reveals structure-property relationships in carbon nanofibers. *Carbon*, *60*, 246–253. https://doi.org/10.1016/j.carbon.2013.04.018
14. Bhudolia, S. K., Kam, K. K. C., Perrotey, P., & Joshi, S. C. (2019). Effect of fixation stitches on out-of-plane response of textile non-crimp fabric composites. *Journal of Industrial Textiles*, *48*(7), 1151–1166. https://doi.org/10.1177/1528083718757525
15. Catalani, L. H., Collins, G., & Jaffe, M. (2007). Evidence for molecular orientation and residual charge in the electrospinning of poly(butylene terephthalate) nanofibers. *Macromolecules*, *40*(5), 1693–1697. https://doi.org/10.1021/ma061342d
16. Chavoshnejad, P., Alsmairat, O., Ke, C., & Razavi, M. J. (2021). Effect of interfiber bonding on the rupture of electrospun fibrous mats. *Journal of Physics D: Applied Physics*, *54*(2). https://doi.org/10.1088/1361-6463/abba95
17. Chavoshnejad, P., & Razavi, M. J. (2020). Effect of the Interfiber Bonding on the Mechanical Behavior of Electrospun Fibrous Mats. *Scientific Reports*, *10*(1), 1–11. https://doi.org/10.1038/s41598-020-64735-5
18. Chen, J., Chen, W., Wang, M., Ding, Y., Zhou, H., Zhao, B., & Fan, J. (2017). Mechanical behaviors and elastic parameters of laminated fabric URETEK3216LV subjected to uniaxial and biaxial loading. *Applied Composite Materials*, *24*(5), 1107–1136. https://doi.org/10.1007/s10443-016-9576-2
19. Chen, K., Hu, H., Zeng, Y., Pan, H., Wang, S., Zhang, Y., Shi, L., Tan, G., Pan, W., & Liu, H. (2022). Recent advances in electrospun nanofibers for wound dressing. *European Polymer Journal*, *178*(August), 111490. https://doi.org/10.1016/j.eurpolymj.2022.111490
20. Chen, N., Koker, M. K. A., Uzun, S., & Silberstein, M. N. (2016). In-situ X-ray study of the deformation mechanisms of non-woven polypropylene. *International Journal of Solids and Structures*, *97_98*, 200–208. https://doi.org/10.1016/j.ijsolstr.2016.07.028
21. Choi, S. S., Lee, S. G., Joo, C. W., Im, S. S., & Kim, S. H. (2004). Formation of interfiber bonding in electrospun poly(etherimide) nanofiber web. *Journal of Materials Science*, *39*(4), 1511–1513. https://doi.org/10.1023/B:JMSC.0000013931.84760.b0
22. Collins, G., Federici, J., Imura, Y., & Catalani, L. H. (2012). Charge generation, charge transport, and residual charge in the electrospinning of polymers: A review of issues and complications. *Journal of Applied Physics*, *111*(4). https://doi.org/10.1063/1.3682464

23. Collins, R. T., Jones, J. J., Harris, M. T., & Basaran, O. A. (2008). Electrohydrodynamic tip streaming and emission of charged drops from liquidcones. *Nature Physics*, *4*(2), 149–154. https://doi.org/10.1038/nphys807
24. Demir, M. M., Yilgor, I., Yilgor, E., & Erman, B. (2002). Electrospinning of polyurethane fibers. *Polymer*, *43*(11), 3303–3309. https://doi.org/10.1016/S0032-3861(02)00136-2
25. Duan, G., Liu, S., Jiang, S., & Hou, H. (2019). High-performance polyamide-imide films and electrospun aligned nanofibers from an amide-containing diamine. *Journal of Materials Science*, *54*(8), 6719–6727. https://doi.org/10.1007/s10853-019-03326-w
26. Duft, D., Achtzehn, T., Muller, R., Huber, B. A., & Leisner, T. (2003). Rayliegh Jets of Microdrops. *Nature*, *421*(January), 2003.
27. Es-Saheb, M., & Elzatahry, A. (2014). Post-heat treatment and mechanical assessment of polyvinyl alcohol nanofiber sheet fabricated by electrospinning technique. *International Journal of Polymer Science*, *2014*(iv). https://doi.org/10.1155/2014/605938
28. Faccini, M., Vaquero, C., & Amantia, D. (2012). Development of protective clothing against nanoparticle based on electrospun nanofibers. *Journal of Nanomaterials*, *2012*. https://doi.org/10.1155/2012/892894
29. Farukh, F., Demirci, E., Sabuncuoglu, B., Acar, M., Pourdeyhimi, B., & Silberschmidt, V. V. (2014). Numerical analysis of progressive damage in nonwoven fibrous networks under tension. *International Journal of Solids and Structures*, *51*(9), 1670–1685. https://doi.org/10.1016/j.ijsolstr.2014.01.015
30. Feng, J. J. (2002). The stretching of an electrified non-Newtonian jet: A model for electrospinning. *Physics of Fluids*, *14*(11), 3912–3926. https://doi.org/10.1063/1.1510664
31. Feng, L., Xie, N., & Zhong, J. (2014). Carbon nanofibers and their composites: A review of synthesizing, properties and applications. *Materials*, *7*(5), 3919–3945. https://doi.org/10.3390/ma7053919
32. Finn, R. (1999). Capillary surface interactions. *Notices of the AMS*, *46*, 770–781. http://www.ams.org/notices/199907/fea-finn.pdf
33. Fridrikh, S. V., Yu, J. H., Brenner, M. P., & Rutledge, G. C. (2003). Controlling the Fiber Diameter during Electrospinning. *Physical Review Letters*, *90*(14), 4. https://doi.org/10.1103/PhysRevLett.90.144502
34. Gañán-Calvo, A. M. (1997). Cone-jet analytical extension of Taylor's electrostatic solution and the asymptotic universal scaling laws in electrospraying. *Physical Review Letters*, *79*(2), 217–220. https://doi.org/10.1103/PhysRevLett.79.217
35. Georgopoulou, A., Michel, S., & Clemens, F. (2021). Sensorized robotic skin based on piezoresistive sensor fiber composites produced with injection molding of liquid silicone. *Polymers*, *13*(8).

https://doi.org/10.3390/polym13081226
36. Gorji, M., Bagherzadeh, R., & Fashandi, H. (2017). Electrospun nanofibers in protective clothing. In *Electrospun Nanofibers*. Elsevier Ltd. https://doi.org/10.1016/B978-0-08-100907-9.00021-0
37. Guan, X., Xu, B., Wu, M., Jing, T., Yang, Y., & Gao, Y. (2021). Breathable, washable and wearable woven-structured triboelectric nanogenerators utilizing electrospun nanofibers for biomechanical energy harvesting and self-powered sensing. *Nano Energy*, *80*(July 2020), 105549. https://doi.org/10.1016/j.nanoen.2020.105549
38. Guo, Z., Shao, C., Zhang, M., Mu, J., Zhang, Z., Zhang, P., Chen, B., & Liu, Y. (2011). Dandelion-like Fe3O4@CuTNPc hierarchical nanostructures as a magnetically separable visible-light photocatalyst. *Journal of Materials Chemistry*, *21*(32), 12083–12088. https://doi.org/10.1039/c1jm11098e
39. Gupta, A. K., Paliwal, D. K., & Bajaj, P. (1998). Melting behavior of acrylonitrile polymers. *Journal of Applied Polymer Science*, *70*(13), 2703–2709. https://doi.org/10.1002/(sici)1097-4628(19981226)70:13<2703::aid-app15>3.0.co;2-2
40. Guzman-Puyol, S., Ceseracciu, L., Heredia-Guerrero, J. A., Anyfantis, G. C., Cingolani, R., Athanassiou, A., & Bayer, I. S. (2015). Effect of trifluoroacetic acid on the properties of polyvinyl alcohol and polyvinyl alcohol-cellulose composites. *Chemical Engineering Journal*, *277*, 242–251. https://doi.org/10.1016/j.cej.2015.04.092
41. Habeeb, S. A., Nadhim, B. A., Kadhim, B. J., Ktab, M. S., Kadhim, A. J., & Murad, F. S. (2023). Improving the Physical Properties of Nanofibers Prepared by Electrospinning from Polyvinyl Chloride and Polyacrylonitrile at Low Concentrations. *Advances in Polymer Technology*, *2023*, 1–12. https://doi.org/10.1155/2023/1811577
42. Hahn, L., Rittner, S., Bauer, C., & Cherif, C. (2018). Development of alternative bondings for the production of stitch-free non-crimp fabrics made of multiple carbon fiber heavy tows for construction industry. *Journal of Industrial Textiles*, *48*(3), 660–681. https://doi.org/10.1177/1528083717736100
43. Han, T., Reneker, D. H., & Yarin, A. L. (2008). Pendulum-like motion of straight electrified jets. *Polymer*, *49*(8), 2160–2169. https://doi.org/10.1016/j.polymer.2008.01.048
44. Hanumantharao, S. N., & Rao, S. (2019). Multi-functional electrospun nanofibers from polymer blends for scaffold tissue engineering. *Fibers*, *7*(66), 1–35.
45. He, J. H., Wu, Y., & Zuo, W. W. (2005). Critical length of straight jet in electrospinning. *Polymer*, *46*(26), 12637–12640. https://doi.org/10.1016/j.polymer.2005.10.130
46. He, W., Horn, S. W., & Hussain, M. D. (2007). Improved bioavailability

of orally administered mifepristone from PLGA nanoparticles. *International Journal of Pharmaceutics*, *334*(1–2), 173–178. https://doi.org/10.1016/j.ijpharm.2006.10.025
47. Helgeson, M. E., Grammatikos, K. N., Deitzel, J. M., & Wagner, N. J. (2008). Theory and kinematic measurements of the mechanics of stable electrospun polymer jets. *Polymer*, *49*(12), 2924–2936. https://doi.org/10.1016/j.polymer.2008.04.025
48. Hohman, M. M., Shin, M., Rutledge, G., & Brenner, M. P. (2001). Electrospinning and electrically forced jets. II. Applications. *Physics of Fluids*, *13*(8), 2221–2236. https://doi.org/10.1063/1.1384013
49. Homaeigohar, S., & Boccaccini, A. R. (2020). Antibacterial biohybrid nanofibers for wound dressings. *Acta Biomaterialia*, *107*(2020), 25–49. https://doi.org/10.1016/j.actbio.2020.02.022
50. Huang, L., Manickam, S. S., & McCutcheon, J. R. (2013). Increasing strength of electrospun nanofiber membranes for water filtration using solvent vapor. *Journal of Membrane Science*, *436*, 213–220. https://doi.org/10.1016/j.memsci.2012.12.037
51. Huang, Z. M., Zhang, Y. Z., Kotaki, M., & Ramakrishna, S. (2003). A review on polymer nanofibers by electrospinning and their applications in nanocomposites. *Composites Science and Technology*, *63*(15), 2223–2253. https://doi.org/10.1016/S0266-3538(03)00178-7
52. Jain, N., Singh, V. K., & Chauhan, S. (2017). A review on mechanical and water absorption properties of polyvinyl alcohol based composites/films. *Journal of the Mechanical Behavior of Materials*, *26*(5–6), 213–222. https://doi.org/10.1515/jmbm-2017-0027
53. Jalalah, M., Ahmad, A., Saleem, A., Qadir, M. B., Khaliq, Z., Khan, M. Q., Nazir, A., Faisal, M., Alsaiari, M., Irfan, M., Alsareii, S. A., & Harraz, F. A. (2022). Electrospun nanofiber/textile supported composite membranes with improved mechanical performance for biomedical applications. *Membranes*, *12*(11). https://doi.org/10.3390/membranes12111158
54. Jamil, T., Munir, S., Wali, Q., Shah, G. J., Khan, M. E., & Jose, R. (2021). Water Purification through a Novel Electrospun Carbon Nanofiber Membrane. *ACS Omega*, *6*(50), 34744–34751. https://doi.org/10.1021/acsomega.1c05197
55. Jin, H., Nayeem, M. O. G., Lee, S., Matsuhisa, N., Inoue, D., Yokota, T., Hashizume, D., & Someya, T. (2019). Highly durable nanofiber-reinforced elastic conductors for skin-tight electronic textiles. *ACS Nano*, *13*(7), 7905–7912. https://doi.org/10.1021/acsnano.9b02297
56. Kanani, G. A., & Bahrami, H. S. (2010). Review on electrospun nanofibers scaffold and biomedical applications. *Trends in Biomaterials and Artificial Organs*, *24*(2), 93–115.
57. Kang, M., Kim, J., Jang, B., Chae, Y., Kim, J. H., & Ahn, J. H. (2017).

Graphene-based three-dimensional capacitive touch sensor for wearable electronics. *ACS Nano*, *11*(8), 7950–7957. https://doi.org/10.1021/acsnano.7b02474
58. Kashyap, S., Pratihar, S. K., & Behera, S. K. (2016). Strong and ductile graphene oxide reinforced PVA nanocomposites. *Journal of Alloys and Compounds*, *684*, 254–260. https://doi.org/10.1016/j.jallcom.2016.05.162
59. Kenawy, E. R., Bowlin, G. L., Mansfield, K., Layman, J., Simpson, D. G., Sanders, E. H., & Wnek, G. E. (2002). Release of tetracycline hydrochloride from electrospun poly(ethylene-co-vinylacetate), poly(lactic acid), and a blend. *Journal of Controlled Release*, *81*(1–2), 57–64. https://doi.org/10.1016/S0168-3659(02)00041-X
60. Kessick, R., Fenn, J., & Tepper, G. (2004). The use of AC potentials in electrospraying and electrospinning processes. *Polymer*, *45*(9), 2981–2984. https://doi.org/10.1016/j.polymer.2004.02.056
61. Kim, G. H. (2008). Electrospun PCL nanofibers with anisotropic mechanical properties as a biomedical scaffold. *Biomedical Materials (Bristol, England)*, *3*(2), 25010. https://doi.org/10.1088/1748-6041/3/2/025010
62. Kucukali-Ozturk, M., Ozden-Yenigun, E., Nergis, B., & Candan, C. (2017). Nanofiber-enhanced lightweight composite textiles for acoustic applications. *Journal of Industrial Textiles*, *46*(7), 1498–1510. https://doi.org/10.1177/1528083715622427
63. Landel, R. F., & Nielsen, L. E. (1993). *Mechanical properties of polymers and composites*. CRC Press.
64. Lasenko, I., Grauda, D., Butkauskas, D., Sanchaniya, J. V., Viluma-Gudmona, A., & Lusis, V. (2022). Testing the physical and mechanical properties of polyacrylonitrile nanofibers reinforced with succinite and silicon dioxide nanoparticles. *Textiles*, *2*(1), 162–173. https://doi.org/10.3390/textiles2010009
65. Lasenko, I., Sanchaniya, J. V., Kanukuntla, S. P., Ladani, Y., Viluma-gudmona, A., Kononova, O., Lusis, V., Tipans, I., & Selga, T. (2023). The mechanical properties of nanocomposites reinforced with PA6 electrospun nanofibers. *Polymers*, *15*(3). https://doi.org/10.3390/polym15030673
66. Lee, J., Yoon, J., Kim, J. H., Lee, T., & Byun, H. (2018). Electrospun PAN–GO composite nanofibers as water purification membranes. *Journal of Applied Polymer Science*, *135*(7), 1–9. https://doi.org/10.1002/app.45858
67. Li, A., Li, F., Mai, K., & Zhang, Z. (2022). Crystallization and Melting Behavior of UHMWPE Composites Filled by Different Carbon Materials. *Advances in Polymer Technology*, *2022*. https://doi.org/10.1155/2022/2447418
68. Li, D., Marquez, M., & Xia, Y. (2007). Capturing electrified nanodroplets under Rayleigh instability by coupling electrospray with a sol-gel reaction.

Chemical Physics Letters, *445*(4–6), 271–275. https://doi.org/10.1016/j.cplett.2007.07.090
69. Li, D., & Xia, Y. (2004). Electrospinning of nanofibers: Reinventing the wheel? *Advanced Materials*, *16*(14), 1151–1170. https://doi.org/10.1002/adma.200400719
70. Li, W. J., Mauck, R. L., Cooper, J. A., Yuan, X., & Tuan, R. S. (2007). Engineering controllable anisotropy in electrospun biodegradable nanofibrous scaffolds for musculoskeletal tissue engineering. *Journal of Biomechanics*, *40*(8), 1686–1693. https://doi.org/10.1016/j.jbiomech.2006.09.004
71. Liang, Y., Cheng, S., Zhao, J., Zhang, C., Sun, S., Zhou, N., Qiu, Y., & Zhang, X. (2013). Heat treatment of electrospun Polyvinylidene fluoride fibrous membrane separators for rechargeable lithium-ion batteries. *Journal of Power Sources*, *240*, 204–211. https://doi.org/10.1016/j.jpowsour.2013.04.019
72. Liao, Y., Loh, C. H., Tian, M., Wang, R., & Fane, A. G. (2018). Progress in electrospun polymeric nanofibrous membranes for water treatment: Fabrication, modification and applications. *Progress in Polymer Science*, *77*, 69–94. https://doi.org/10.1016/j.progpolymsci.2017.10.003
73. Liu, F., Guo, R., Shen, M., Wang, S., & Shi, X. (2009). Effect of processing variables on the morphology of electrospun poly[(lactic acid)-co-(glycolic acid)] nanofibers. *Macromolecular Materials and Engineering*, *294*(10), 666–672. https://doi.org/10.1002/mame.200900110
74. Liu, Y., & Dzenis, Y. (2016). Explicit 3D finite-element model of continuous nanofibre networks. *Micro and Nano Letters*, *11*(11), 727–730. https://doi.org/10.1049/mnl.2016.0147
75. Maccaferri, E., Cocchi, D., Mazzocchetti, L., Benelli, T., Brugo, T. M., Giorgini, L., & Zucchelli, A. (2021). How Nanofibers Carry the Load: Toward a Universal and Reliable Approach for Tensile Testing of Polymeric Nanofibrous Membranes. *Macromolecular Materials and Engineering*, *306*(7). https://doi.org/10.1002/mame.202100183
76. Magazzù, A., & Marcuello, C. (2023). Investigation of soft matter nanomechanics by atomic force microscopy and optical tweezers: A comprehensive review. In *Nanomaterials* (Vol. 13, Issue 6). https://doi.org/10.3390/nano13060963
77. Maheshwari, S., & Chang, H. C. (2009). Assembly of multi-stranded nanofiber threads through AC electrospinning. *Advanced Materials*, *21*(3), 349–354. https://doi.org/10.1002/adma.200800722
78. Mao, X., Simeon, F., Rutledge, G. C., & Hatton, T. A. (2013). Electrospun carbon nanofiber webs with controlled density of states for sensor applications. *Advanced Materials*, *25*(9), 1309–1314. https://doi.org/10.1002/adma.201203045
79. Marcuello, C., Chabbert, B., Berzin, F., Bercu, N. B., Molinari, M., &

Aguié-Béghin, V. (2023). Influence of surface chemistry of fiber and lignocellulosic materials on adhesion properties with polybutylene succinate at nanoscale. *Materials*, *16*(6). https://doi.org/10.3390/ma16062440

80. Meena, J. S., Choi, S. Bin, Jung, S.-B., & Kim, J.-W. (2023). Electronic textiles: new age of wearable technology for healthcare and fitness solutions. *Materials Today Bio*, *19*(December 2022), 100565. https://doi.org/10.1016/j.mtbio.2023.100565
81. Mondal, J., An, J. M., Surwase, S. S., Chakraborty, K., Sutradhar, S. C., Hwang, J., Lee, J., & Lee, Y. K. (2022). Carbon Nanotube and Its Derived Nanomaterials Based High Performance Biosensing Platform. *Biosensors*, *12*(9). https://doi.org/10.3390/bios12090731
82. Munir, M. U., Mayer-Gall, T., Gutmann, J. S., Ali, W., Etemad-Parishanzadeh, O., Khanzada, H., & Mikučioniene, D. (2023). Development of carbon-nanodot-loaded PLA nanofibers and study of their barrier performance for medical applications. *Nanomaterials*, *13*(7). https://doi.org/10.3390/nano13071195
83. Musale, D. A., & Kumar, A. (2000). Solvent and pH resistance of surface crosslinked chitosan/poly(acrylonitrile) composite nanofiltration membranes. *Journal of Applied Polymer Science*, *77*(8), 1782–1793. https://doi.org/10.1002/1097-4628(20000822)77:8<1782::AID-APP15>3.0.CO;2-5
84. Nataraj, S. K., Yang, K. S., & Aminabhavi, T. M. (2012). Polyacrylonitrile-based nanofibers - A state-of-the-art review. *Progress in Polymer Science (Oxford)*, *37*(3), 487–513. https://doi.org/10.1016/j.progpolymsci.2011.07.001
85. Nathanael, A. J., & Oh, T. H. (2021). Encapsulation of calcium phosphates on electrospun nanofibers for tissue engineering applications. *Crystals*, *11*(2), 1–23. https://doi.org/10.3390/cryst11020199
86. Nemati, S., Kim, S. jeong, Shin, Y. M., & Shin, H. (2019). Current progress in application of polymeric nanofibers to tissue engineering. *Nano Convergence*, *6*(1). https://doi.org/10.1186/s40580-019-0209-y
87. Niu, Y., Zhang, X., Pan, W., Zhao, J., & Li, Y. (2014). Enhancement and wettability of self-assembled GO sheets as interfacial layers of CF/PI composites. *RSC Advances*, *4*(15), 7511–7515. https://doi.org/10.1039/c3ra46881j
88. Pai, C. L., Boyce, M. C., & Rutledge, G. C. (2011). On the importance of fiber curvature to the elastic moduli of electrospun nonwoven fiber meshes. *Polymer*, *52*(26), 6126–6133. https://doi.org/10.1016/j.polymer.2011.10.055
89. Papkov, D., Delpouve, N., Delbreilh, L., Araujo, S., Stockdale, T., Mamedov, S., Maleckis, K., Zou, Y., Andalib, M. N., Dargent, E., Dravid, V. P., Holt, M. V., Pellerin, C., & Dzenis, Y. A. (2019). Quantifying

Polymer Chain Orientation in Strong and Tough Nanofibers with Low Crystallinity: Toward Next Generation Nanostructured Superfibers [Review-article]. *ACS Nano*, *13*(5), 4893–4927. https://doi.org/10.1021/acsnano.8b08725

90. Papkov, D., Goponenko, A., Compton, O. C., An, Z., Moravsky, A., Li, X. Z., Nguyen, S. T., & Dzenis, Y. A. (2013). Improved graphitic structure of continuous carbon nanofibers via graphene oxide templating. *Advanced Functional Materials*, *23*(46), 5763–5770. https://doi.org/10.1002/adfm.201300653
91. Papkov, D., Zou, Y., Andalib, M. N., Goponenko, A., Cheng, S. Z. D., & Dzenis, Y. A. (2013). Simultaneously strong and tough ultrafine continuous nanofibers. *ACS Nano*, *7*(4), 3324–3331. https://doi.org/10.1021/nn400028p
92. Papkov, Di., Goponenko, A., Compton, O. C., An, Z., Nguyen, S. T., & Dzenis, Y. A. (2019). Controlled Nanofabrication of Uniform Continuous Graphene Oxide/Polyacrylonitrile Nanofibers for Templated Carbonization. *Journal of Micro and Nano-Manufacturing*, *7*(4), 1–9. https://doi.org/10.1115/1.4045211
93. Pham, L. Q., Uspenskaya, M. V., Olekhnovich, R. O., & Baranov, M. A. (2021). The mechanical properties of PVC nanofiber mats obtained by electrospinning. *Fibers*, *9*(1), 1–12. https://doi.org/10.3390/fib9010002
94. Püspöki, Z., Storath, M., Sage, D., & Unser, M. (2016). Transforms and operators for directional bioimage analysis: A survey. *Advances in Anatomy Embryology and Cell Biology*, *219*, 69–93. https://doi.org/10.1007/978-3-319-28549-8_3
95. Qiu, Q., Chen, S., Li, Y., Yang, Y., Zhang, H., Quan, Z., Qin, X., Wang, R., & Yu, J. (2020). Functional nanofibers embedded into textiles for durable antibacterial properties. *Chemical Engineering Journal*, *384*(June 2019), 123241. https://doi.org/10.1016/j.cej.2019.123241
96. Radu, E. R., Voicu, S. I., & Thankur, V. K. (2023). Polymeric membranes for biomedical applications. *Polymers*, *15*(3), 1–28. https://doi.org/https://doi.org/10.3390/polym15030619
97. Ramaswamy, S., Clarke, L. I., & Gorga, R. E. (2011). Morphological, mechanical, and electrical properties as a function of thermal bonding in electrospun nanocomposites. *Polymer*, *52*(14), 3183–3189. https://doi.org/10.1016/j.polymer.2011.05.023
98. Reneker, D. H., & Hao, F. (2006). Polymeric nanofibers: Introduction. *ACS Symposium Series*, *918*, 1–6. https://doi.org/10.1021/bk-2006-0918.ch001
99. Reneker, D. H., Kataphinan, W., Theron, A., Zussman, E., & Yarin, A. L. (2002). Nanofiber garlands of polycaprolactone by electrospinning. *Polymer*, *43*(25), 6785–6794. https://doi.org/10.1016/S0032-3861(02)00595-5

100. Reneker, D. H., & Yarin, A. L. (2008). Electrospinning jets and polymer nanofibers. *Polymer*, *49*(10), 2387–2425. https://doi.org/10.1016/j.polymer.2008.02.002
101. Rezakhaniha, R., Agianniotis, A., Schrauwen, J. T. C., Griffa, A., Sage, D., Bouten, C. V. C., Van De Vosse, F. N., Unser, M., & Stergiopulos, N. (2012). Experimental investigation of collagen waviness and orientation in the arterial adventitia using confocal laser scanning microscopy. *Biomechanics and Modeling in Mechanobiology*, *11*(3–4), 461–473. https://doi.org/10.1007/s10237-011-0325-z
102. Ridruejo, A., González, C., & Llorca, J. (2011). Micromechanisms of deformation and fracture of polypropylene nonwoven fabrics. *International Journal of Solids and Structures*, *48*(1), 153–162. https://doi.org/10.1016/j.ijsolstr.2010.09.013
103. Rodriguez-Millan, M., Garcia-Gonzalez, D., Rusinek, A., & Arias, A. (2018). Influence of stress state on the mechanical impact and deformation behaviors of aluminum alloys. *Metals*, *8*(7). https://doi.org/10.3390/met8070520
104. Sallakhniknezhad, R., Khorsi, M., Niknejad, A. S., Bazgir, S., Kargari, A., Sazegar, M., Rasouli, M., & Chae, S. (2021). Enhancement of physical characteristics of styrene–acrylonitrile nanofiber membranes using various post-treatments for membrane distillation. *Membranes*, *11*(12). https://doi.org/10.3390/membranes11120969
105. Sanchaniya, J.-V., Kanukuntla, S.-P., Modappathi, P., & Macanovskis, A. (2022). Mechanical behaviour numerical investigation of composite structure, consisting of polymeric nanocomposite mat and textile. *21st International Scientific Conference Engineering for Rural Development Proceedings*, *21*, 720–726. https://doi.org/10.22616/erdev.2022.21.tf225
106. Sanchaniya, J. V. (2024). COMPARATIVE ANALYSIS OF THERMAL CHARACTERISTICS: VIRGIN POLYACRYLONITRILE (PAN) VERSUS ELECTROSPUN PAN NANOFIBER MATS. *Latvian Journal of Physics and Technical Sciences*. https://doi.org/Accepted Article
107. Sanchaniya, J. V., Kanukuntla, S.-P., Simon, S., & Gerina-Ancane, A. (2022). Analysis of mechanical properties of composite nanofibers constructed on rotating drum and collector plate. *21st International Scientific Conference Engineering for Rural Development Proceedings*, *21*, 737–744. https://doi.org/10.22616/erdev.2022.21.tf227
108. Sanchaniya, J. V., Lasenko, I., Gobins, V., & Kobeissi, A. (2024). A Finite Element Method for Determining the Mechanical Properties of Electrospun Nanofibrous Mats. *Polymers (Basel)*, *16*(6), 852. https://doi.org/10.3390/polym16060852
109. Sanchaniya, J. V., Lasenko, I., Kanukuntala, S.-P., Smogor, H., Viluma-Gudmona, A., Krasnikovs, A., Gobins, V., & Tipans, I. (2023). Mechanical

and thermal characteristics of annealed-oriented PAN nanofibers. *Polymers*. https://doi.org/doi.org/10.3390/polym15153287
110. Sanchaniya, J. V., Lasenko, I., Kanukuntla, S. P., Mannodi, A., Vilumagudmona, A., & Gobins, V. (2023). Preparation and Characterization of Non-Crimping Laminated Textile Composites Reinforced with Electrospun Nanofibers. *Nanomaterials*, *13*(13), 1949. https://doi.org/10.3390/nano13131949
111. Sanchaniya, J. V., Lasenko, I., Vijayan, V., Smogor, H., Gobins, V., Kobeissi, A., & Goljandin, D. (2024). A Novel Method to Enhance the Mechanical Properties of Polyacrylonitrile Nanofiber Mats: An Experimental and Numerical Investigation. *Polymers*, *16*(7), 992. https://doi.org/10.3390/polym16070992
112. Sarkar, S., Deevi, S., & Tepper, G. (2007). Biased AC electrospinning of aligned polymer nanofibers. *Macromolecular Rapid Communications*, *28*(9), 1034–1039. https://doi.org/10.1002/marc.200700053
113. Scharnagl, N., & Buschatz, H. (2001). Polyacrylonitrile (PAN) membranes for ultra- and microfiltration. *Desalination*, *139*(1–3), 191–198. https://doi.org/10.1016/S0011-9164(01)00310-1
114. Schneider, C. A., Rasband, W. S., & Eliceiri, K. W. (2012). NIH Image to ImageJ: 25 years of image analysis. *Nature Methods*, *9*(7), 671–675. https://doi.org/10.1038/nmeth.2089
115. Sharma, S., Chhetry, A., Zhang, S., Yoon, H., Park, C., Kim, H., Sharifuzzaman, M., Hui, X., & Park, J. Y. (2021). Hydrogen-Bond-Triggered hybrid nanofibrous membrane-based wearable pressure sensor with ultrahigh sensitivity over a broad pressure range. *ACS Nano*, *15*(3), 4380–4393. https://doi.org/10.1021/acsnano.0c07847
116. Sheng, J., Li, Y., Wang, X., Si, Y., Yu, J., & Ding, B. (2016). Thermal inter-fiber adhesion of the polyacrylonitrile/fluorinated polyurethane nanofibrous membranes with enhanced waterproof-breathable performance. *Separation and Purification Technology*, *158*, 53–61. https://doi.org/10.1016/j.seppur.2015.11.046
117. Song, W., Zhang, Y., Yu, D. G., Tran, C. H., Wang, M., Varyambath, A., Kim, J., & Kim, I. (2021). Efficient Synthesis of Folate-Conjugated Hollow Polymeric Capsules for Accurate Drug Delivery to Cancer Cells. *Biomacromolecules*, *22*(2), 732–742. https://doi.org/10.1021/acs.biomac.0c01520
118. Song, Z., Hou, X., Zhang, L., & Wu, S. (2010). Enhancing crystallinity and orientation by hot-stretching to improve the mechanical properties of electrospun partially aligned polyacrylonitrile (PAN) nanocomposites. *Materials*, *4*(4), 621–632. https://doi.org/10.3390/ma4040621
119. Sonker, A. K., Wagner, H. D., Bajpai, R., Tenne, R., & Sui, X. M. (2016). Effects of tungsten disulphide nanotubes and glutaric acid on the thermal and mechanical properties of polyvinyl alcohol. *Composites Science and*

Technology, *127*, 47–53. https://doi.org/10.1016/j.compscitech.2016.02.030
120. Srithep, Y., Nealey, P., & Turang, L.-S. (2013). Effects of Annealing Time and Temperature on the Crystallinity and Heat Resistance Behavior of Injection-Molded Poly(lactic acid). *Polymer Engineering & Science*, *53*(3), 1–10. https://doi.org/https://doi.org/10.1002/pen.23304
121. Stanishevsky, A., Brayer, W. A., Pokorny, P., Kalous, T., & Lukáš, D. (2016). Nanofibrous alumina structures fabricated using high-yield alternating current electrospinning. *Ceramics International*, *42*(15), 17154–17161. https://doi.org/10.1016/j.ceramint.2016.08.003
122. Stockdale, T. A., Cole, D. P., Staniszewski, J. M., Roenbeck, M. R., Papkov, D., Lustig, S. R., Dzenis, Y. A., & Strawhecker, K. E. (2020). Hierarchical Mechanisms of Lateral Interactions in High-Performance Fibers. *ACS Applied Materials and Interfaces*, *12*(19), 22256–22267. https://doi.org/10.1021/acsami.9b23459
123. Sun, B., Long, Y. Z., Zhang, H. D., Li, M. M., Duvail, J. L., Jiang, X. Y., & Yin, H. L. (2014). Advances in three-dimensional nanofibrous macrostructures via electrospinning. *Progress in Polymer Science*, *39*(5), 862–890. https://doi.org/10.1016/j.progpolymsci.2013.06.002
124. Sun, G., Sun, L., Xie, H., & Liu, J. (2016). Electrospinning of nanofibers for energy applications. *Nanomaterials*, *6*(7). https://doi.org/10.3390/nano6070129
125. Sundarrajan, S., Tan, K. L., Lim, S. H., & Ramakrishna, S. (2014). Electrospun nanofibers for air filtration applications. *Procedia Engineering*, *75*, 159–163. https://doi.org/10.1016/j.proeng.2013.11.034
126. Tan, E. P. S., & Lim, C. T. (2006). Effects of annealing on the structural and mechanical properties of electrospun polymeric nanofibres. *Nanotechnology*, *17*(10), 2649–2654. https://doi.org/10.1088/0957-4484/17/10/034
127. Tang, X., & Yan, X. (2017). Dip-coating for fibrous materials: mechanism, methods and applications. *Journal of Sol-Gel Science and Technology*, *81*(2), 378–404. https://doi.org/10.1007/s10971-016-4197-7
128. Tanioka, A., Matsumoto, H., & Tsuboi, K. (2010). Electrospun Nanofiber Networks for Electronics and Optics. *MRS Online Proceedings Library*, *1242*, 1–6. https://doi.org/https://doi.org/10.1557/PROC-1240-WW10-04
129. Taylor, G., & Dyke, M. D. Van. (1969). Electrically driven jets With an appendix by. *Proc. Roy. Soc. Lond. A*, *313*, 453–475.
130. Terada, D., Kobayashi, H., Zhang, K., Tiwari, A., Yoshikawa, C., & Hanagata, N. (2012). Transient charge-masking effect of applied voltage on electrospinning of pure chitosan nanofibers from aqueous solutions. *Science and Technology of Advanced Materials*, *13*(1). https://doi.org/10.1088/1468-6996/13/1/015003

131. Thomas, D., Zhuravlev, E., Wurm, A., Schick, C., & Cebe, P. (2018). Fundamental thermal properties of polyvinyl alcohol by fast scanning calorimetry. *Polymer*, *137*, 145–155. https://doi.org/10.1016/j.polymer.2018.01.004
132. TONG, H.-W., & WANG, M. (2012). Negative Voltage Electrospinning and Positive Voltage Electrospinning of Tissue Engineering Scaffolds: a Comparative Study and Charge Retention on Scaffolds. *Nano LIFE*, *02*(01), 1250004. https://doi.org/10.1142/s1793984411000384
133. Tsioptsias, C., Fardis, D., Ntampou, X., Tsivintzelis, I., & Panayiotou, C. (2023). Thermal Behavior of Poly(vinyl alcohol) in the Form of Physically Crosslinked Film. *Polymers*, *15*(8), 1843. https://doi.org/10.3390/polym15081843
134. Vargas, E. A. T., do Vale Baracho, N. C., de Brito, J., & de Queiroz, A. A. A. (2010). Hyperbranched polyglycerol electrospun nanofibers for wound dressing applications. *Acta Biomaterialia*, *6*(3), 1069–1078. https://doi.org/10.1016/j.actbio.2009.09.018
135. Wang, Y., Tong, Y., Zhang, B., Su, H., & Xu, L. (2018). Formation of surface morphology in polyacrylonitrile (PAN) fibers during wet-spinning. *Journal of Engineered Fibers and Fabrics*, *13*(2), 52–57. https://doi.org/10.1177/155892501801300208
136. Wang, Z., Cai, N., Dai, Q., Li, C., Hou, D., Luo, X., Xue, Y., & Yu, F. (2014). Effect of thermal annealing on mechanical properties of polyelectrolyte complex nanofiber membranes. *Fibers and Polymers*, *15*(7), 1406–1413. https://doi.org/10.1007/s12221-014-1406-2
137. Wang, Z., Sahadevan, R., Crandall, C., Menkhaus, T. J., & Fong, H. (2020). Hot-pressed PAN/PVDF hybrid electrospun nanofiber membranes for ultrafiltration. *Journal of Membrane Science*, *611*(May), 118327. https://doi.org/10.1016/j.memsci.2020.118327
138. Wijerathne, D., Gong, Y., Afroj, S., Karim, N., & Abeykoon, C. (2023). Mechanical and thermal properties of graphene nanoplatelets-reinforced recycled polycarbonate composites. *International Journal of Lightweight Materials and Manufacture*, *6*(1), 117–128. https://doi.org/10.1016/j.ijlmm.2022.09.001
139. Wong, S. C., Baji, A., & Leng, S. (2008). Effect of fiber diameter on tensile properties of electrospun poly(ε-caprolactone). *Polymer*, *49*(21), 4713–4722. https://doi.org/10.1016/j.polymer.2008.08.022
140. Xiang, C., & Frey, M. W. (2016). Increasing mechanical properties of 2-D-structured electrospun nylon 6 non-woven fiber mats. *Materials*, *9*(4). https://doi.org/10.3390/ma9040270
141. Xu, T. C., Han, D. H., Zhu, Y. M., Duan, G. G., Liu, K. M., & Hou, H. Q. (2020). High Strength Electrospun Single Copolyacrylonitrile (coPAN) Nanofibers with Improved Molecular Orientation by Drawing. *Chinese Journal of Polymer Science (English Edition)*.

https://doi.org/10.1007/s10118-021-2516-0
142. Xue, J., Wu, T., Dai, Y., & Xia, Y. (2019a). Electrospinning and electrospun nanofibers: Methods, materials, and applications. In *Chemical Reviews* (Vol. 119, Issue 8, pp. 5298–5415). https://doi.org/10.1021/acs.chemrev.8b00593
143. Xue, J., Wu, T., Dai, Y., & Xia, Y. (2019b). Electrospinning and electrospun nanofibers: Methods, materials, and applications [Review-article]. *Chemical Reviews*, *119*(8), 5298–5415. https://doi.org/10.1021/acs.chemrev.8b00593
144. Xue, J., Xie, J., Liu, W., Xia, Y., States, U., Holland, D., Medicine, R., States, U., States, U., & States, U. (2019). *HHS Public Access*. *50*(8), 1976–1987. https://doi.org/10.1021/acs.accounts.7b00218.Electrospun
145. Yao, J., Bastiaansen, C. W. M., & Peijs, T. (2014). High strength and high modulus electrospun nanofibers. *Fibers*, *2*(2), 158–187. https://doi.org/10.3390/fib2020158
146. Yarin, A. L., Kataphinan, W., & Reneker, D. H. (2005). Branching in electrospinning of nanofibers. *Journal of Applied Physics*, *98*(6). https://doi.org/10.1063/1.2060928
147. Yarin, A. L., Koombhongse, S., & Reneker, D. H. (2001a). Bending instability in electrospinning of nanofibers. *Journal of Applied Physics*, *89*(5), 3018–3026. https://doi.org/10.1063/1.1333035
148. Yarin, A. L., Koombhongse, S., & Reneker, D. H. (2001b). Taylor cone and jetting from liquid droplets in electrospinning of nanofibers. *Journal of Applied Physics*, *90*(9), 4836–4846. https://doi.org/10.1063/1.1408260
149. Yin, Y., Pan, Z., & Xiong, J. (2018). A tensile constitutive relationship and a finite element model of electrospun nanofibrous mats. *Nanomaterials*, *8*(1). https://doi.org/10.3390/nano8010029
150. Yin, Y., Pu, D., & Xiong, J. (2017). Analysis of the comprehensive tensile relationship in electrospun silk fibroin/polycaprolactone nanofiber membranes. *Membranes*, *7*(4). https://doi.org/10.3390/membranes7040067
151. Yin, Y., & Xiong, J. (2018). Finite element analysis of electrospun nanofibrous mats under biaxial tension. *Nanomaterials*, *8*(5), 1–19. https://doi.org/10.3390/nano8050348
152. You, X., He, J., Nan, N., Sun, X., Qi, K., Zhou, Y., Shao, W., Liu, F., & Cui, S. (2018). Stretchable capacitive fabric electronic skin woven by electrospun nanofiber coated yarns for detecting tactile and multimodal mechanical stimuli. *Journal of Materials Chemistry C*, *6*(47), 12981–12991. https://doi.org/10.1039/C8TC03631D
153. Zhang, H., Nie, H., Yu, D., Wu, C., Zhang, Y., White, C. J. B., & Zhu, L. (2010). Surface modification of electrospun polyacrylonitrile nanofiber towards developing an affinity membrane for bromelain adsorption. *Desalination*, *256*(1–3), 141–147.

https://doi.org/10.1016/j.desal.2010.01.026
154. Zhang, M., Chen, Y., Chiang, F. P., Gouma, P. I., & Wang, L. (2019). Modeling the large deformation and microstructure evolution of nonwoven polymer fiber networks. *Journal of Applied Mechanics, Transactions ASME*, *86*(1), 1–11. https://doi.org/10.1115/1.4041677
155. Zhang, P., Shao, C., Zhang, Z., Zhang, M., Mu, J., Guo, Z., & Liu, Y. (2011). In situ assembly of well-dispersed Ag nanoparticles (AgNPs) on electrospun carbon nanofibers (CNFs) for catalytic reduction of 4-nitrophenol. *Nanoscale*, *3*(8), 3357–3363. https://doi.org/10.1039/c1nr10405e
156. Zhang, Y., Lu, Y., Xu, Y., Zhou, Z., Li, Y., Ling, W., & Song, W. (2023). Bio-Inspired Drug Delivery Systems: From Synthetic Polypeptide Vesicles to Outer Membrane Vesicles. *Pharmaceutics*, *15*(2). https://doi.org/10.3390/pharmaceutics15020368
157. Zhao, Z., Li, B., & Ma, P. (2023). Advances in mechanical properties of flexible textile composites. *Composite Structures*, *303*(October 2022), 116350. https://doi.org/10.1016/j.compstruct.2022.116350
158. Zhou, Y., Liu, Y., Zhang, M., Feng, Z., Yu, D. G., & Wang, K. (2022). Electrospun Nanofiber Membranes for Air Filtration: A Review. *Nanomaterials*, *12*(7). https://doi.org/10.3390/nano12071077
159. Zulkifli, M. Z. A., Nordin, D., Shaari, N., & Kamarudin, S. K. (2023). Overview of Electrospinning for Tissue Engineering Applications. *Polymers*, *15*(11), 1–27. https://doi.org/10.3390/polym15112418

Jaymin Vrajlal Sanchaniya, born in 1992 in Rajkot, India, holds a Bachelor's degree in Mechanical Engineering from Gujarat Technical University, India (2015), and a Master's degree in Mechanics and Mechanical Engineering from Riga Technical University, Latvia (2020). Since 2020, he has been working as a research assistant at Riga Technical University. He has gained extensive experience through collaborations and training at renowned institutions such as KTH Royal Institute of Technology (Sweden), RWTH Aachen University (Germany), University of Technology of Compiegne (France), University of Rouen Normandy (France), and Tallinn University of Technology (Estonia). His research interests revolve around the fabrication, characterization, finite element modeling, and mechanics of nanofibers and nanofiber mats. His dedication to the field is reflected in his impressive publication record, with more than 20 journal and conference articles indexed in the SCOPUS database, spanning areas such as fabricating and characterizing nanofiber mats for the fields of environment and smart materials.